Development of Histotripsy Focused Ultrasound Devices Using Rapid Prototyping Methods

Hannah O. Sheppard

Thesis submitted to the faculty of the Virginia Polytechnic Institute and State University
in partial fulfillment of the requirements for the degree of

Master of Science
In
Biomedical Engineering

Eli Vlaisavljevich, Chair
Andre A. Muelenaer
Christopher B. Arena

April 25, 2022
Blacksburg, Virginia

Keywords: histotripsy, prototyping, injection molding, transducer

Development of Histotripsy Focused Ultrasound Devices Using Rapid Prototyping Methods

Hannah O. Sheppard

ABSTRACT

Histotripsy is a nonthermal ultrasound therapy used to treat cancer noninvasively by tissue mechanical fractionation with cavitation bubble clouds. Histotripsy is conducted through focused ultrasound transducers, where the piezoceramic (PZT) plate or disc, which emits the ultrasound wave, is the fundamental unit of the transducer. For modular prototype histotripsy designs, these PZTs are housed in a 3D printed focused lens. However, 3D printing transducer components can be time consuming and expensive when scaling up manufacturing, and 3D printing is limited in material selection for transducer applications. This thesis investigates the use of a novel fabrication process for prototype focused ultrasound transducers, injection molding, with an in-house benchtop injection molding machine. Acoustic material properties for investigated injection molded materials, ABS, GPPS, 30% glass filled nylon, nylon 6/6, and nylon 101, are quantified experimentally. Single elements are constructed with injection molded lenses made from ABS, 30% glass-filled nylon, nylon 6/6, and nylon 101 on an in-house benchtop machine. Results show that injection molding is a novel feasible method for applications in focused ultrasound devices and the investigated plastics have favorable properties for developing prototype histotripsy transducers, comparable to 3D printed transducer housings. Future work aims to apply injection molding to various transducer designs and additional materials for focused ultrasound therapy devices.

Development of Histotripsy Focused Ultrasound Devices Using Rapid Prototyping Methods

Hannah O. Sheppard

GENERAL AUDIENCE ABSTRACT

Histotripsy is a cancer therapy that can noninvasively treat tumors without surgery. This is done through devices called focused ultrasound transducers which emit ultrasound waves to administer treatment to ablate tumors. These transducers are constructed using 3D printing methods, but this can be limiting when scaling up manufacturing or in material selection for transducer applications, therefore additional fabrication methods are needed. This thesis presents injection molding as a novel method for making transducer components with an in-house benchtop injection molding machine. Five plastic materials are investigated to determine ultrasound properties that would identify preferred transducer materials. Single element transducers are made from injection molded materials, tested, and compared with 3D printed single element transducers. Results of this thesis show that injection molding is a feasible manufacturing method capable of producing transducers for histotripsy, and researched materials have favorable properties for this application. In future research, additional injection molded materials should be investigated and multiple transducer designs created for injection molding fabrication. These injection molded transducers can be applied to histotripsy or applied to other focused ultrasound therapies.

DEDICATION

To my Lord and Savior, Jesus Christ, who has proved His faithfulness to me time and time again. You knew I needed this thesis experience more than I thought I did, and I'm so grateful for the many answered prayers for both the big and the small.

I am especially grateful for the eternal hope I can only find in You.

Thank you for saving me.

ACKNOWLEDGEMENTS

I have been abundantly blessed in the six years I've been at Virginia Tech. I have many thanks to give to people who have supported me in all kinds of ways to help me get here and complete my thesis.

First, I want to thank my thesis advisor, Eli Vlaisavljevich. Thank you for offering me a position in your lab despite the world entering into the pandemic and all the uncertainty. You made my degree possible to pursue, I owe a lot to you, and I'm very grateful. To my lab mates who have truly become some of my closest friends in this season. Lauren Arnold Ruger – you are amazing and don't forget it. Thank you for the advice, the heart-to-hearts, the mentoring, the conference bonding moments, the text check-ins, the cat pictures, and this friendship that I know will continue. Thank you to Connor Edsall, my unofficial additional advisor. Thank you for letting me bug you about orders, my many materials questions, and every minor and major success in my research I had along the way. I will always look up to you and Danae both professionally and simply as high-quality people. You are both a joy to be around. To Alex Simon, you will never know how much you taught me. Thank you for the coconut La Croix, the conversations about Dune and all sci-fi, for giving me a hard time when I broke things in lab, and for making me a better person. Thank you to Jess Gannon, you are a joy to be around. Thank you for affirming my drape-cutting skills, the mutual respect for finding ways to be fashionable in lab, and for being someone I know I can go to for advice, casual discussion, and a good time. To Barath Udayasuryan and Raffae Ahmad, for welcoming me and providing frequent encouragement, picture sessions, and even a Starbucks gift card. Thank you to Victor Lopez. You've only been here a year but it feels like so much longer. Thank you for the

treasured friendship and kindred spirit. You never failed to be there for me in the highs and lows of this thesis. Best of luck in the next few years, and I'm praying for each of you!

To some incredible, hard-working, enjoyable, intelligent, female-in-stem undergrads: Lauren Potter who bravely began this injection molding journey with me and become a sweet friend, Renata Farrell who committed so much time to this project and truly cared about me succeeding, finishing this thesis, and eating dinner, Laura Huynh for her willingness to CAD away at anything I asked for and for all the entertainment she brings to life, and to Loulou Vos who worked so diligently while engaging in many deep conversations and podcasts with me. I also want to give a shout out to Mariam Hasan and Ty Kwak (even though you're not a woman, Ty) for your hard work and willingness to learn in lab. All of you have big things in store and I better get some updates when you're famous.

I have quite a few particular professionals who guided me on this injection molding and material testing journey. Thank you to Adam Maxwell for his direction on materials to investigate and feedback on all things focused ultrasound. Thank you to Jon Buttram for the advice he so generously offered over the phone and through emails on material testing. Go Hokies! Thank you to George Pabis, the OG, who gave me contact information to hunt down injection molders and makes sure my mom doesn't work too late. I owe a huge thank you to Total Plastic Solutions in Lynchburg, VA. Thank you especially to Marc Robinson and Johnny Eagle (Go Hokies, ACC Champs!), who answered so many of my injection molding questions, gave an abundance of design advice, and have sent me many encouraging emails. Without you both I don't think I'd have made it to the 4th chapter of this thesis. Your professional guidance was especially crucial in this final semester.

Thank you to all my roommates, past and present, who have loved, supported, and been genuinely interested in what I do. Namely, Sarah Bright, Lauren Causey, Jenna McKeown, Heather Andrews, Taryn Hollis, Kaitlin Probus, Jessie McCauley, Kelly Flanagan, Emma Hilt, and Mimi Hilt. You all are awesome and some of the best friends I could ask for. I can't wait to celebrate with most of you soon!

To my spiritual family, mostly found in Chi Alpha and Blacksburg Christian Fellowship. You all prayed so much for me and for the injection molding machine. Thank you for being givers when I needed to receive and listeners when I needed to express my thoughts and emotions. I couldn't have done this without your friendships and accountability: Amanda Huang, Audra Barnard, Analiesa DeReuix, really all of my lifegroup, Julie Faith, Chris Faith, Susan Garner, Sara Frazier, and Emma Kidane. Thank you as well to all the staff and friends at the Bradley Study Center. You make help make Blacksburg feel like home.

I have to say thank you to all the intramural sports, teams, and friends that kept me sane. Thanks to the countless teammates who joined the adventures of basketball, Spikeball, innertube water polo, flag football and more.

To the family I will soon acquire, the Covell family. Thank you for the love and patience and for wanting to know what I do. Thank you for all the games of Dutch Blitz and pickleball that allowed me to enjoy living life outside of the lab. I'm excited for the memories to come.

A huge, exponentially increasing thank you to my family who I love so much. Zachary, thank you for being a big brother who works hard when it's not always fun, you inspire me, and I love you. To my brother, Logan, grad school has given us a chance to be

at the same place at the same time. I love our weekly lunches and the friendship we have developed the past 4 years. Thank you for your perspective and submission to God's word. I love you. To my incredible sister and best friend, Kellyn. Thank you for your late-night phone calls, being a delivery woman for this project, and for the fun we have together. I would still give you my kidney. Mom and Dad, thank you for also delivering me molds and plastic squares from Lynchburg. I owe you a lot in gas money… But seriously thank you for the many phone calls, excitement and support, and the engineering advice. Thank you, Dad, for your allen wrenches and helping me with equipment over FaceTime and being willing to put up with VT parking rules. I love you both so much. Thank you for giving me the opportunity to pursue an engineering degree in the first place and for giving me a family that I wouldn't trade for anything.

Lastly, an unquantifiable thank you to my fiancé, Bryan. I might cry when writing this because I am so thankful and you know I'm a deep feeler. I owe a lot to God for giving me this thesis that brought us back together in the first place. Thank you for visiting so much simply to make me dinner, clean my apartment, and make sure I was taking care of myself. You have encouraged me more than anyone. You are my best friend I am so excited to marry you. I love you.

Table of Contents

List of Figures

List of Tables

Chapter 1. Introduction

1.1 Histotripsy Background

Histotripsy is an emerging focused ultrasound therapy that can be used to noninvasively ablate cancerous tissue in the body (**Figure 1-1**). Unlike many other technologies used to treat cancer, such as noninvasive high-intensity focused ultrasound (HIFU), or minimally invasive techniques such as microwave ablation or radiofrequency ablation (RFA), which rely on heating the target tissue to temperatures > 50°C [1, 2], histotripsy is nonthermal. Histotripsy's nonthermal mechanism allows it to avoid some of the challenges of thermal ablation techniques, including heat-sink effects [3] in surrounding vasculature that can result in poor efficacy of treatment in the targeted tissue. Histotripsy has been previously divided into three categories: intrinsic threshold histotripsy, shock-scattering histotripsy, and boiling histotripsy [4, 5]. Unless otherwise indicated, throughout this document, histotripsy refers to intrinsic threshold histotripsy. Intrinsic threshold histotripsy uses single cycle pulses with large peak negative pressures (p- >25 MPa) to exert a tensile force on a medium, resulting in a cavitation bubble cloud [4-6]. In short, histotripsy breaks down tissue using high amplitude, low duty cycle (<1%) sonication [4]. The high amplitude, short duration pressure pulse incites cavitation, and the rapid expansion and collapse of the microbubbles mechanically shears the targeted tissue into an acellular debris with no remaining viable cells [7-9]. During treatment, real-time ultrasound imaging can be used to monitor and visualize the hyperechoic bubble cloud in the tissue [10, 11]. These cavitation bubble clouds, based on recent documentation and current devices operating in the most commonly investigated histotripsy frequencies from 500 kHz-3 MHz, range in size from 0.1-10 mm in the axial direction [7]. This small target area allows for precise targeting, creating a defined boundary of fractionated

acellular material and untargeted, intact tissue after a sufficient number of pulses have been applied to the tissue. Previous studies have shown that ~1,000 pulses per point is sufficient to ablate softer tissues such as the kidney whereas >2,000-10,000 are required to ablate more fibrous tissues such as cholangiocarcinoma liver tumors or uterine fibroids [12, 13].

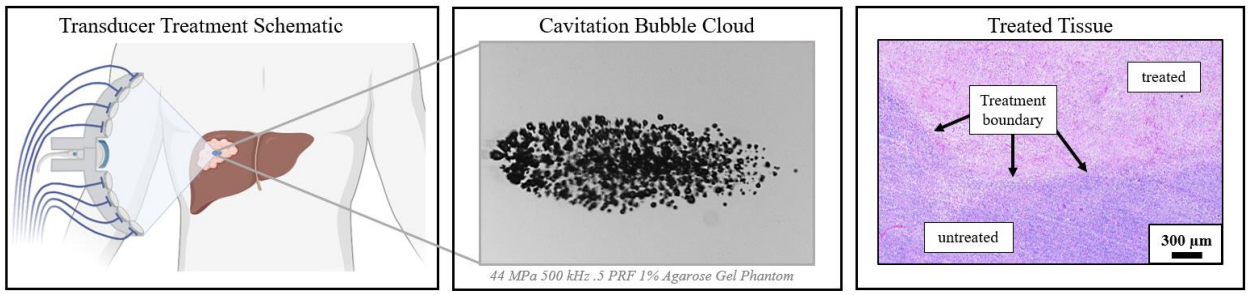

Figure 1-1. Histotripsy treatment showing schematic with transducer treating liver tumor, example cavitation bubble cloud at 500 kHz, and resulting treated tissue with defined margins of treated and untreated tissue.

1.2 Applications of Histotripsy

The history of histotripsy and its development is outlined in multiple review articles [4, 9, 14]. Early studies explored the effects of cavitation ablation of the kidneys, liver, and thrombus using animal models under the name of shock wave therapy [15-19]. From there, histotripsy has been better defined and has been investigated for various applications, including ablation of liver [20-24] and kidney tumors [25, 26], treatment of thrombosis [27-30] and hematomas [31], and the removal of biofilms [32-34]. Histotripsy has also been investigated in more fibrous tissues such as ablation of benign prostatic hyperplasia [11, 35, 36] and primary bone tumors [37]. Phase I human clinical trials have been conducted and are ongoing in benign prostatic hyperplasia (BPH) [38], calcified aortic stenosis (CAS) [39], and the ablation of liver tumors [40].

1.3 Histotripsy Transducers for Preclinical Research

Histotripsy therapy is applied using focused transducers typically operating within frequencies of 0.1 to 10 MHz and capable of generating very large peak negative pressure levels often

>30 MPa [4-6]. Histotripsy transducers are developed based on the needs of the application. For instance, lower frequencies (500-700 kHz) are used to treat deeper (7-10 cm) tissues because higher frequencies (1-3 MHz) experience more pressure attenuation. Higher frequencies produce smaller bubble clouds than lower frequencies [7], allowing for more precise treatment than lower frequencies, whereas a low frequency treatment is more time efficient for treating large masses. Prototype histotripsy devices are still being designed, tailored, and optimized for various applications.

A hard piezoelectric (PZT) plate or disc is the fundamental unit of prototype histotripsy transducers. When high voltage is applied to the PZT, an ultrasound wave is emitted by the plate, generating a pressure wave. Illustrated in **Figure 1-2**, the ultrasound pressure wave travels through the focused housing matching layer lens as well as any additional layers between the flat PZT disc and the lens before passing through the coupling medium (typically degassed water) and finally passing into the patient. The pressure wave must exceed the negative pressure threshold required for a cavitation bubble cloud, based on the target media, which has previously been shown to be ~25-30 MPa for water-based soft tissues when using single cycle intrinsic threshold histotripsy pulsing [5]. For higher frequencies used for prototype histotripsy devices (500 kHz - 3 MHz), these high peak negative pressures are not generated from a single transducer element. Instead, multiple PZT elements are assembled in an ultrasound array with a geometric focus matching the focus of the individual elements. The focus location is where the pressure waves of all PZTs are superimposed for cavitation and is predetermined by the housing lens and array design, referred to as a scaffold, pictured in **Figure 1-3**. The housing lenses and scaffold are often made by 3D printing, which can produce detailed part designs and is ideal for initial prototyping. However, 3D

printing is not sustainable for scale-up manufacturing due to significant post-processing and multiple hour print times compared to alternative manufacturing methods.

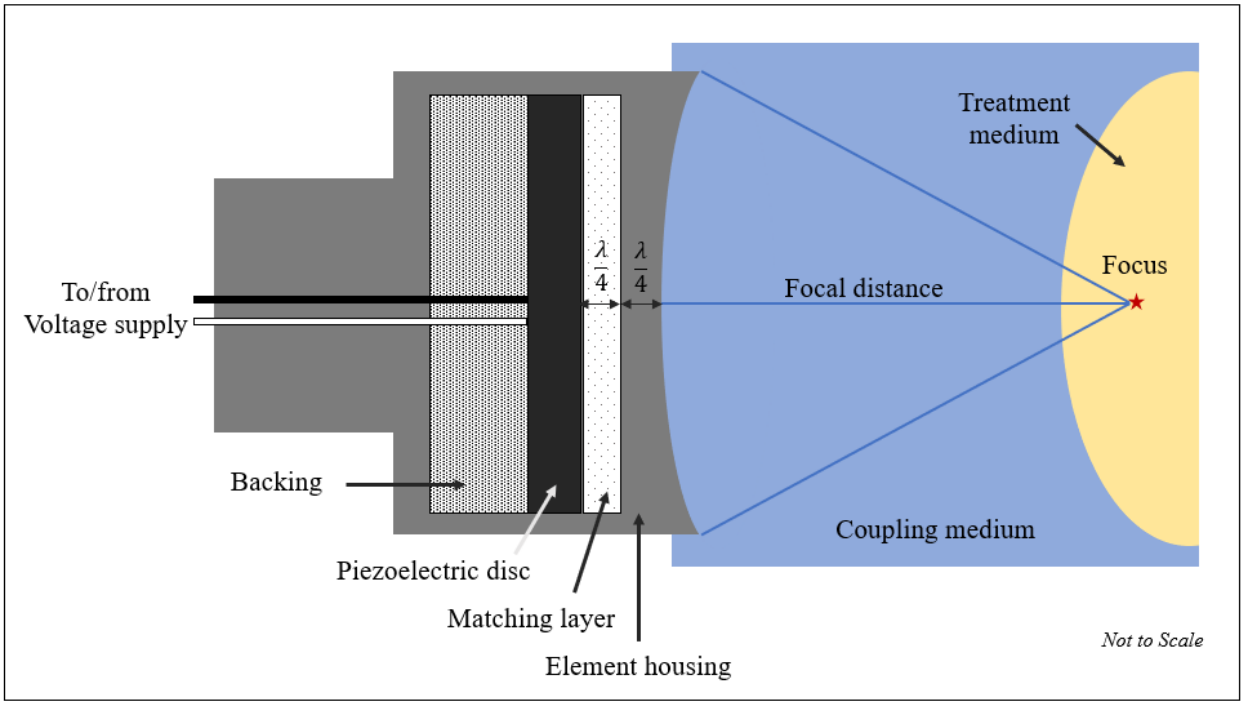

Figure 1-2. The components of a transducer element and wave propagation media. A voltage is sent to the piezoelectric (PZT) disc. The disc vibrates to emit a pressure wave that travels through the ¼-wavelength (λ) thick matching layer and element housing, through the coupling medium, and to the treatment focus. The focus distance is determined by the radius of curvature of the element housing.

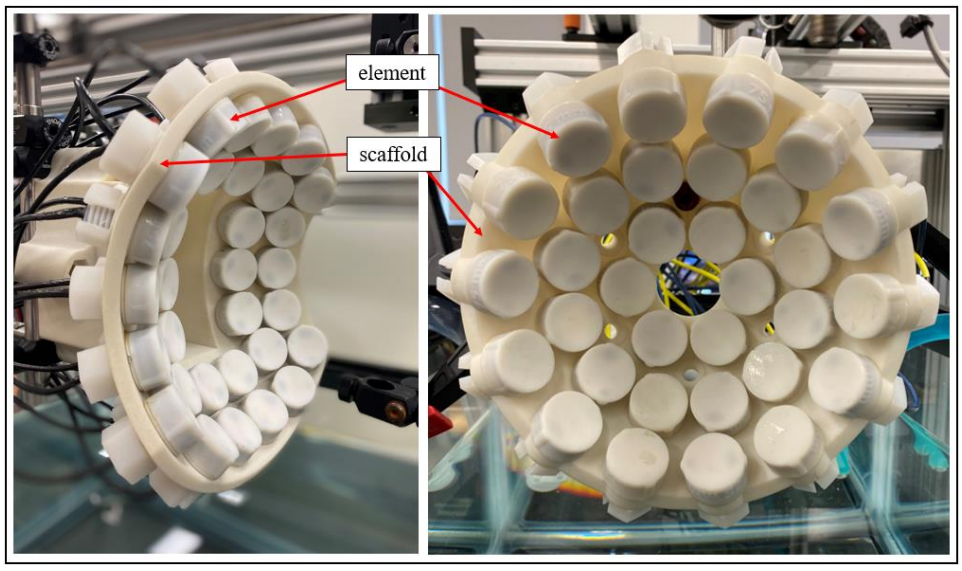

Figure 1-3. Image of transducer array with circular elements. Two different transducers are pictured, both with 32 elements and a focal distance of 75 mm.

Pressure loss and acoustic attenuation occurs based on the mediums and matching layers that the wave must travel through. A matching layer is a quarter-wavelength in thickness so that the reverberations of the sound wave will share the same phase to constructively interfere for best energy transmission [41]. Acoustic impedance, denoted with a Z, is a material property defined by *Eq.* 1.1 [41-43]

$$Z = v\rho \qquad (Eq.\ 1.1)$$

where v is the acoustic velocity and ρ is the density of the wave propagation media. Because materials have varying acoustic impedance properties, when designing a housing lens for the PZT, the acoustic impedance of the lens material must be assessed. The more the matching layer impedance differs from the geometric average of the impedance of the PZT and the impedance of the propagation medium, the greater the loss of power of the pressure-sound wave due to reflection which will inhibit effective treatment. Put another way, when the matching layer's acoustic impedance is equal to the geometric average of the PZT and propagation medium's impedances, the reflection, or attenuation between the mediums, approaches zero [42]. For two mediums, such as a matching layer and housing lens as in **Figure 1-2**, the amplitude reflection coefficient, R, can be calculated using *Eq.* 1.2 [41, 44]

$$R = \frac{Z_2 - Z_1}{Z_2 + Z_1} \times 100 \qquad (Eq.\ 1.2)$$

where Z_1 and Z_2 are the acoustic impedances of mediums 1 and 2, respectively. From the reflection coefficient, the percentage of reflection of the initial pressure pulse of energy can be calculated, and subtracting from 100 gives the percentage of energy transmitted. For an ideal matching layer acoustic impedance, the geometric mean can be calculated from two mediums using *Eq.* 1.3 [41, 43]

$$Z_m = \sqrt{Z_1 Z_2} \qquad (Eq.\ 1.3)$$

where Z_1 and Z_2 are the acoustic impedances of mediums 1 and 2, respectively. Additional matching layers may be used to maximize the transmitted energy between the PZT and propagation media, with consideration for ease of assembly and wave propagation efficiency tradeoffs. Using multiple matching layers or improving the impedance of the matching layer materials results in a greater pulse bandwidth for PZT use and decreases stress in the PZT to avoid mechanical failure at high amplitude pulses.

While histotripsy transducers and their applications are the focus of this document, the materials and injection molding principles used for device modification and design discussed in Chapters 3 and 4 can be expanded to other focused ultrasound applications such as neuromodulation [45] and blood brain barrier disruption for drug delivery [46].

1.4 Outline of Thesis

The goal of this thesis was to investigate novel techniques for histotripsy device fabrication through the presentation and discussion of how histotripsy transducers are currently made and used in the clinical setting, the quantification of acoustic impedance for injection molded materials, and the application of the optimal injection molded materials in histotripsy transducer design. This thesis is broken into three primary chapters, 2-4, which investigate the goals of this work.

Chapter 2 discusses the modular prototype histotripsy device currently used for the majority of preclinical histotripsy studies [37, 47]. The first part of this chapter describes the current devices and prototyping methods used in our lab and discusses the many factors considered when designing a transducer such as tissue depth, size, and acoustic window. Next, Chapter 2 discusses device fabrication prototyping methods and developing the matching layer for the two types of PZTs used in a modular transducer, Pz36 and SM111. Transitioning to using the device, Chapter

2 then outlines the setup and inputs for *in vivo* studies of canine soft tissue sarcoma and canine osteosarcoma targeting utilizing a prototype histotripsy device. This chapter concludes with the results and discussion of these studies with a focus on the transducer strengths, limitations, and potential modifications for future histotripsy devices uses in these applications.

Current histotripsy transducers are constructed using 3D printing methods which, while ideal for initial prototyping, is a limiting manufacturing process due to post-processing, hours-long production times per part, and limitations in the types of materials that can be utilized. Alternatively, for the first time in literature, Chapter 3 introduces a novel manufacturing method for histotripsy transducer applications, injection molding, which is known to consistently manufacture components quickly and accurately. Chapter 3 discusses the workflow process of injection molding and injection molded material properties for investigated materials of interest. CAD models of molds specific to our injection molding machine are given. For 5 injection molded materials and two 3D printed materials, sound speed and acoustic impedance values obtained by experimentation are presented. These values are compared with literature. Additionally, similar materials injected on two different machines, an in-house benchtop machine and industry-grade machine, are compared. This chapter aims to suggest injection molding as a feasible prototyping method for transducer components.

Chapter 4 discusses the design, construction, and results of experiments using single element transducers built using the injection molding methods developed in Chapter 3. Attention is given to design for manufacturing considerations, and single element testing with waveform data for each injection molded housing material of interest.

Chapter 5 summarizes and concludes this thesis, reiterating main outcomes of injection molding for histotripsy devices. Additionally, this chapter indicates future directions and potential investigations for injection molding as a novel technique for transducer applications.

1.5 References

[1] Y. Keisari, "Tumor abolition and antitumor immunostimulation by physico-chemical tumor ablation," *Frontiers in Bioscience-Landmark,* vol. 22, no. 2, pp. 310-347, 2017-01-01 2017, doi: 10.2741/4487.

[2] C. J. Simon, D. E. Dupuy, and W. W. Mayo-Smith, "Microwave Ablation: Principles and Applications," *RadioGraphics,* vol. 25, no. suppl_1, pp. S69-S83, 2005, doi: 10.1148/rg.25si055501.

[3] D. S. K. Lu *et al.*, "Influence of Large Peritumoral Vessels on Outcome of Radiofrequency Ablation of Liver Tumors," *Journal of Vascular and Interventional Radiology,* vol. 14, no. 10, pp. 1267-1274, 2003/10/01/ 2003, doi: https://doi.org/10.1097/01.RVI.0000092666.72261.6B.

[4] K. B. Bader, E. Vlaisavljevich, and A. D. Maxwell, "For Whom the Bubble Grows: Physical Principles of Bubble Nucleation and Dynamics in Histotripsy Ultrasound Therapy," *Ultrasound in Medicine & Biology,* vol. 45, no. 5, pp. 1056-1080, 2019/05/01/ 2019, doi: https://doi.org/10.1016/j.ultrasmedbio.2018.10.035.

[5] E. Vlaisavljevich *et al.*, "Effects of Ultrasound Frequency and Tissue Stiffness on the Histotripsy Intrinsic Threshold for Cavitation," *Ultrasound in Medicine & Biology,* vol. 41, no. 6, pp. 1651-1667, 2015/06/01/ 2015, doi: https://doi.org/10.1016/j.ultrasmedbio.2015.01.028.

[6] A. D. Maxwell, C. A. Cain, T. L. Hall, J. B. Fowlkes, and Z. Xu, "Probability of Cavitation for Single Ultrasound Pulses Applied to Tissues and Tissue-Mimicking Materials," *Ultrasound in Medicine & Biology,* vol. 39, no. 3, pp. 449-465, 2013/03/01/ 2013, doi: https://doi.org/10.1016/j.ultrasmedbio.2012.09.004.

[7] C. Edsall, E. Ham, H. Holmes, T. L. Hall, and E. Vlaisavljevich, "Effects of frequency on bubble-cloud behavior and ablation efficiency in intrinsic threshold histotripsy," *Physics in Medicine & Biology,* vol. 66, no. 22, p. 225009, 2021.

[8] Z. Xu, M. Raghavan, T. L. Hall, M. A. Mycek, J. B. Fowlkes, and C. A. Cain, "Evolution of bubble clouds induced by pulsed cavitational ultrasound therapy - Histotripsy," *IEEE Transactions on Ultrasonics, Ferroelectrics, and Frequency Control,* vol. 55, no. 5, pp. 1122-1132, 2008, doi: 10.1109/TUFFC.2008.764.

[9] W. W. Roberts, "Development and translation of histotripsy: current status and future directions," (in eng), *Curr Opin Urol,* vol. 24, no. 1, pp. 104-110, 2014, doi: 10.1097/MOU.0000000000000001.

[10] T. L. Hall, C. R. Hempel, K. Wojno, Z. Xu, C. A. Cain, and W. W. Roberts, "Histotripsy of the prostate: dose effects in a chronic canine model," (in eng), *Urology,* vol. 74, no. 4, pp. 932-937, 2009, doi: 10.1016/j.urology.2009.03.049.

[11] A. M. Lake, T. L. Hall, K. Kieran, J. B. Fowlkes, C. A. Cain, and W. W. Roberts, "Histotripsy: minimally invasive technology for prostatic tissue ablation in an in vivo canine model," (in eng), *Urology,* vol. 72, no. 3, pp. 682-686, 2008, doi: 10.1016/j.urology.2008.01.037.

[12] W. W. Roberts, T. L. Hall, K. Ives, J. S. Wolf, J. B. Fowlkes, and C. A. Cain, "Pulsed cavitational ultrasound: a noninvasive technology for controlled tissue ablation

(histotripsy) in the rabbit kidney," *The Journal of urology*, vol. 175, no. 2, pp. 734-738, 2006.

[13] A. Hendricks *et al.*, "Histotripsy for the Treatment of Cholangiocarcinoma Liver Tumors: In Vivo Feasibility and Ex Vivo Dosimetry Study," *IEEE transactions on ultrasonics, ferroelectrics, and frequency control*, 2021.

[14] Z. Xu, T. L. Hall, E. Vlaisavljevich, and F. T. Lee Jr, "Histotripsy: the first noninvasive, non-ionizing, non-thermal ablation technique based on ultrasound," *International Journal of Hyperthermia*, vol. 38, no. 1, pp. 561-575, 2021.

[15] M. Delius, R. Denk, C. Berding, H.-G. Liebich, M. Jordan, and W. Brendel, "Biological effects of shock waves: Cavitation by shock waves in piglet liver," *Ultrasound in Medicine & Biology*, vol. 16, no. 5, pp. 467-472, 1990/01/01/ 1990, doi: https://doi.org/10.1016/0301-5629(90)90169-D.

[16] M. Delius, G. Enders, Z. Xuan, H.-G. Liebich, and W. Brendel, "Biological effects of shock waves: Kidney damage by shock waves in dogs—Dose dependence," *Ultrasound in Medicine & Biology*, vol. 14, no. 2, pp. 117-122, 1988/01/01/ 1988, doi: https://doi.org/10.1016/0301-5629(88)90178-0.

[17] A. Arefiev, F. Prat, J. Y. Chapelon, J. Tavakkoli, and D. Cathignol, "Ultrasound-induced tissue ablation: studies on isolated, perfused porcine liver," *Ultrasound in Medicine & Biology*, vol. 24, no. 7, pp. 1033-1043, 1998/09/01/ 1998, doi: https://doi.org/10.1016/S0301-5629(98)00046-5.

[18] F. Prat *et al.*, "Focused liver ablation by cavitation in the rabbit: a potential new method of extracorporeal treatment," *Gut*, vol. 35, no. 3, pp. 395-400, 1994.

[19] U. Rosenschein *et al.*, "Shock-wave thrombus ablation, a new method for noninvasive mechanical thrombolysis," *The American Journal of Cardiology*, vol. 70, no. 15, pp. 1358-1361, 1992/11/15/ 1992, doi: https://doi.org/10.1016/0002-9149(92)90775-T.

[20] E. Vlaisavljevich *et al.*, "Non-invasive ultrasound liver ablation using histotripsy: chronic study in an in vivo rodent model," *Ultrasound in medicine & biology*, vol. 42, no. 8, pp. 1890-1902, 2016.

[21] E. Vlaisavljevich *et al.*, "Image-guided non-invasive ultrasound liver ablation using histotripsy: feasibility study in an in vivo porcine model," *Ultrasound in medicine & biology*, vol. 39, no. 8, pp. 1398-1409, 2013.

[22] A. R. Smolock *et al.*, "Robotically assisted sonic therapy as a noninvasive nonthermal ablation modality: proof of concept in a porcine liver model," *Radiology*, vol. 287, no. 2, pp. 485-493, 2018.

[23] T. Worlikar *et al.*, "Effects of histotripsy on local tumor progression in an in vivo orthotopic rodent liver tumor model," *BME frontiers*, 2020.

[24] T. Worlikar *et al.*, "Histotripsy for non-invasive ablation of hepatocellular carcinoma (HCC) tumor in a subcutaneous xenograft murine model," in *2018 40th Annual International Conference of the IEEE Engineering in Medicine and Biology Society (EMBC)*, 2018: IEEE, pp. 6064-6067.

[25] T. L. Hall, K. Kieran, K. Ives, J. B. Fowlkes, C. A. Cain, and W. W. Roberts, "Histotripsy of rabbit renal tissue in vivo: temporal histologic trends," *Journal of endourology*, vol. 21, no. 10, pp. 1159-1166, 2007.

[26] N. R. Styn, T. L. Hall, J. B. Fowlkes, C. A. Cain, and W. W. Roberts, "Histotripsy of renal implanted VX-2 tumor in a rabbit model: investigation of metastases," *Urology*, vol. 80, no. 3, pp. 724-729, 2012.

[27] A. D. Maxwell, G. Owens, H. S. Gurm, K. Ives, D. D. Myers Jr, and Z. Xu, "Noninvasive treatment of deep venous thrombosis using pulsed ultrasound cavitation therapy (histotripsy) in a porcine model," *Journal of vascular and interventional radiology*, vol. 22, no. 3, pp. 369-377, 2011.

[28] X. Zhang *et al.*, "Non-invasive thrombolysis using microtripsy in a porcine deep vein thrombosis model," *Ultrasound in medicine & biology*, vol. 43, no. 7, pp. 1378-1390, 2017.

[29] V. Bollen *et al.*, "In vitro thrombolytic efficacy of single-and five-cycle histotripsy pulses and rt-PA," *Ultrasound in medicine & biology*, vol. 46, no. 2, pp. 336-349, 2020.

[30] K. B. Bader, S. A. Hendley, and V. Bollen, "Assessment of Collaborative Robot (Cobot)-assisted histotripsy for venous clot ablation," *IEEE Transactions on Biomedical Engineering*, vol. 68, no. 4, pp. 1220-1228, 2020.

[31] Y. Li *et al.*, "Histotripsy liquefaction of large hematoma for intracerebral hemorrhage using millisecond-length ultrasound pulse groups combined with fundamental and second harmonic superposition: A preliminary study," *Ultrasound in medicine & biology*, vol. 46, no. 5, pp. 1244-1257, 2020.

[32] C. Childers *et al.*, "Focused Ultrasound Biofilm Ablation: Investigation of Histotripsy for the Treatment of Catheter-Associated Urinary Tract Infections (CAUTIs)," *IEEE Transactions on Ultrasonics, Ferroelectrics, and Frequency Control*, 2021.

[33] T. A. Bigelow, T. Northagen, T. M. Hill, and F. C. Sailer, "Ultrasound histotripsy and the destruction of Escherichia coli biofilms," in *2008 30th Annual International Conference of the IEEE Engineering in Medicine and Biology Society*, 2008: IEEE, pp. 4467-4470.

[34] T. A. Bigelow, C. L. Thomas, and H. Wu, "Scan parameter optimization for histotripsy treatment of S. Aureus biofilms on surgical mesh," *IEEE transactions on ultrasonics, ferroelectrics, and frequency control*, vol. 67, no. 2, pp. 341-349, 2019.

[35] G. R. Schade *et al.*, "Histotripsy focal ablation of implanted prostate tumor in an ACE-1 canine cancer model," *The Journal of urology*, vol. 188, no. 5, pp. 1957-1964, 2012.

[36] C. R. Hempel, T. L. Hall, C. A. Cain, J. B. Fowlkes, Z. Xu, and W. W. Roberts, "Histotripsy fractionation of prostate tissue: local effects and systemic response in a canine model," *The Journal of urology*, vol. 185, no. 4, pp. 1484-1489, 2011.

[37] L. Arnold *et al.*, "Histotripsy Ablation of Bone Tumors: Feasibility Study in Excised Canine Osteosarcoma Tumors," *Ultrasound in Medicine & Biology*, vol. 47, no. 12, pp. 3435-3446, 2021.

[38] T. G. Schuster, J. T. Wei, K. Hendlin, R. Jahnke, and W. W. Roberts, "Histotripsy treatment of benign prostatic enlargement using the Vortx Rx system: initial human safety and efficacy outcomes," *Urology*, vol. 114, pp. 184-187, 2018.

[39] E. Messas *et al.*, "Feasibility and performance of noninvasive ultrasound therapy in patients with severe symptomatic aortic valve stenosis: a first-in-human study," *Circulation*, vol. 143, no. 9, pp. 968-970, 2021.

[40] J. V. Jove, "Phase I study of safety and efficacy of hepatic histotripsy: Preliminary results of first in man experience with robotically-assisted sonic therapy," *International Society of Therapeutic Ultrasound, Barcelona, Spain*, 2019.

[41] V. T. Rathod, "A review of acoustic impedance matching techniques for piezoelectric sensors and transducers," *Sensors,* vol. 20, no. 14, p. 4051, 2020.

[42] T. Gudra and K. J. Opieliński, "Influence of acoustic impedance of multilayer acoustic systems on the transfer function of ultrasonic airborne transducers," *Ultrasonics,* vol. 40, no. 1-8, pp. 457-463, 2002.

[43] T. L. Szabo, "Chapter 5 - Transducers," in *Diagnostic Ultrasound Imaging: Inside Out (Second Edition)*, T. L. Szabo Ed. Boston: Academic Press, 2014, pp. 121-165.

[44] H. Choi and J. S. Popovics, "NDE application of ultrasonic tomography to a full-scale concrete structure," *IEEE transactions on ultrasonics, ferroelectrics, and frequency control,* vol. 62, no. 6, pp. 1076-1085, 2015.

[45] H. Guo *et al.*, "Ultrasound Produces Extensive Brain Activation via a Cochlear Pathway," *Neuron,* vol. 98, no. 5, pp. 1020-1030.e4, 2018/06/06/ 2018, doi: https://doi.org/10.1016/j.neuron.2018.04.036.

[46] A. Burgess and K. Hynynen, "Noninvasive and Targeted Drug Delivery to the Brain Using Focused Ultrasound," *ACS Chemical Neuroscience,* vol. 4, no. 4, pp. 519-526, 2013/04/17 2013, doi: 10.1021/cn300191b.

[47] A. Hendricks-Wenger *et al.*, "Histotripsy Ablation in Preclinical Animal Models of Cancer and Spontaneous Tumors in Veterinary Patients: A Review," *IEEE Transactions on Ultrasonics, Ferroelectrics, and Frequency Control,* vol. 69, no. 1, pp. 5-26, 2022, doi: 10.1109/TUFFC.2021.3110083.

Chapter 2. Modular Prototype Histotripsy Device

2.1 Introduction: Device Description and Parameters

Currently, prototype histotripsy transducer PZT housings and transducer scaffolds are made using additive manufacturing methods, specifically 3D printing with stereolithography (SLA) and selective laser sintering (SLS) [1-3]. SLA is a prototyping method that relies on photo-polymerization to harden a polyether, polyester, or polycarbonate liquid resin [4, 5] layer by layer. SLA maximizes resolution (as fine as 10 μm) over material variety [4] and is used to make the PZT housings for prototype histotripsy transducers. SLS is another 3D printing method that, also layer by layer, uses a laser to heat and fuse powder together; a roller applies the next layer of powder on top of the hardened layer [4, 6]. SLS uses amorphous or semi-crystalline thermoplastic polymers in powder form to create a component, and is a faster manufacturing method than SLA, making it a preferable 3D printing method for large components [4, 6]. Therefore, SLS is often used to make transducer scaffolds for prototype histotripsy systems.

The 3D prototype transducers discussed in this document are modular in style, as shown in **Figure 1-3**. In these systems, individual, focused PZT elements are loaded into a scaffold where the elements and scaffold have the same focus. Element lenses can be made from aluminum [7-9], silicone [10, 11], resin [10, 12], or other plastics [2]. Aluminum has a higher acoustic impedance, giving better matching between the PZT and water than lower acoustic impedance found in plastics [8]. Aluminum lenses are preferred over plastics for smaller, single element devices because a greater acoustic gain can be achieved with a less extreme focus than plastic housings [10]. The element lenses most commonly used for prototype transducers and used in our lab are made using PerFORM or Watershed plastics from Proto Labs (Maple Plain, MN, USA) having focuses of 36 or 75 mm, and the scaffolds are made using PA 12 mineral-filled nylon also from Proto Labs

(Maple Plain, MN, USA). The element housings' materials, as opposed to the scaffold, are the focus of the device sections of this chapter.

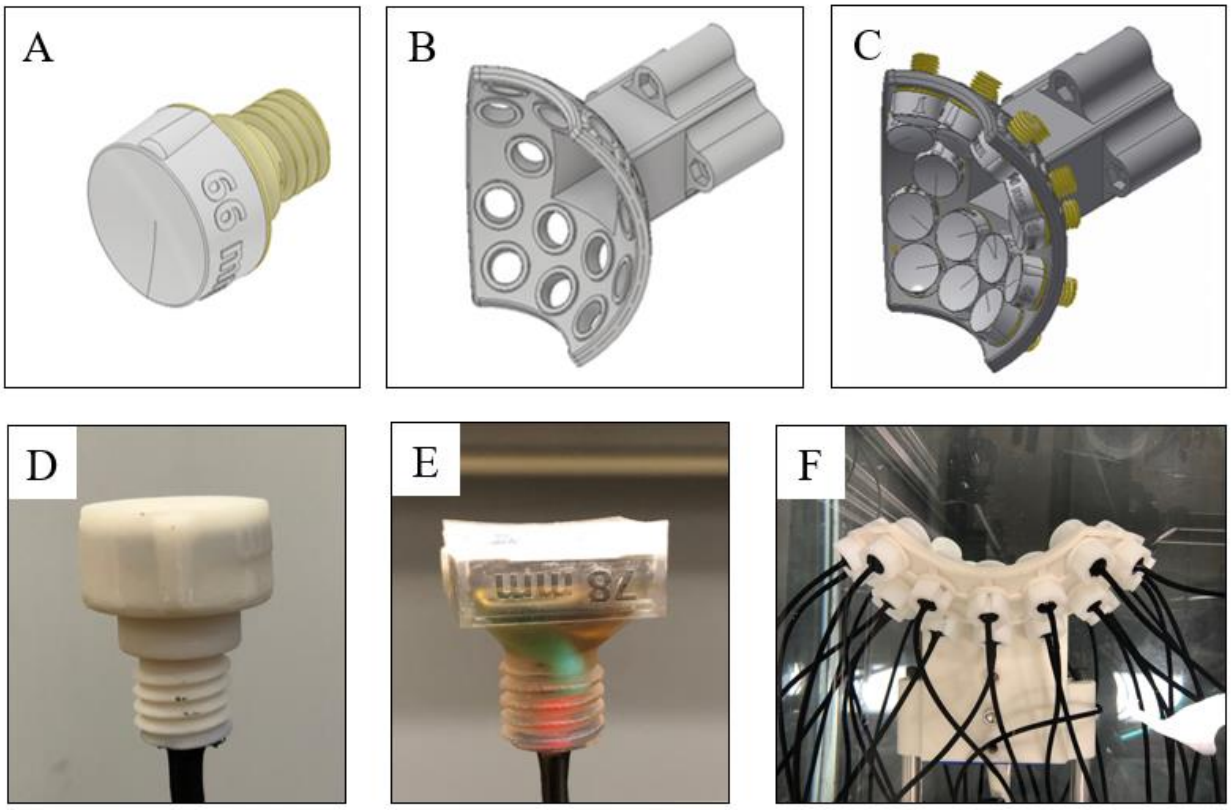

Figure 2-1. Prototype histotripsy transducer examples. (Top) Computer-aided design models of a prototype, histotripsy modular transducer. (A) singular circular element housing with 66 mm focus, (B) empty 16-element scaffold with 66 mm focus, (C) 16 elements loaded into scaffold with 66 mm focus. (Bottom) Life images of transducer components. (D) PZT 36 circular element, 500kHz with 36 mm focus lens made from PerFORM 3D printed plastic (Ceramic-Like Advanced HighTemp PerFORM, Proto Labs, Maple Plain, MN, USA), (E) Sm111 rectangular plate with 78 mm focus lens made from WaterShed plastic (ABS-Like Translucent/Clear WaterShed XC 11122, Proto Labs, Maple Plain, MN, USA), (F) assembled 500 kHz, 32-element histotripsy transducer with 7.8 cm geometric focus.

Several factors are considered when designing a histotripsy transducer. The size, depth, and acoustic window of the target tissue can all factor into choosing the f-number for a histotripsy device. F-number is defined as the ratio of focal distance to aperture diameter [13]. A transducer with a small f-number, < 0.6, is considered to be focused, generating a higher density bubble cloud when compared with less-focused transducers, f-number > 0.6 but < 0.89 [14]. In addition to bubble cloud size considerations, as f-number increases, the pressure wave becomes less linear

[13], requiring more transducer output to achieve cavitation at the focus. Beyond an f-number of 1, acoustic saturation can occur, making it difficult to generate a cavitation bubble cloud at the focus using intrinsic threshold methods [13].

The size of the tissue can determine the most efficient frequency to use for the application. The bubble cloud size is highly dependent on the transducer frequency [15]. A higher frequency will have a smaller bubble cloud and be more precise when treating, while a lower frequency will have a larger cloud [15] which can be more efficient for treating larger tissues. The depth of the tissue impacts consideration for the working distance of the device. The working distance affects the maximum depth at which the transducer can target and is defined as the distance from the most protruding edge of the transducer to the focus of the device. If the transducer has a short working distance, then the transducer may be limited to more superficial applications. Often, there is a tradeoff between the f-number and working distance. As described, the application of the transducer strongly affects how it is designed, and certain parameters are prioritized for most effective treatment. **Figure 2-2** illustrates this point, showing geometry, focal distance, and a focal pressure map for an example array combination.

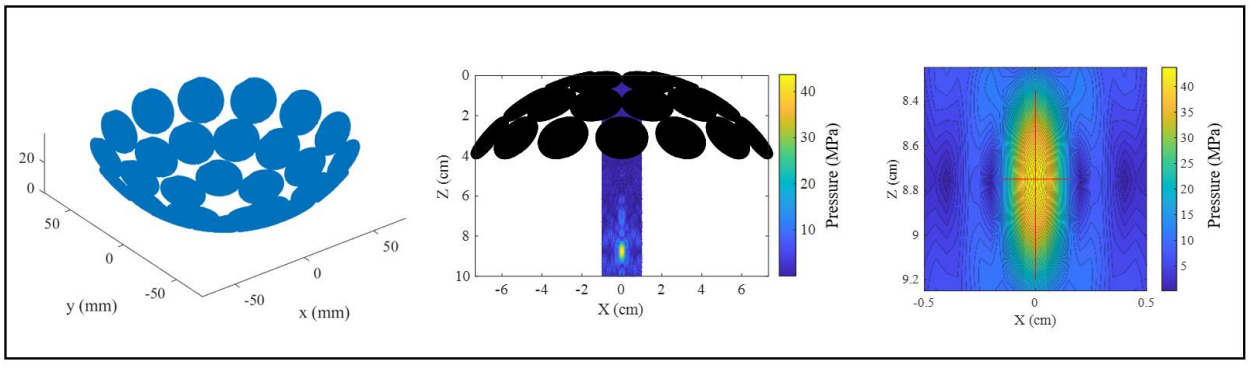

Figure 2-2. Sample 500 kHz transducer array with focal pressures and beam profiles. From left to right, element geometry simulation, pressure color map simulation, and focal pressure map.

In the following sections, the fabrication of a prototype 500kHz histotripsy array transducer developed for large animal histotripsy studies is described (Section 2.2) along with the use of this

device for a series of *in-vivo* studies (Sections 2.3-2.4) testing histotripsy for the treatment of soft tissue sarcoma, osteosarcoma, and pancreatic cancer.

2.2 Methods: Device Fabrication

SLA is the primary prototyping method currently used to fabricate transducer scaffolds and element housings. Starting with a CAD model which is translated into layer by layer printing using computer-aided manufacturing (CAM) software, SLA can be used to create detailed, highly accurate, customizable parts within hours [4, 5]. PerFORM and WaterShed plastics (Proto Labs, Maple Plain, MN, USA) are element housings used for histotripsy prototype transducers made with resolution up to 0.002 in or 0.05 mm (Proto Labs, Maple Plain, MN, USA). These plastic housings are printed as a focused lens, typically 36 mm or 78 mm based on our applications. The scaffold's focus matches the focal point of the lens on each individual element.

Transducer elements are often constructed with a matching layer, depending on the desired power output of the transducer. The matching layer, as shown in **Figure 1-2**, is located between the element housing and PZT. The ideal matching layer acoustic impedance is calculated from the acoustic impedances of the PZT and the element housing. The histotripsy prototype transducers discussed here are made using Pz36 disc piezoelectrics (FerropermPz36 low acoustic impedance PZT, Meggitt A/S, Meggitt PLC Energy & Equipment, Coventry, United Kingdom) or SM111 plate piezoelectrics (STEMiNC, Miami, Florida, USA). Pz36 discs have an acoustic impedance of 14 MRayl, and the element housing used for this PZT is made from PerFORM which has a tested acoustic impedance of 5.12 MRayl. As stated in Chapter 1.3, reflection is an indicator of power transmission between materials. The reflection coefficient calculated (*Eq.* 1.2) between the Pz36 and PerFORM material is 46%, indicating an energy transmission percentage of 54%. This energy transmission has been determined sufficiently high for current histotripsy applications [1].

Therefore, this PZT and housing combination does not require a matching layer. The other type of PZTs used are SM111 plates which have an acoustic impedance of 33.5 MRayl. The housing paired with these PZTs is WaterShed which has a tested acoustic impedance of 2.75 MRayl, making the reflection coefficient between this combination 85%, meaning only 15% of the incident pressure wave energy is transmitted. Therefore, a matching layer is used to improve the energy transmission. Based on *Eq.* 1.3, the ideal matching layer impedance between SM111 and WaterShed to improve energy transmission is 9.59 MRayl. The matching layer for the SM111 and WaterShed element was made from an aluminum oxide (Al_2O_3 White #500 Grit Abrasive CAS# 1344-28-1, AGSCO Corporation, Libertyville, IL, USA) and resin (INF-114-2 Infusion Resin Part A, INF-212-2 Infusion Hardener Part B, Pro-Set, Dallas, TX, USA) combination. All elements are backed with epoxy (Marine Epoxy A-side Resin 314, B-side Hardener 143, TAP Plastics, Stockton, CA, USA). The acoustic impedances of the PZTs, housing material, and traditional matching layer used is summarized in **Table 2-1**.

Table 2-1. Piezoelectric, housing material, and matching layer densities and acoustic impedances.

Type	Material	Density (g/cm^3)	Acoustic Impedance (MRayl)
PZT[1]	Pz36	6.00	14.0
PZT[2]	SM111	7.90	33.5
Housing[3]	PerFORM	1.61	5.12
Housing[4]	WaterShed	1.12	2.75
Matching Layer[5]	Al_2O_3	2.29	6.82

1 – data sheet FerropermPz36 low acoustic impedance PZT from Meggitt A/S, Meggitt PLC Energy & Equipment, Coventry, United Kingdom
2 – data sheet SM111 from STEMiNC, Miami, Florida, USA
3 – data sheet Ceramic-Like (Advanced HighTemp PerFORM) from Proto Labs, Maple Plain, MN, USA
4 – data sheet ABS-Like Translucent/Clear (WaterShed XC 11122) from Proto Labs, Maple Plain, MN, USA
5 - Aluminum oxide calculations from in-lab testing

2.3 Methods: Device *In Vivo* Studies

The methods for using a prototype histotripsy transducer in clinical settings are still being developed and optimized for multiple different clinical applications. In the current state and in the following studies, this process follows **Figure 2-3**. All studies detailed in this chapter were conducted at the Virginia-Maryland College of Veterinary Medicine under IACUC approved protocols. A 500 kHz, 32-element device with a geometric focus of 7.8 cm and a working distance of 3.7 cm is used for these studies.

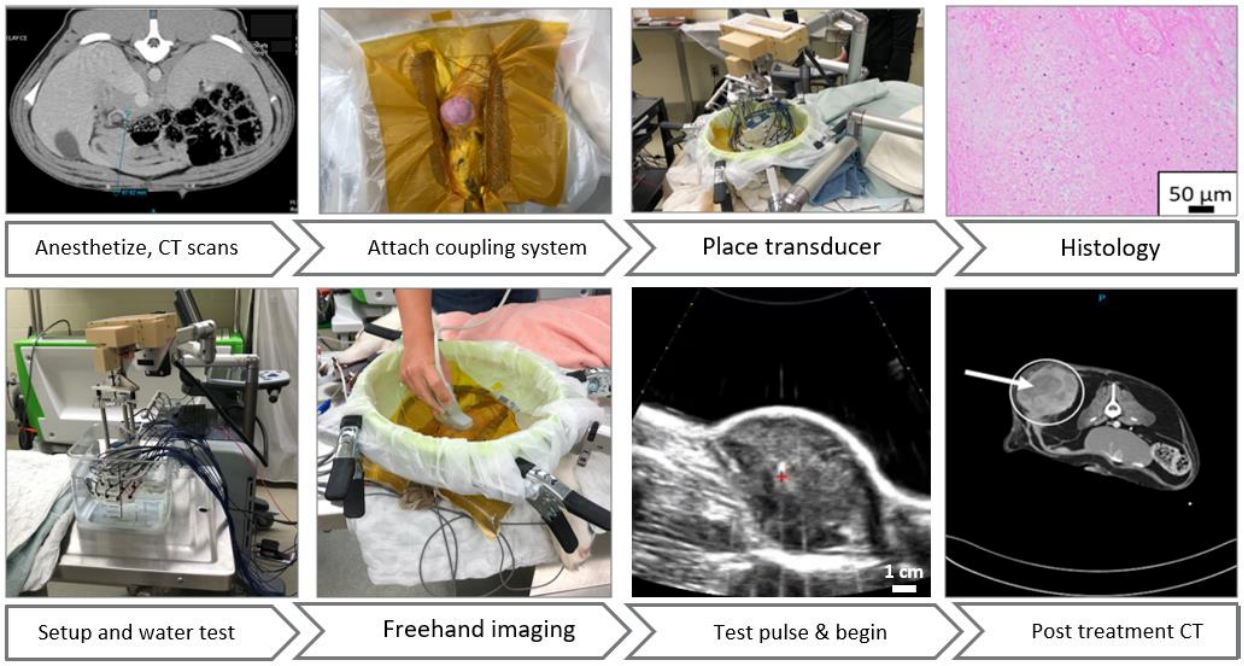

Figure 2-3. Current clinical process using prototype histotripsy transducer. Images are in line with caption arrows, read left to right. CT scans are not of the same patient. From left to right, clinical cart setup and transducer testing in parallel with anesthetizing patient and obtaining CT scans. The coupling drape is attached to the shaved skin of the patient then the acoustic window is determined through freehand imaging. The transducer is placed over the patient and a test pulse is initiated. The treatment ensues and is followed with assessment of ablation through CT, surgery, histology, and/or necropsy.

Prior to treatment, a water test, where the transducer is fired in open water, is run to check the entire treatment system for appropriate acoustic firing. Following an initial CT scan that is used for treatment planning, the patient is anesthetized, and the treatment area is removed of hair in order to allow acoustic transmission through the skin. A coupling system is used to fill the space

between the transducer and patient with degassed water since ultrasound waves require a propagation medium for effective treatment. Freehand imaging can be utilized throughout the pre- or post-treatment process to ensure correct placement of the transducer relative to the target tissue and inspect the target tissue following treatment. Then, the therapy transducer is placed manually over the treatment region by adjusting the articulating arm. An electronic micro-positioning system attached to the transducer can be used to finely move the transducer to the desired acoustic window for treatment. An ultrasound imaging probe coaxially aligned with the transducer is used for real-time guidance during this process as well as live imaging of the treatment. Next, a test pulse is applied in which the pressure is slowly increased until a bubble cloud is generated and maintained in the tissue. This test pulse identifies the cavitation threshold needed for the treatment tissue [16, 17]. Appropriate treatment volume, shape, and location is determined and treatment begins, initiated by the clinical cart user.

The clinical cart, transducer, and electrical components used for the clinical studies in this chapter are illustrated in **Figure 2-4**. The transducer used in these studies is a 500 kHz, 32-element transducer with an f-number of 0.70 in the elevational and 0.61 in the transverse directions, an aperture size of 112 mm in the elevational and 128 mm in the transverse directions, a geometric focus of 7.8 cm, and a working distance of 3.7 cm. This transducer is also used in a previous feasibility study [18]. 500 kHz frequency, towards the lower range of histotripsy frequencies, was chosen based on previous research suggesting that, with lower frequencies, bubble size increases. Using this lower frequency would better optimize bubble expansion and bubble lifespan in stiffer tissues such as osteosarcoma tumors [18], and minimize treatment time. A lower frequency will also experience less attenuation when treating deeper tissue. The transducer was integrated with a clinical cart (HistoSonics, Ann Arbor, MI, USA) and was designed to fit an ultrasound probe

(Model C5-2, Analogic Corp., Peabody, MA, USA) coaxially for live imaging during treatment. For all the following *in vivo* studies, the transducer was used to fire 1-2 cycle histotripsy pulses, through the use of a custom high-voltage pulser controlled by a field-programmable gate array (FPGA) board (Altera DE0-Nano Terasic Technology, Dover, DE, USA), at the transducer focus with a pulse repetition frequency (PRF) of 500 Hz. A custom MATLAB script (The MathWorks, Natick, MA, USA) is used to control the treatment parameters by defining inputs such as PRF, elements to fire, and the number of pulses. The treatment and transducer system are powered by a DC power supply (GENH750W, TDK-Lambda, National City, CA, USA).

Before clinical use, the transducer was calibrated in degassed water using a custom-constructed fiber optic hydrophone [19], and beam profiles of the focus were determined using a rod hydrophone. Presented as full-width half-maximum measurements, the beam profiles of the focus are 2.1, 2.1, and 6.6 mm in the transverse, elevational, and axial directions [15]. Waveforms for the transducer were collected with the fiber optic hydrophone up to a negative pressure of 20 MPa, before sustained cavitation could occur at the fiber's tip, damaging the hydrophone. Focal measurements beyond this pressure were estimated by summing individual element pressures [15].

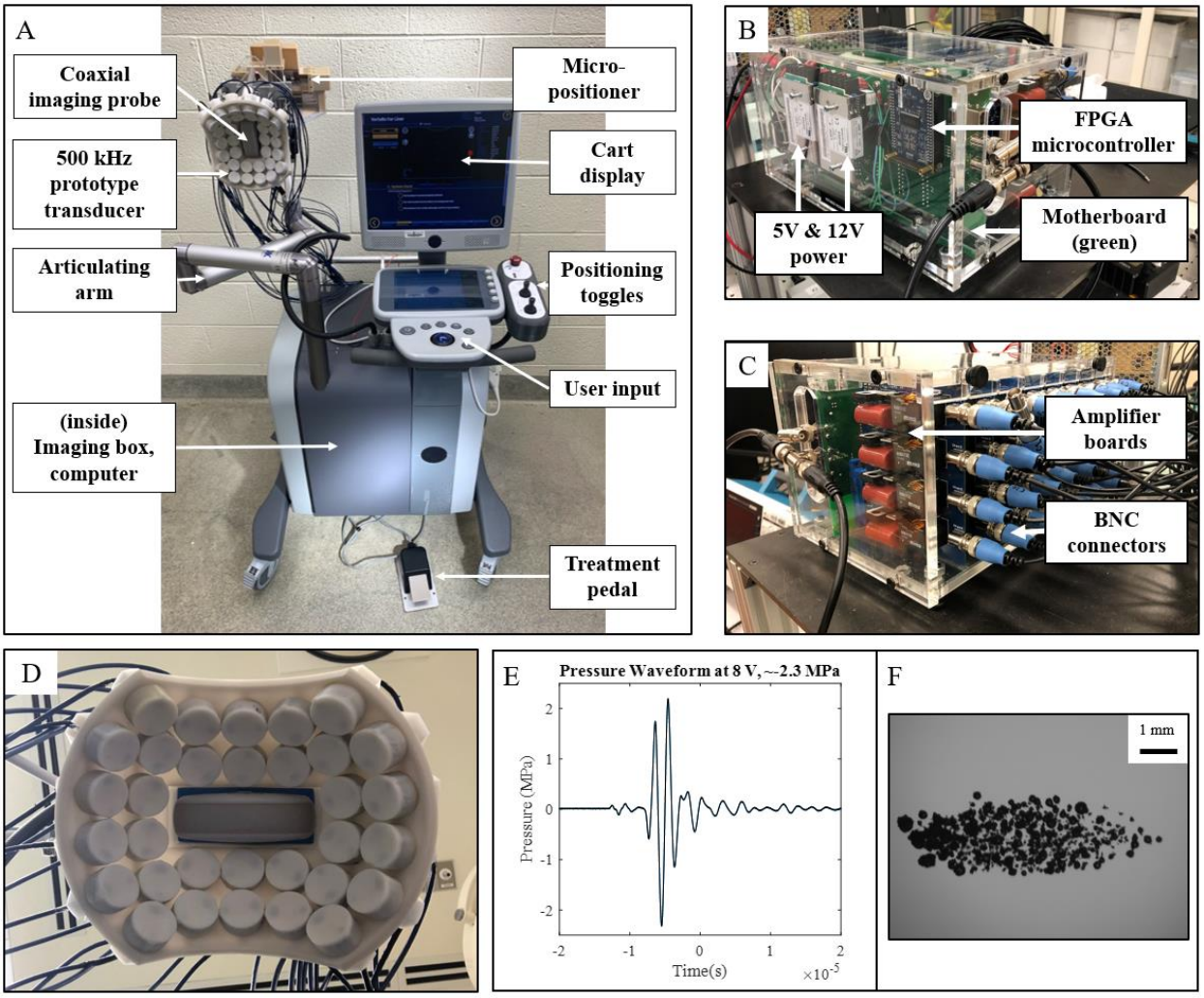

Figure 2-4. Clinical cart and prototype components used in Chapter 2 clinical treatments. (A) clinical cart and labeled components provided by *HistoSonics, Inc.* (Ann Arbor, MI, USA) The cart is outfitted with a prototype histotripsy transducer. (B) Motherboard side of amplifier box constructed in-house. (C) Amplifier side of amplifier box with BNC connections connecting amplifier boards with transducer elements. (D) 500 kHz, 32 element, histotripsy prototype transducer with coaxial imaging probe. (E) Pressure waveform for 500 kHz transducer with peak negative pressure of 2.33 MPa. (F) Sample bubble cloud in agarose gel phantom.

2.3.1 Canine Soft Tissue Sarcoma

Soft tissue sarcoma (STS) is a spontaneously occurring cancer that, while having low potential for metastasis, is locally aggressive and, before this study, had not yet been treated *in vivo* with histotripsy.

In this study, canine patients (n=10) with STS ≥2 cm in diameter were treated with our transducer. The University Institutional Animal Care and Use Committee (#20-049) and the College of Veterinary Medicine Hospital Board approved this study. **Figure 2-5** shows sample photos of some patient tumors before treatment. As seen in this figure, tumors ranged in size, location, and shape. Each patient was given a CT scan before treatment to visualize the tumor and develop a treatment plan. The tumors were superficial, easily accessible for physical examination and freehand ultrasound imaging. Patients with varying coat consistencies were shaved and removed of hair with a hair removal cream (Nair, Church & Dwight Co., Inc., Ewing, New Jersey, USA) before treatment. The patients were treated for a 2-3 cm diameter spherical volume entirely within the tumor limits where each point was treated for 500 pulses. The points were spaced equally, 3.5 mm apart axially and 1.5 mm laterally and elevationally. This way, the bubble cloud would overlap between locations, fully ablating tissue between treatment points. The patients underwent a post-treatment CT scan 1 day after treatment, the tumors were surgically resected 4-6 days following treatment, and the tumor was harvested to examine ablative results both grossly and microscopically.

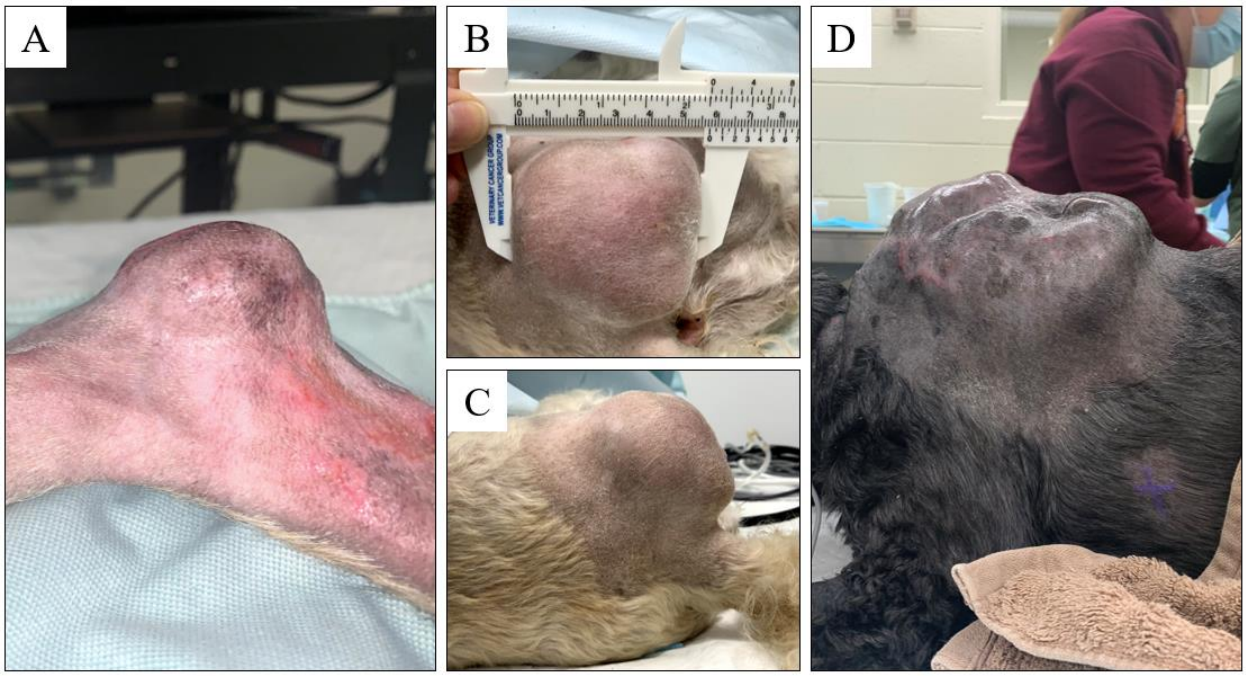

Figure 2-5. Soft tissue sarcoma patient images before treatment. (A) STS on limb of patient. (B and C) STS on right hip of patient, measuring approximately 5.5 cm in diameter. (D) STS on left shoulder.

2.3.2 Canine Osteosarcoma

Osteosarcoma (OS) is a type of primary bone tumor. OS is commonly treated by limb amputation in dogs which is the current standard of care. Since limited nonsurgical options yet exist for OS, the application of histotripsy was explored for this tumor type.

The feasibility of histotripsy ablation of OS in canines was recently explored *ex vivo* in a previous study [18], where tumor samples were treated with our 500 kHz transducer at 4000 pulses per point. This previous study suggests that histotripsy can ablate OS without causing damage to critical structures or overlying tissue. In the current study, canine patients with bone tumors (n=20) were treated with our transducer. This clinical trial was approved through the Virginia Tech Institutional Animal Care and Use Committee protocol (#19-229). **Figure 2-6** shows sample images of the varying bone tumors treated during this study. The tumors ranged in size and consisted of various lytic and proliferative components between dogs. The bone tumors were on joints or limbs of the patients. Before treatment, the patients underwent a CT scan to observe the

composition of the tumor and best treatment plan. The patients were anesthetized during treatment and hair on the surface of the treatment location was shaved and removed with a hair removal cream (Nair, Church & Dwight Co., Inc., Ewing, New Jersey, USA). The patients were treated with histotripsy for spheres of 1.25-3 cm in diameter at 500 pulses per treatment point for the first 5 dogs and 1000 pulses per treatment point for following dogs. The treatment points were spaced 3.5 mm axially and 1.5 mm laterally and elevationally, close enough for the bubble cloud to overlap between treatment points for full ablation. A post-treatment CT scan was given 18-24 hours following histotripsy ablation, and, immediately following, the patients underwent standard of care surgery for the affected limb. Following surgery, the tumor was evaluated for histotripsy treatment both grossly and microscopically.

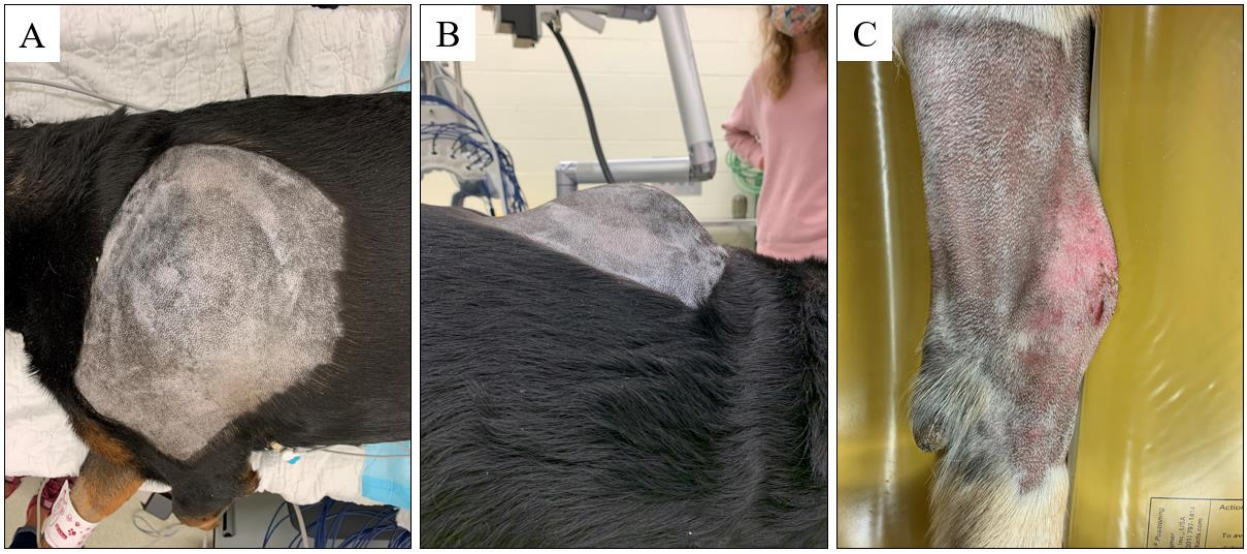

Figure 2-6. Osteosarcoma patient images before treatment. (A and B) The top and side views of the same patient with the tumor on front left shoulder. (C) Tumor is on the front left leg with positioning pads on both sides of the limb for coupling system support.

2.4 Results

2.4.1 Canine Soft Tissue Sarcoma

10 canine patients with STS were treated using our prototype histotripsy transducer and treatment system. Due to the minimally fibrous and superficial nature of these tumors, the canines

were treated with 500 pulses per point with voltage inputs determined by the test pulse corresponding to an average peak negative pressure of 22.60 ± 7.21 MPa. The tumors were ablated with defined margins for target volumes ranging between 2-3 cm in spherical diameter, centered within the tumor. Treatments were conducted between 14 min to 1 hour, based on the size of the treatment volume. In 5 out of 10 of the canines, skin irritation was visible but resolved within 4-6 days of treatment with the exception of one dog. Histotripsy bubble clouds were clearly visualized during real-time ultrasound imaging for 9 out of 10 patients. For this one patient, the tumor was treated through a surgical drape rather than an open acoustic window and cavitation was monitored using passive cavitation detection (PCD) [20]. In post-treatment CT scans, clear ablation zones were seen in 7 out of 10 patients. The 3 patients without clear ablation zones had considerable tissue necrosis in the treated region. **Figure 2-7** illustrates before and after treatment CT scans with untreated and treated histology images the STS tissue, showing characteristic differences between treated and untreated tissue. Complete ablation is characterized by the dark ablated region and necrosis, acellular debris, and hemorrhage in the treated region. Intact, untreated tissue is characterized by the cellular matrix and observable nuclei.

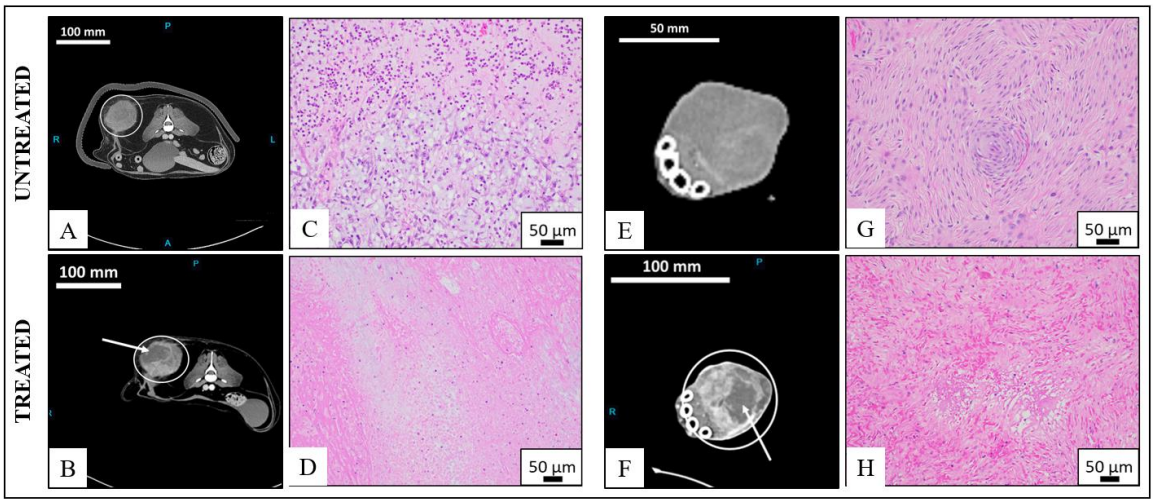

Figure 2-7. Before and after CT scans with treated and untreated histology STS tissue samples. (A-D) from one patient and (E-H) of second patient. Top row: untreated STS tissue with CT scans and histology,

characterized by no clear ablated region and a dense population of tumor cells and intact extracellular matrix (ECM), respectively. Bottom row: treated STS tissue with CT scans and histology characterized by dark ablated region and necrosis, acellular debris, and hemorrhage, respectively.

2.4.2 Canine Osteosarcoma

In this clinical study, dogs with OS (n=20) were treated with histotripsy using our 500 kHz prototype transducer. These bone tumors were generally stiffer in composition than STS and therefore treatment pulses per point were increased from 500 to 1000 after the first 5 dogs. After determining a cavitation threshold, the average peak negative pressure used during treatments was 27.00 ± 5.24 MPa. Ranging from 1.25-3 cm in diameter, spherical volumes of the tumor were treated. Cavitation was not always visible with ultrasound imaging during treatment, although cavitation at the focus was evidenced continually during treatment through PCD monitoring [20]. PCD data also showed occasional prefocal cavitation during treatment of varying severity. The treatments were accomplished in less than an hour. The sizes of the tumors observed on post-treatment CT scans increased by 4.76 ± 5.58 cm^2 cross-sectionally, most likely due to histotripsy-induced swelling. Successful ablation was confirmed through gross examination and histology results, shown in **Figure 2-8**. Tissue heterogeneity is clearly evidenced in histology examples.

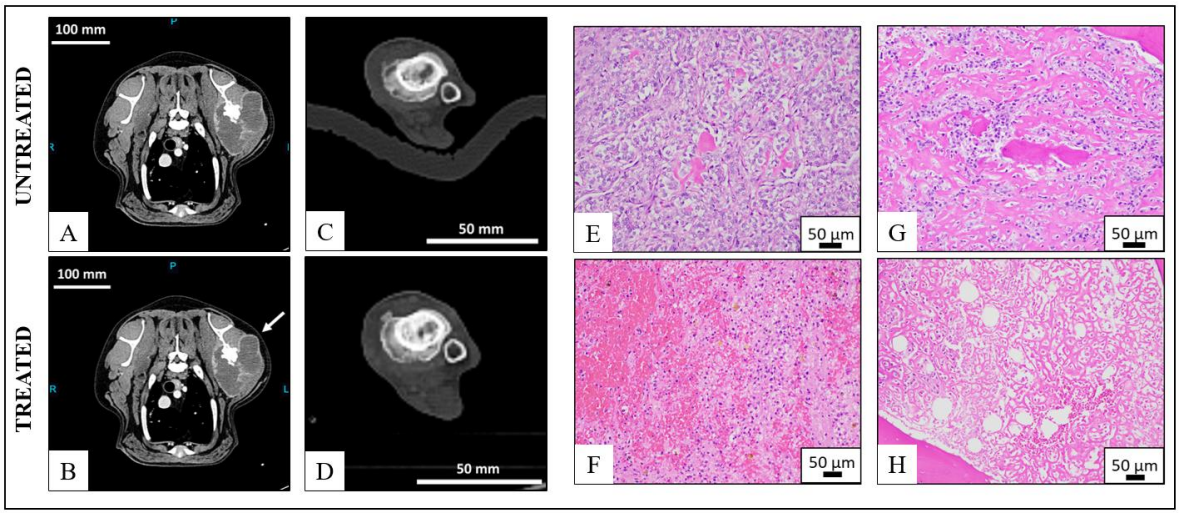

Figure 2-8. Before (top row) and after (bottom row) CT scans with untreated (top row) and treated (bottom row) histology bone tumor tissue samples. (A, B) Before and after CT scans of the same patient, with no

visual change in treatment region. (C, D) Before and after CT scans of the same patient, with slight tumor enlargement post-treatment. (E, F) Treated and untreated histology of the same patient with acellular debris and hemorrhage in treated tissue. (G, H) Treated and untreated histology of the same patient with ablated nuclei but preserved bone structure. White empty spots most likely left from ablated adipocytes.

2.5 Discussion

SLA is an effective prototyping method for developing low-volume, customized histotripsy transducer housings and scaffolds. However, due to the nature of the machining process, SLA is limited to primarily low-molecular weight, minimally viscous resins, that, when cured, are stiff and brittle, making it easy to crack or break the component if dropped [5]. This is the case with the PerFORM SLA material currently used to make the lenses of the Pz36 elements. Although 3D printing is classically considered ideal as a rapid prototyping method, SLA is time consuming, on the order of hours per print, making it less ideal for manufacturing high quantities of identical parts. Another prototyping method should be considered for a broader range of resilient plastic materials, sustainable cost benefits, and speed of production when expanding use and manufacturing of histotripsy devices.

Our prototype 500 kHz histotripsy transducer, made using SLA and SLS methods, was utilized for two *in vivo* studies using clinical veterinary patients: STS and OS in canines. Ablation was evident in the STS tissue, treated at 500 pulses per treatment point and a peak negative pressure average of 22.60 ± 7.21 MPa. Full ablation of the tumors was not completed in these studies due to the large size of these tumors but is hypothesized to be completed in future studies by increasing the target volume or number of treatments. Due to the superficial nature of STS, prefocal cavitation on the skin was observed.

In the bone tumor tissue, mostly OS in this trial, treated at 1000 pulses per treatment point and a peak negative pressure average of 27.00 ± 5.24 MPa, ablation was observed through histological results, although not as clearly seen in CT scans. The composition of OS tissue can

vary throughout the tissue and a singular test pulse in one region of the tissue may not account for heterogeneity throughout the treatment region, resulting in partial ablation. Between patients, the treatment threshold can vary and histotripsy treatment has yet to be optimized across OS. Similar to STS but more frequently, prefocal cavitation can occur during treatment due to the high peak negative pressure. In both STS and OS, prefocal cavitation could possibly be minimized by adjusting the f-number to create a more focused transducer for this application or by increasing the frequency of the elements for superficial targeting. Although STS and OS are superficial, the working distance of the transducer and ability to target deeper tissue should be considered if making these changes due to the unique shapes and locations of these tissues, highly variable from patient to patient.

2.6 Conclusions

Our current 500 kHz histotripsy transducer designed with SLA and SLS prototyping methods is an effective tool for ablating tissue *in vivo*. STS and bone tumors feasible histotripsy applications each requiring inputs specific to the design and programming of the transducer system. The current transducer could be further optimized for these applications by adjusting the f-number, frequency, and working distance of the device. Prototype histotripsy transducers are commonly constructed with PerFORM and WaterShed plastics, sometimes in combination with an Al_2O_3 matching layer. These element housings used for our prototype histotripsy devices, while effective, are expensive and time consuming to print, justifying investigation into an alternative prototyping method while not compromising effective application of histotripsy *in vivo*.

2.7 References

[1] G. E. Stocker, M. Zhang, Z. Xu, and T. L. Hall, "Endocavity Histotripsy for Efficient Tissue Ablation–Transducer Design and Characterization," *IEEE Transactions on*

Ultrasonics, Ferroelectrics, and Frequency Control, vol. 68, no. 9, pp. 2896-2905, 2021, doi: 10.1109/TUFFC.2021.3055138.

[2] Y. Kim, A. D. Maxwell, T. L. Hall, Z. Xu, K. Lin, and C. A. Cain, "Rapid prototyping fabrication of focused ultrasound transducers," *IEEE Transactions on Ultrasonics, Ferroelectrics, and Frequency Control,* vol. 61, no. 9, pp. 1559-1574, 2014, doi: 10.1109/TUFFC.2014.3070.

[3] A. D. Maxwell, K. J. Haworth, C. K. Holland, S. A. Hendley, W. Kreider, and K. B. Bader, "Design and Characterization of an Ultrasound Transducer for Combined Histotripsy-Thrombolytic Therapy," *IEEE Transactions on Ultrasonics, Ferroelectrics, and Frequency Control,* vol. 69, no. 1, pp. 156-165, 2021, doi: 10.1109/TUFFC.2021.3113635.

[4] A. Kafle, E. Luis, R. Silwal, H. M. Pan, P. L. Shrestha, and A. K. Bastola, "3D/4D Printing of Polymers: Fused Deposition Modelling (FDM), Selective Laser Sintering (SLS), and Stereolithography (SLA)," *Polymers,* vol. 13, no. 18, p. 3101, 2021. [Online]. Available: https://www.mdpi.com/2073-4360/13/18/3101.

[5] F. P. W. Melchels, J. Feijen, and D. W. Grijpma, "A review on stereolithography and its applications in biomedical engineering," *Biomaterials,* vol. 31, no. 24, pp. 6121-6130, 2010/08/01/ 2010, doi: https://doi.org/10.1016/j.biomaterials.2010.04.050.

[6] A. Mazzoli, "Selective laser sintering in biomedical engineering," *Medical & biological engineering & computing,* vol. 51, no. 3, pp. 245-256, 2013.

[7] J. K. Woodacre, T. G. Landry, and J. A. Brown, "A low-cost miniature histotripsy transducer for precision tissue ablation," *IEEE transactions on ultrasonics, ferroelectrics, and frequency control,* vol. 65, no. 11, pp. 2131-2140, 2018.

[8] J. K. Woodacre, T. G. Landry, and J. A. Brown, "Fabrication and Characterization of a 5 mm x 5mm Aluminum Lens Based Histotripsy Transducer," *IEEE Transactions on Ultrasonics, Ferroelectrics, and Frequency Control*, 2022.

[9] J. Woodacre, E. Simpson, and J. Brown, "A 5 mm× 5 mm Square, Aluminum Lens Based Histotripsy Transducer: Reaching the Endoscopic Form Factor," in *2018 IEEE International Ultrasonics Symposium (IUS)*, 2018: IEEE, pp. 1-4.

[10] M. G. Mallay, J. K. Woodacre, T. G. Landry, N. A. Campbell, and J. A. Brown, "A Dual-Frequency Lens-Focused Endoscopic Histotripsy Transducer," *IEEE Transactions on Ultrasonics, Ferroelectrics, and Frequency Control*, vol. 68, no. 9, pp. 2906-2916, 2021.

[11] M. Mallay, T. Landry, J. Woodacre, and J. Brown, "An Endoscopic Tri-Frequency (1 MHz, 5 MHz, 30 MHz) Transducer for Combined Imaging and Therapy," in *2020 IEEE International Ultrasonics Symposium (IUS)*, 2020: IEEE, pp. 1-4.

[12] M. Mallay, J. Woodacre, T. Take, E. Napier, S. Gorgey, and J. Brown, "A Miniature 16-element Endoscopic Histotripsy Transducer with Electronically Steerable Focus," in *2019 IEEE International Ultrasonics Symposium (IUS)*, 2019: IEEE, pp. 1797-1800.

[13] K. B. Bader, E. Vlaisavljevich, and A. D. Maxwell, "For Whom the Bubble Grows: Physical Principles of Bubble Nucleation and Dynamics in Histotripsy Ultrasound Therapy," *Ultrasound in Medicine & Biology*, vol. 45, no. 5, pp. 1056-1080, 2019/05/01/ 2019, doi: https://doi.org/10.1016/j.ultrasmedbio.2018.10.035.

[14] E. Vlaisavljevich, T. Gerhardson, T. Hall, and Z. Xu, "Effects of f-number on the histotripsy intrinsic threshold and cavitation bubble cloud behavior," (in eng), *Phys Med Biol*, vol. 62, no. 4, pp. 1269-1290, 2017, doi: 10.1088/1361-6560/aa54c7.

[15] C. Edsall, E. Ham, H. Holmes, T. L. Hall, and E. Vlaisavljevich, "Effects of frequency on bubble-cloud behavior and ablation efficiency in intrinsic threshold histotripsy," *Physics in Medicine & Biology,* vol. 66, no. 22, p. 225009, 2021.

[16] A. R. Smolock *et al.*, "Robotically assisted sonic therapy as a noninvasive nonthermal ablation modality: proof of concept in a porcine liver model," *Radiology,* vol. 287, no. 2, pp. 485-493, 2018.

[17] E. Vlaisavljevich *et al.,* "Image-guided non-invasive ultrasound liver ablation using histotripsy: feasibility study in an in vivo porcine model," *Ultrasound in medicine & biology,* vol. 39, no. 8, pp. 1398-1409, 2013.

[18] L. Arnold *et al.,* "Histotripsy Ablation of Bone Tumors: Feasibility Study in Excised Canine Osteosarcoma Tumors," *Ultrasound in Medicine & Biology,* vol. 47, no. 12, pp. 3435-3446, 2021.

[19] J. E. Parsons, C. A. Cain, and J. B. Fowlkes, "Cost-effective assembly of a basic fiber-optic hydrophone for measurement of high-amplitude therapeutic ultrasound fields," *The Journal of the Acoustical Society of America,* vol. 119, no. 3, pp. 1432-1440, 2006.

[20] A. D. Maxwell, C. A. Cain, T. L. Hall, J. B. Fowlkes, and Z. Xu, "Probability of Cavitation for Single Ultrasound Pulses Applied to Tissues and Tissue-Mimicking Materials," *Ultrasound in Medicine & Biology,* vol. 39, no. 3, pp. 449-465, 2013/03/01/ 2013, doi: https://doi.org/10.1016/j.ultrasmedbio.2012.09.004.

Chapter 3. Injection Molding and Material Acoustic Testing

3.1 Injection Molding Background

Injection molding (IM) is a manufacturing process used to make plastics with high repeatability and precision. By weight, almost a third of plastic components in the world are made using IM [1]. In IM, plastic pellets are loaded into the injection molding machine (IMM) and fed into a heated chamber, often equipped with a turning screw, that melts and pressurizes the plastic [2]. On the other end of the heated barrel, a two or more-part cavity is closed forming a negative space representing the component shape. This cavity is additionally comprised of the gate and runners, which feed the plastic into the component cavity. A valve opens between the pressurized barrel and mold cavity allowing the pressurized melted plastic to flow into the mold where it is held at a holding pressure and allowed to cool. The mold then opens and the hardened plastic part can be removed by hand or with ejector pins. This process is repeated to create identical parts in a matter of seconds. Proper part design, material selection, tool design, and an optimized process are the primary elements that should be considered when making an IM component [3]. The focus of this chapter is on material selection and part design for IM manufacturing for prototype histotripsy transducers, with this work representing the first time IM has been explored for this purpose.

IM can be applied across a range of materials, primarily thermoplastics and thermosets [1, 2]. Examples of thermoplastics include high and low density polyethylene, polystyrene, acrylonitrile butadiene styrene (ABS), acrylics, cellulosics, nylons, polycarbonates, and fluroplastics [2]. Examples of thermosets include reinforced plastics, urethane foam, phenolic or resins, polyester, and epoxy [2]. Some materials, such as nylons, acrylics, and polycarbonates, require drying before injection [2]. Without proper drying before use, water absorbed by the plastic can react during

plasticizing, reducing the molecular weight which affects the physical properties of the material [2]. This moisture can also affect the manufacturing process, turning into steam and contributing to the formation of air bubbles in the injected components. To dry, the plastic is heated in a convection oven for multiple hours at a temperature typically around 80°C. Two crucial material properties to consider in IM are melting temperature and melt flow index or rate (MFR) which is an indicator of the material's viscosity [2]. A low MFR indicates a highly viscous material that will require high forces to inject which could be beyond a machine's capabilities.

3.2 Methods

3.2.1 Injection Molding Design and Inputs

The table-top size, relatively inexpensive APSX-PIM Plastic Injection Molding Machine (Advanced Production Systems LLC., Blue Ash, OH, USA) pictured in **Figure 3-1** (B) and (C) is the injection machine used by our lab to explore the possibility of creating prototype injection molded transducer components. This machine has a footprint of 4x1 ft^2 with a maximum injection mold size of 4.8x6x2 in^3, maximum injection temperature of 315°C (599°F), and maximum injection pressure of 345 bar. Full IMM specifications for the APSX-PIM can be found in Appendix A. A new mold takes approximately 15 minutes to install, and each injection run is a minute or less in length depending on pre-set cooling times. This machine can be used for cyclic running, designed to include ejector pins if desired, or individual part runs where the user removes the part from the mold following each run. This machine has the capability to be run with 3D printed molds made with *Formlabs* High Temp V2 resin (Somerville, MA, USA) for materials with processing temperatures less than 238°C, making it an ideal IMM for prototyping and mold design experimentation, particularly in an academic laboratory setting. See Appendix B for more detail on 3D printed molds.

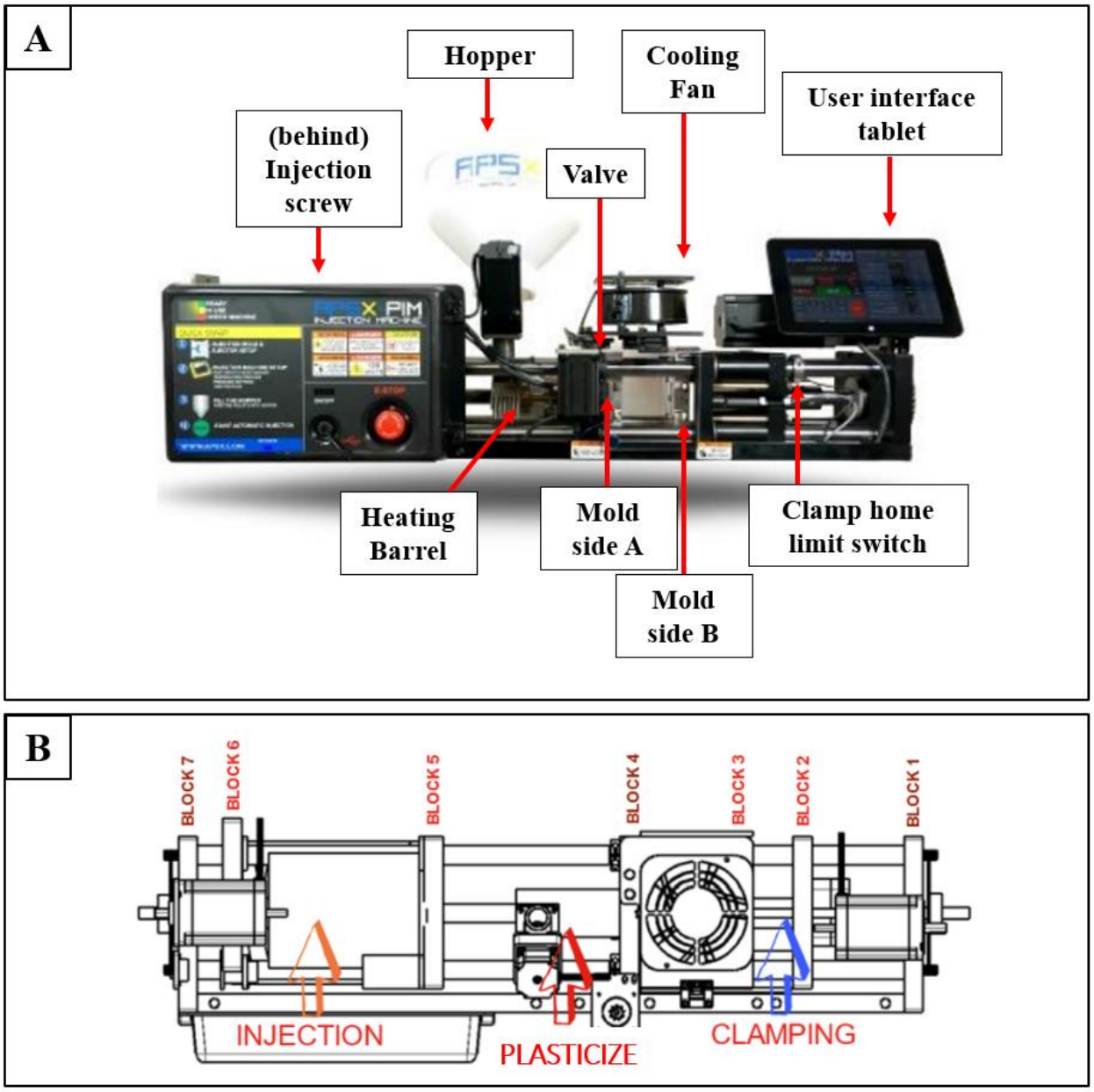

Figure 3-1. APSX-PIM Plastic Injection Molding Machine (APSX LLC., Blue Ash, OH, USA). (A) Front view of APSX-PIM with labeled important components. (B) Top view of APSX-PIM with labeled regions for primary injection steps: injection, plasticize, and clamping.

Figure 3-2 describes the injection molding process for our machine. First, we design a CAD model of the desired part and derive the mold for that part. The CAD file is used to 3D print a resin mold or machine a two-part aluminum mold with a cavity for the component. The two parts of this mold are referred to as sides A and B where side A has a central hole for the sprue, or injection

opening of the mold that allows melted plastic to enter. The molds are mounted on the machine and aligned, a process that takes 15-30 minutes on our machine. The plastic material, which has been pre-dried for multiple hours, is loaded into the machine and appropriate parameters are set. Pressure builds in the barrel until it reaches and maintains a set injection pressure. A valve opens and plastic is injected into the mold. The part cools and is ejected as the mold opens. This injection process, which takes less than a minute, is repeated for multiple parts, and parameters can be adjusted to determine ideal injection inputs.

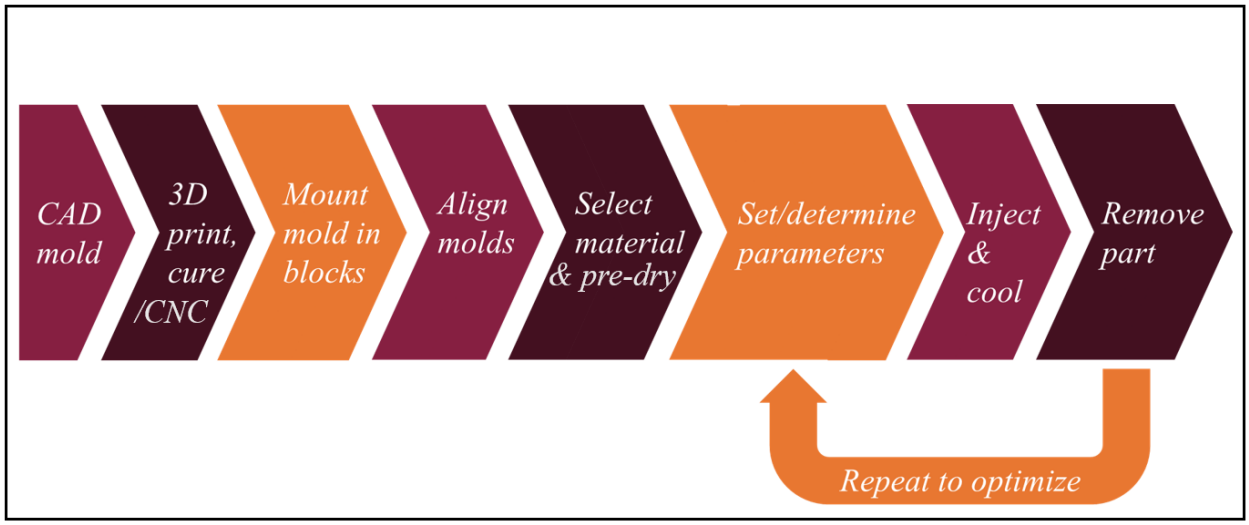

Figure 3-2. Graphic for our injection molding process. The molds are designed using CAD, machined or printed, then mounted and aligned. The selected material is pre-dried and loaded into the machine. Appropriate parameters are set and the plastic is injected. The process is repeated for optimization.

Figure 3-1 (A) points out key components of the APSX-PIM. The hopper is where the pre-dried plastic is loaded into the IMM. The heated barrel melts the plastic. The mold cooling fan is placed on top of the machine as a safety precaution and way to cool the molds. Sides A and B of the mold close while pressure builds in the barrel via the injection screw and the closed injection valve. This valve opens to release melted plastic into the closed mold. The injection barrel also holds the plastic at a set holding pressure once injected. The clamp home limit switch is used to stop the side B mold when homing and can be adjusted based on the mold design and length of

ejector pins. **Figure 3-1** (B) provides a top view and divides the machine into primary function regions of injection, plasticizing or melting, and clamping.

Injection molding inputs must be optimized for each material. These inputs interact with one another and vary across materials. Finding the ideal injection molding inputs can be a complicated process and, while documented for many materials, can vary between IMMs. Artificial intelligence has been recently explored as a tool to control and determine the ideal injection inputs [4], however, the machine used in this document is operated based on trial and error. The APSX-PIM user interface (**Figure 3-3**) allows for IM inputs to be adjusted to achieve best results. The barrel temperature is set to the material's processing temperature, often provided in the material specification sheet. The mold temperature is used to control the fan, turning it on if the measured mold temperature exceeds the set mold temperature. Minimum barrel temperature maintains a lower boundary for the heated barrel. The injection pressure, also commonly called the first stage pressure, is a crucial input adjusted between materials based primarily on the materials' viscosities, torturous mold path, mold opening, and part detail. Up to 95% of the mold capacity is injected at injection pressure, with the remaining 5-10% of the cavity filled at holding pressure. The clamp force is the force at which sides A and B of the mold are held together during injection. The holding time is the time for which the material is held under holding pressure before the valve is shut and pressure is removed from the plastic in the mold. The part then cools for a time set by the cooling time. Heater boost is utilized for multiple run mode on the machine when the barrel temperature drops below the minimum barrel temperature. Clamp time is the amount of time given for side B of the mold to move and clamp to side A. If this is set too low, then the mold will not close, allowing plastic to flow into the open gap between molds. The cut off amount is a safety measure indicating the maximum amount of plastic that the machine would inject per run. The first stage

amount is set to 90-95% of the mold cavity volume and is the volume of plastic injected at injection pressure. Valve fill position, ranging from 0 to 200 degrees, is the amount of rotation that the injection valve turns when permitting plastic to fill the mold. A fully open valve is set to 180 degrees. The hopper multiplier controls how much plastic is allowed to enter the barrel from the hopper following each run. Lastly, the injected amount is observed during the run to determine the amount of plastic injected into the mold each run.

Figure 3-3. APSX-PIM user interface featured on tablet screen (APSX LLC., Blue Ash, OH, USA).

The resulting parts can indicate if these inputs are working congruously and if the mold was correctly designed. **Figure 3-4** shows examples of 2-8 mm thick, 25x25 mm squares injected from various materials that failed because of incorrect inputs. In the first example, mold misalignment combined with too low of a clamp force caused flashing in the part. Too low of a processing temperature resulted in the part prematurely cooling in layers instead of as one homogenous piece.

In the second example, the squares were burned, and while this could be interpreted as too high of a processing temperature, trapped air due to improper venting or the plastic being injected too quickly can also cause burning. In the third example, the component was stuck in the mold, which was 3D printed, indicating that the mold was poorly designed without significant enough draft angles and with undercuts [5, 6]. Draft angles allow the part to be removed cleanly, breaking the seal between the part and mold and preventing a negative pressure space which could damage the cooling part. Undercuts are where the injected component fills a space within the mold that prevents the part from being ejected. Undercuts can be avoided by using a core in the mold or changing the location of the parting line between the molds [5, 6]. In the fourth example, the component did not cool properly before the mold separated, resulting in a warped part that was intended to be an 8x25x25 mm^3 square. This can be prevented by increasing the holding and cooling times. Each material has a glass transition temperature where the temperature is cool enough that the plastic begins to solidify [5]. A long enough cooling time allows the plastic to return to this temperature. Lastly, the sixth example in **Figure 3-4** shows bubbling in general purpose polystyrene (GPPS) squares. The large internal bubble can result from trapped moisture due to the material not being properly dried before injection. Surface pimpling, or small bubbles on the surface of the part, can occur as a result of too high of an injection speed. The injection speed is not a parameter that can be controlled on the APSX-PIM but can be adjusted on more sophisticated IMMs. Understanding the adjustable injection parameters, relevant material properties, and mold design is a critical element of the IM manufacturing process.

Example	Diagnosis	Affected Input
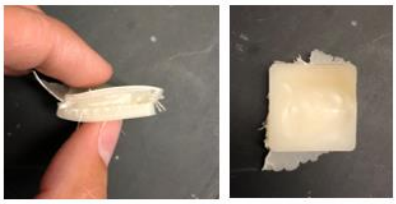	• Warping • Flashing	• Mold alignment • Clamp force • Processing temperature
	• Burning • Flashing	• Venting • Processing temperature • Injection pressure
	• Stuck in mold	• Undercuts • Draft angles
	• Warping	• Holding time • Cooling time
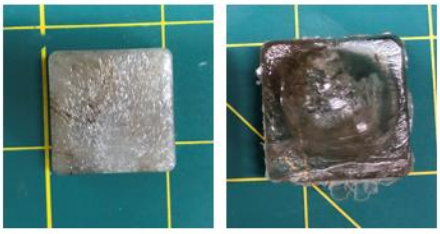	• Surface bubbling and/or air bubbles	• Injection speed • Drying time/temperature

Figure 3-4. Injection molding errors based on incorrect inputs. The top 3 examples are made from polypropylene, 4th example is made from ABS, and 5th example is made from general purpose polystyrene (GPPS).

To investigate injection molded materials for the purpose of prototyping histotripsy devices, sound speed and material acoustic impedance values needed to be quantified. Using our in-house APSX-PIM IM machine, we injected 5 materials: acrylonitrile butadiene styrene or ABS (POLYMAXX 2P100, UL Prospector, Overland Park, KS, USA), general purpose polystyrene or

GPPS (441147 Polystyrene, Millipore Sigma, Burlington, MA, USA), 30% glass-filled nylon (Nylon 6 with 30% glass-fiber filled, Professional Plastics, Fullerton, CA, USA), nylon 6/6 (429171 Nylon 6/6, Millipore Sigma, Burlington, MA, USA), and nylon 101 (Zytel 101L, DuPont, Wilmington, DE, USA). With the exception of ABS, small squares of these materials were made using a custom-designed CAD (Autodesk Inventor Professional 2022, San Rafael, CA, USA) mold that was then machined out of aluminum by Proto Labs (Maple Plain, MN, USA) at a cost of ~$700. This mold is pictured in **Figure 3-5**, and is designed to create two 8x25x25 mm^3 squares at a time. Side A of the mold has a central hole, or sprue where the plastic enters the mold. Runner channels are designed from the sprue to the components, connected by a gate, the term used to describe the plane the plastic flows through where the runner connects to the part cavity. Side B is designed with the majority of the cavity in its surface to avoid requiring backflow into side A which could inhibit part filling. This mold was not designed with draft angles or ejector pins. At the beginning of a set of runs, mold release (CRC 03301 food grade silicone mold release, CRC Industries Americas, Horsham, PA, USA) was sprayed on the mold to minimize part adhesion to the aluminum. ABS was injected into a 3D printed High Temp V2 Proto Labs resin mold designed and printed in-house to test the mold design before machining the aluminum mold. Appendix B gives images of this 3D printed mold, also designed to injected two 8x25x25 mm^3 squares.

Simulations of the fill for the square part were run using Fusion 360's Injection Molding simulation tool (Autodesk Fusion 360 2020, San Rafael, CA, USA). Two simulations were run. One simulation was run for a singular square of generic ABS at an injection temperature of 230°C. The second simulation included the two squares, runners, and gate and was run for nylon 6/6 at an injection temperature of 290°C. These materials were chosen because there were determined to be a fair representation of the range of plastics tested in temperature and density ranges.

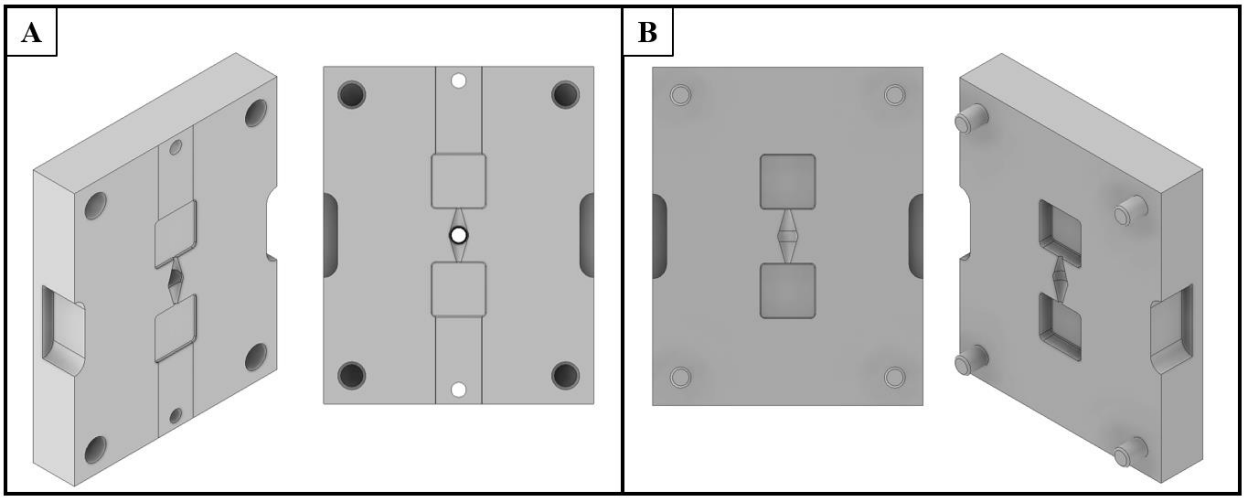

Figure 3-5. 8x25x25 mm^3 square mold design CAD for use in the APSX-PIM. (A) CAD renderings of side A of the mold. Side A has a central sprue hole and small venting channels. The small venting channels were too small to be machined, so stickers were used for venting. (B) CAD rendering of side B of the mold.

Each material was injected on the APSX-PIM with the inputs found in **Table 3-1**. These inputs were determined by trial and error, observing the response of the machine and the output squares. For nylon 101, a PEEK insulator (Mold Insulator (PEEK), Advanced Production Systems LLC., Blue Ash, OH, USA) was used between the injection valve and mold side A to prevent the plastic from cooling too quickly. The insulator was received after nylon 6/6 had been injected, but is recommended for this material too due to the rapid cooling rate of nylon 6/6. Additionally, the venting channels on the mold were too small to be machined by Proto Labs, therefore, stickers were placed on the face of the side B mold to provide a minimal gap for air but no plastic to escape the mold during injection.

Table 3-1. Injection molded inputs for 5 tested materials: ABS, GPPS, 30% glass-filled nylon, nylon 6/6 and nylon 101 on the APSX-PIM.

	****ABS Black**	**GPPS**	**30% glass-filled nylon**	**Nylon 6/6**	**Nylon 101**
Dry Time (hr)	2-5	2-3	4-6	4-6	4-6
Dry Temp (Celsius)	80-85	80	75-80	80-85	80-85
Barrel Temp (Celsius)	235	205	245	265	295
Mold Temp (Celsius)	38	38	38	56	56
Min Barrel Temp (Celsius)	175	200	200	200	200
Inj. P (Bar)	200	300	310	180	110
Hold P (Bar)	100	50	25	135	100
Clamp Force (Kg)	500	1000	2000	2000	1500
Holding Time (mSec)	20000	10000	10000	10000	10000
Cooling Time (mSec)	80000	55000	20000	20000	20000
Heater Boost (Sec)	0	0	0	0	0
Clamp Time (mSec)	12000	12200	12200	*11200	11000
Cut Off Amount (cu-cm)	10.0	12.0	12.0	12.0	12.0
First Stage (cu-cm)	*9.0	7.0	7.0	*9.0	7.0
Valve Fill Position	180	180	180	180	180
Hopper Multiplier	90	*145	*110	80	70

** indicates that these parameters are recommended to be further investigated in future runs*
*** indicates that this material was injected with a 3D printed High Temp V2 mold instead of aluminum mold*

Parameters like the barrel temperature, injection pressure, holding pressure, cooling time and even mold design are impacted by material properties such as melting temperature, density, flexural modulus, and melt flow rate (MFR). The material properties for the injected materials are found in **Table 3-2**. The melting temperature range of a material determines the barrel temperature used during injection and partially determines the cooling time before ejection of the component. Density quantifies the character of a material in simple terms and can impact the final part cost [2]. Flexural modulus, often referred to as Young's modulus, is an indication of material stiffness and directly affects the force needed to inject and hold a plastic in a mold. MFR is a commonly used parameter in IM to describe viscosity of a material [1, 2, 6]. For a standardized set of injection parameters, MFR is defined and measured as the amount of material injected over a period of 10

minutes. Our nylon 6/6 material does not currently have a recorded MFR, therefore this value is omitted. On our IMM, MFR most directly impacts the injection pressure and hold pressure.

Table 3-2. Material properties for specific injection molded materials for materials presented in Section 3.2.1. Our nylon 6/6 does not have a recorded melt flow rate (MFR).

Material	Melting point (Celsius)	Density (g/cm3)	Flexural modulus (MPa)	MFR (g/10min)
ABS	190-240	1.04	2160	18
GPPS	200	1.04	2550	2-4
30% glass-filled nylon	235-282	1.36	7200	4-145
Nylon 6/6	250-260	1.15	1650	-
Nylon 101	262	1.14	2800	115

3.2.2 Acoustic Properties Testing

Following injection, 5 squares of each material, ABS, GPPS, 30% glass-filled nylon, nylon 6/6, and nylon 101, were tested to quantify the materials' acoustic properties: sound speed, impedance, and attenuation. The squares were sanded on the front and back surfaces with various sanding grits (200-600) to ensure a flat face when testing. Testing setup is as shown in **Figure 3-6**. A single 3 MHz transducer element constructed in house was set horizontally in a tank of deionized, degassed water (~26% dissolved O_2). A high-sensitivity rod hydrophone (HNR-0500, Onda Corp., Sunnyvale, CA, USA) was aligned at the focus of the element, 75 mm away for this element. The 8 mm squares were held in a 3D printed PLA holder with their front faces perpendicular to the direction of the ultrasound wave and parallel to the rod hydrophone tip. The back faces of the squares were positioned about 10 mm away from the hydrophone tip, and a mechanical stop **Figure 3-6** (D) was utilized to maintain a consistent distance between the square and hydrophone during testing when removing the holder to repeatedly switch out squares. The material square was positioned centrally with respect to the hydrophone in height and depth. Measurements were taken at 20 V which corresponds to a peak negative pressure of 0.33 MPa.

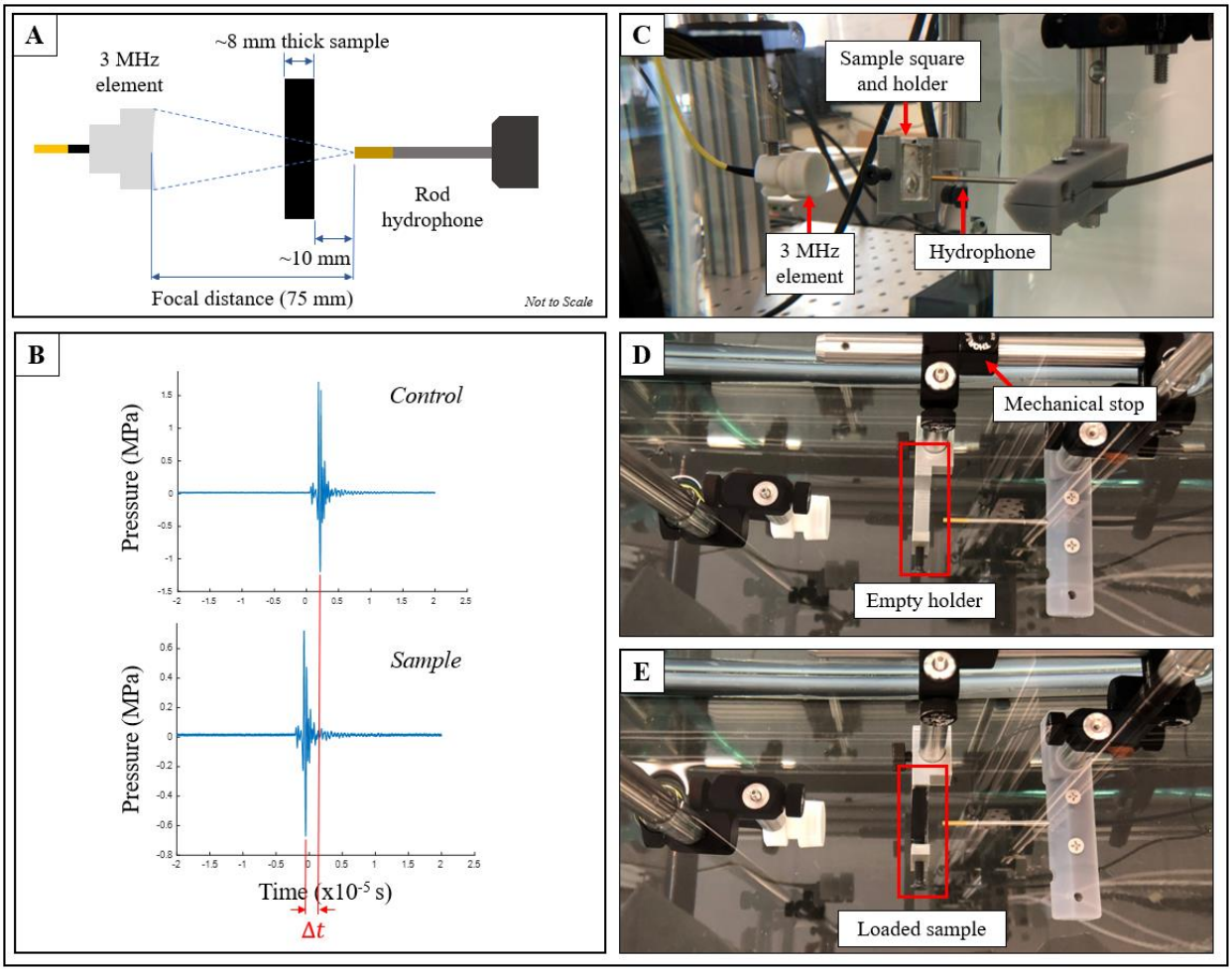

Figure 3-6. Acoustic impedance testing setup with 3 MHz transducer element and rod hydrophone at the element's focus. Sample squares of ABS, GPPS, 30% glass filled nylon, nylon 6/6, nylon 101, PerFORM, and WaterShed were tested, approximately 8 mm in thickness. (A) Schematic of test setup for our scenario with sample positioned about 10 mm from the rod hydrophone tip. (B) MATLAB figures illustrating the time difference used to calculate speed of sound through the sample material. (C) Side view of test setup with material square holder. (D) Control measurement setup with empty holder. (E) Sample measurement setup with occupied holder.

A control waveform created by the element and captured by the hydrophone was measured where the empty holder was positioned between the element and hydrophone. To measure a sample, the waveform was captured with the material square in the holder. As shown in **Figure 3-6** (B), the time difference between these waveforms was assessed to determine the sound speed and acoustic impedance of the injection molded materials. A MATLAB (R2021a, The Math-Works, Natick, MA, USA) function was used to calculate the sound speed and acoustic impedance

for each material and can be found in Appendix C. The function requires inputs of the material squares' densities, exact thicknesses, and waveform data. The waveform peak negative pressure times are compared to the peak negative pressure of the control value and the speed of sound through the material can be calculated according to equations in the methods of reference [7]. Using *Eq.* 1.1 in Section 1.3 of this document, the speed of sound and material density is used to calculate the acoustic impedance of the material.

3.3 Results

3.3.1 Injection Molding Design and Inputs

ABS, GPPS, 30% glass-filled nylon, nylon 6/6, and nylon 101 were injected molded into 8 mm thick, 25x25 mm^2 squares using our custom-made mold on the table-top APSX-PIM. Simulations of the component were run (Fusion 360) and results are presented in **Figure 3-7**. **Figure 3-7** (A) shows results for ABS while (B) shows results for nylon 6/6. The yellow arrows in the figure represent the location where plastic enters the mold. The simulation indicates that, in both cases, the mold easily fills. No visual defects in the form of sink marks are anticipated for either simulation but in simulation (B) weld lines, where plastic meets plastic after partially cooling, could occur at the filleted corners and one edge of the squares. Lastly, the simulations give expected tolerance levels for warpage analysis. A maximum of 0.15 mm warpage could be observed following injection in (A) while up to 0.62 mm warpage could occur in (B). Maximum warpage is observed, as expected, at the locations furthest from the injection location and where plastic will fill the mold last. This warpage, compared to the thickness of the mold and requirements for our part thickness for the purpose of impedance testing, is insignificant.

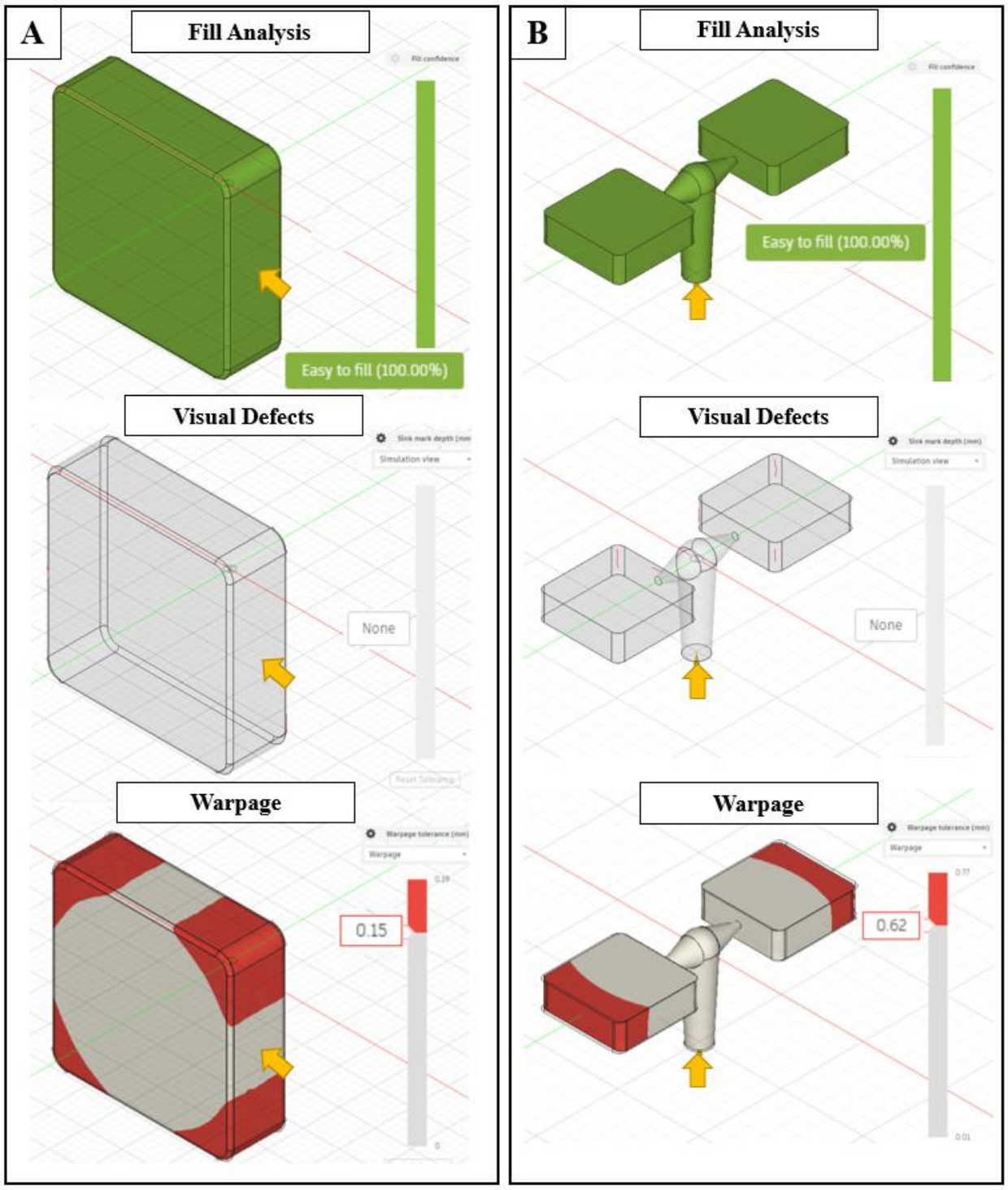

Figure 3-7. Fusion 360 (Autodesk Fusion 360 2020, San Rafael, CA, USA) simulation results of mold fill, visual defects, and warpage for (A) ABS 8x25x25 mm^3 sample square injected at 230°C and (B) nylon 6/6 entire mold cavity injected at 290°C. The yellow arrow indicates the injection location. Pink lines indicated weld lines. Warpage values are in millimeters.

The 5 plastics were injected, and example raw squares are pictured in **Figure 3-8**. Each run cycle took 2.5 minutes or less, with two parts injected per run. Due to the simple part features, the injected plastic could be removed by hand despite the lack of draft angles and ejector pins. Successfully injected squares were measured in the width and length directions as compared to the mold dimensions to assess component shrinkage for each material. Shrinkage data is presented in **Table 3-3**. These values were compared to literature values, or values observed in plastic injection molding industry, as per Reference [8]. The widths and lengths were measured as opposed to the depth because the depths of the squares were sanded to create a flat surface which would affect the measurement results. The widths and lengths were removed of any flashing, but not sanded. ABS experienced the least amount of shrinkage while the nylons experienced the most, up to 3.23%. These experimental values follow the trend found in literature, where nylons have the highest shrinkage.

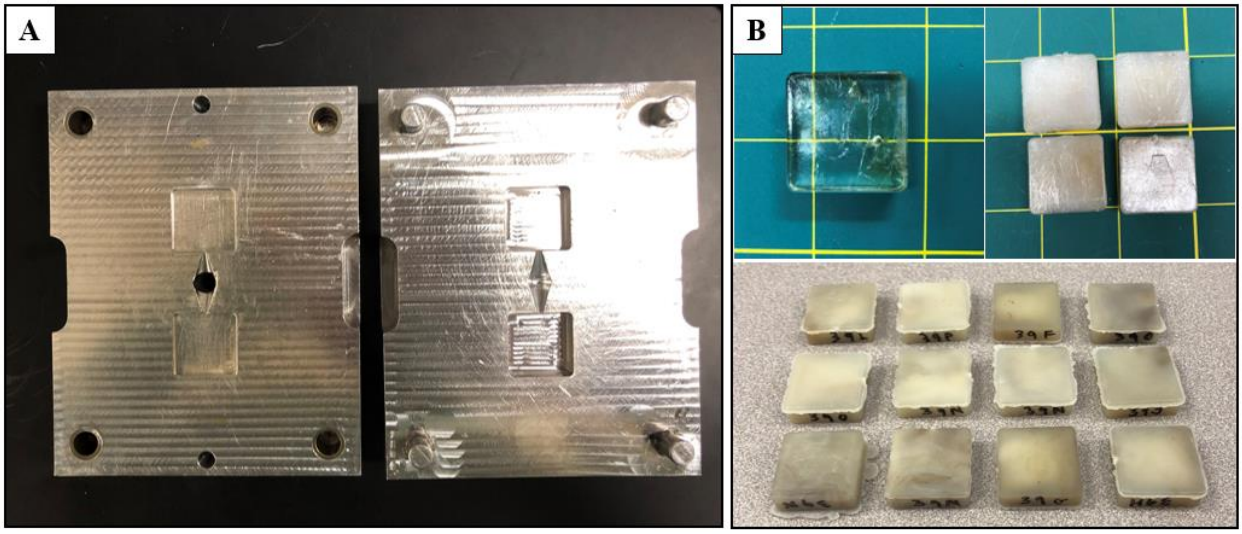

Figure 3-8. 8x25x25 mm^3 squares injected in the APSX-PIM. (A) Life image of the molds, sides A and B. (B) Resultant square samples of GPPS (top left), nylon 101 (top right), and 30% glass-filled nylon (bottom).

Table 3-3. Shrinkage measurements of injected materials compared with literature data from Reference [8]. Data is compared to dimensions of aluminum mold measuring 25.05 mm in width and 25.03 mm in length. Depths were not compared due to sanding affecting this dimension.

Material	Average width measurement (mm)	Average length measurement (mm)	Literature	Experimental
ABS*	24.88	24.92	0.60%	0.40%
GPPS	24.74	24.76	0.60%	1.17%
30% GF Nylon	24.64	24.71	0.40%	1.45%
Nylon 6/6	24.26	24.29	1.50%	3.04%
Nylon 101	24.25	24.22	1.50%	3.23%

**ABS was injected with and therefore compared to 3D printed mold dimensions, 25.19 mm in width and 25.11 mm in length.*

Overall, at least 5 suitable squares of each material were achieved through injection molding on the APSX-PIM using the parameters in **Table 3-1**. During this trial and error process of determining the best IM inputs, some squares were burned or had air bubbles due to reasons listed in **Figure 3-4**. The acoustic impedance values of these samples were tested and compared. The samples were tested at 12.5 V input, correlating to a peak negative pressure of ~0.28 MPa. Samples of burned 30% glass-filled nylon squares with acoustic impedance comparisons are shown in **Figure 3-9**. All samples were tested 3 times each with 5 burned, unsanded samples tested and 3 unburned, unsanded squares tested (limited due to unsanded sample availability). The unburned squares had an acoustic impedance measured to be 3.46 ± 0.07 MRayl while the burned squares had an average acoustic impedance of 3.50 ± 0.03 MRayl.

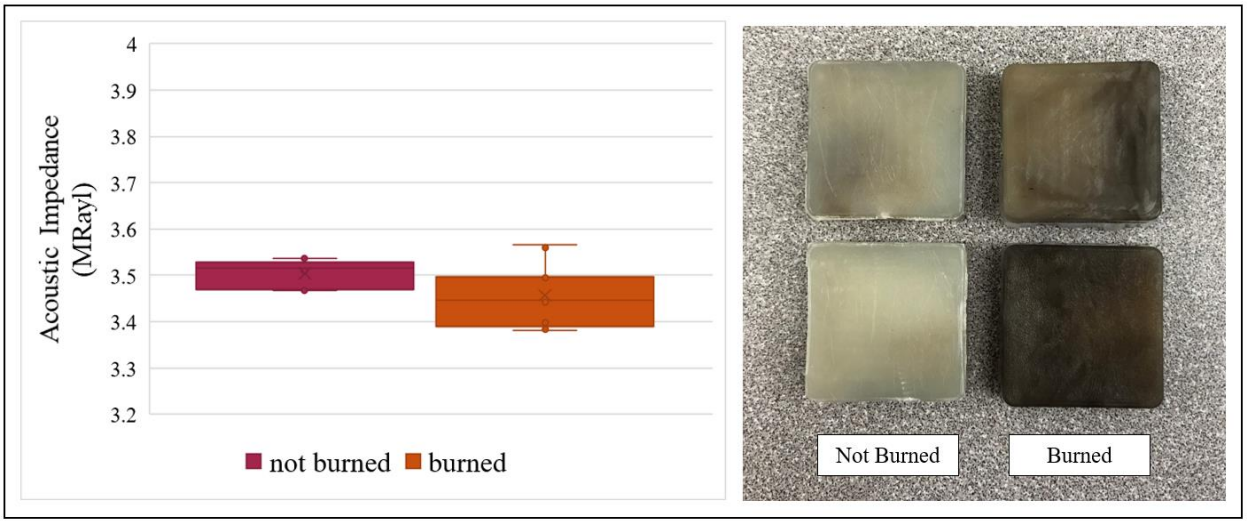

Figure 3-9. Acoustic impedance values comparing burned versus unburned 30% glass-filled nylon samples. All samples were unsanded. 3 unburned samples and 5 burned were tested 3 times each at 12.5V corresponding to a peak negative pressure of ~0.28 MPa. Examples of unburned and burned sample squares are pictured on the right.

Similarly, samples of GPPS with varying air bubble sizes and presence were compared. The results are shown in **Figure 3-10** where bubble severity is rated 1-4 with 1 being less severe, or bubbles occupying a visually-inspected <5% by volume, and 4 being most severe, with bubbles occupying > 30% by volume. Based on these results, bubbling did not seem to affect the acoustic impedance significantly except for a bubble rating of 4, as explained by the figure. For ratings 1-3, the average acoustic impedance of GPPS ranged from 3.39 ± 0.01 MRayl to 2.33 ± 0.03 MRayl. For a bubble rating of 4 the average acoustic impedance was 3.72 ± 1.63 MRayl, a high standard deviation. All samples were tested 3 times each with 5 samples of ratings 1-3 and 3 samples of rating 4 due to sample availability. These bubbles were most likely a result of improper drying of the pellets before injection resulting from moisture trapped as steam in the injection barrel.

Figure 3-10. Bubble comparison of acoustic impedance for GPPS sample squares. 5 squares of each rating 1-3 were tested and 3 samples of rating level 4 were tested 3 times each at 12.5V corresponding to a peak negative pressure of ~0.28 MPa. All samples with a rating of 1 were sanded. Examples of the squares arranged by rating are picture on the right and a table explaining the ratings from 1-4 of least severe bubble occupancy to highest, respectively, is pictured.

3.3.2 Acoustic Impedance Testing

ABS, GPPS, 30% glass-filled nylon, nylon 6/6, and nylon 101 injection molded 8 mm thick, 25x25 mm^2 squares were acoustically tested to determine sound speed and acoustic impedance. In addition to these injection molded materials, equivalently-sized squares of PerFORM and WaterShed were 3D printed and supplied by Proto Labs to be used for acoustic testing. 5 samples of each of the 7 materials were tested. The peak negative pressure waveform shifts were quantified and converted to sound speed and acoustic impedance via our MATLAB code in Appendix C. Sound speed and acoustic impedance results are shown in **Figure 3-11**. Of the IM materials, 30% glass-filled nylon has the highest acoustic impedance, 3.80 ± 0.05 MRayl. Nylon 6/6 and nylon 101 have the next highest impedances, 3.05 ± 0.03 MRayl and 2.96 ± 0.04 MRayl, respectively. GPPS was found to have an acoustic impedance of 2.45 ± <0.01 MRayl, and ABS with an acoustic impedance of 2.32 ± 0.03 MRayl.

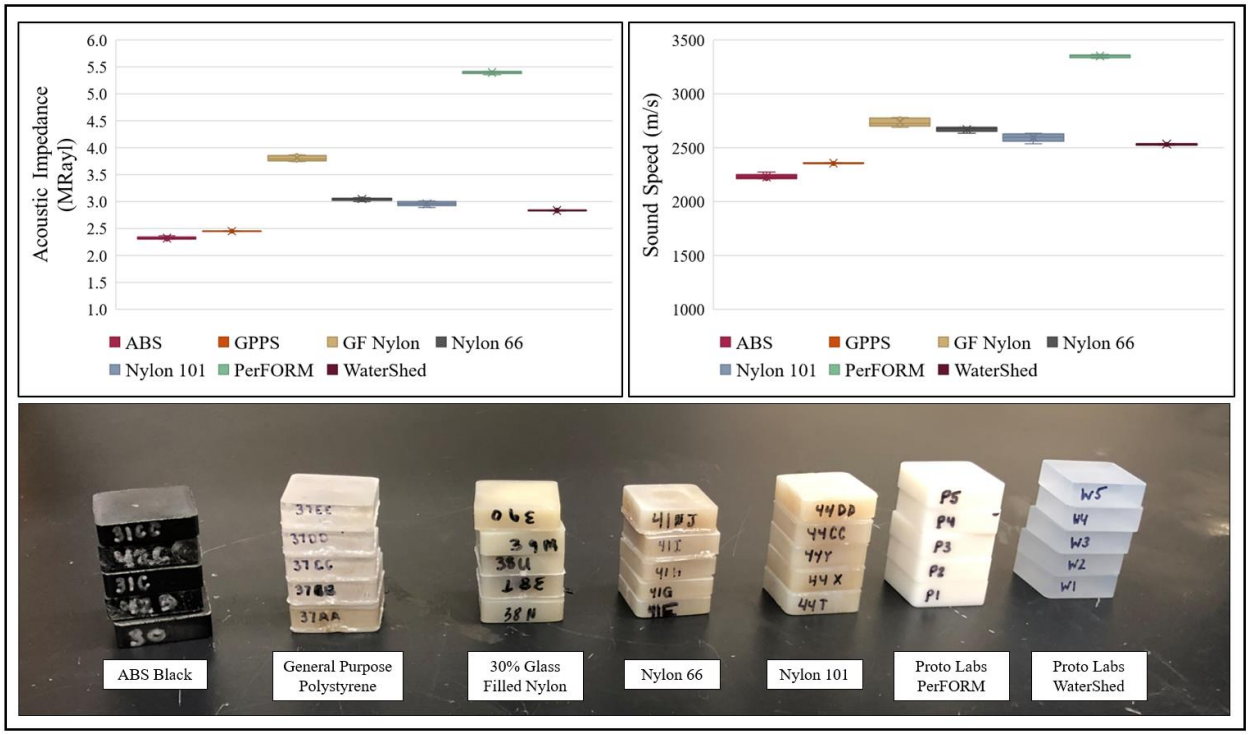

Figure 3-11. Acoustic impedance and sound speed graphed results with images of samples for injection molded ABS Black, GPPS, 30% glass-filled nylon, nylon 6/6, nylon 101 plastics. Additionally, results for Proto Labs 3D printed PerFORM, and WaterShed plastics are shown. 5 smooth or sanded samples of each material type were tested.

Experimental acoustic impedances were compared with anticipated values calculated from material properties specific to each material's data sheet, referred to here as the literature value. This comparison is shown in **Figure 3-12**. The literature value for acoustic impedance is calculated based on the flexural modulus and density, derived from the longitudinal speed of sound in bulk solids from Reference [9] and defined as *Eq.* 3.1

$$Z = \rho\sqrt{\frac{K+\frac{4}{3}G}{\rho}} = \rho\sqrt{\frac{E(1-\nu)}{\rho(1+\nu)(1-2\nu)}} \qquad (Eq.\ 3.1)$$

where ρ is the density of the material, K is the bulk modulus, G is the shear modulus, E is the flexural or Young's modulus, and ν is Poisson's ratio. Data used for density and modulus for these materials is found in **Table 3-2** and references [10-12], with the exception of 3D printed materials which can be found in their respective data sheets (Form Labs, Maple Plain, MN, USA). Based on

this comparison, experimental values were found to be higher than literature values, with the exception of 30% glass-filled nylon, which was slightly lower. Injection molded values differed by 5% (30% glass-filled nylon) to 18% (GPPS) compared to literature values. The experimental values follow the trend found in literature for all sample types measured experimentally.

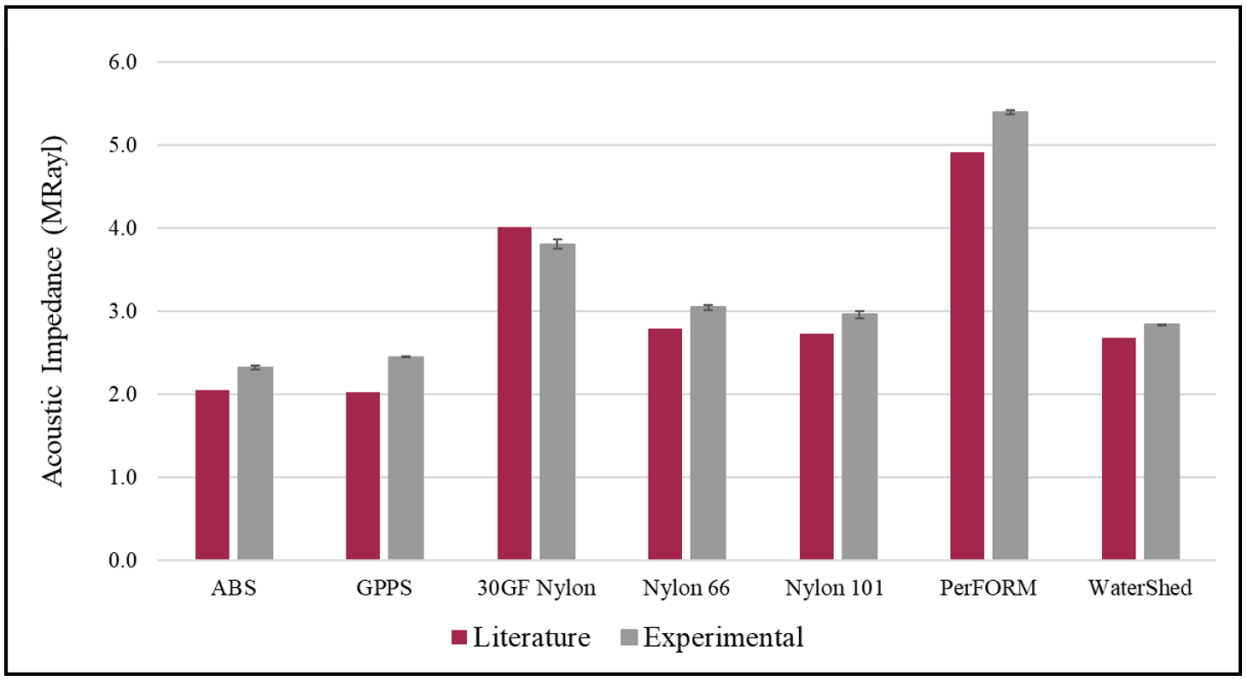

Figure 3-12. Acoustic impedance values comparing literature values with experimental tested values. Literature values based on flexural modulus and density found in each material's specific data sheet and additional references [10-12] when not provided. Acoustic impedance values comparing literature values with experimental tested values. Literature values based on flexural modulus and density found in each material's specific data sheet.

Following testing, GPPS was confirmed to have a MFR outside the capacity of the APSX-PIM and was not further investigated beyond the results presented here due to limited in-house processing capabilities.

Additionally, attenuation of the injection molded materials was assessed at a frequency of 3 MHz. Peak negative pressures of each materials' waveform (n=5) were compared with the amplitude of the control. Attenuation results are presented in **Figure 3-13**. In order of most attenuation to least, GPPS had an acoustic attenuation loss of 7.23 ± 1.15 dB/cm, nylon 6/6 4.30

± 0.76 dB/cm, ABS 3.97 ± 1.32 dB/cm, nylon 101 2.29 ± 1.28 dB/cm, while 30% glass-filled nylon had the lowest, 2.04 ± 0.88 dB/cm. Results for 3D printed PerFORM and WaterShed are included as well, with both 30% glass filled nylon and nylon 101 lower in attenuation. Lower attenuation is preferred for histotripsy transducer applications. 3D printed materials may have less variability in attenuation results due to the smooth surface that was not sanded unlike the IM materials, consistency perfected in a professional 3D printing setting while our IM process is still being developed, or homogeneity compared to the IM squares which likely have varied internal cooling due to high component thickness.

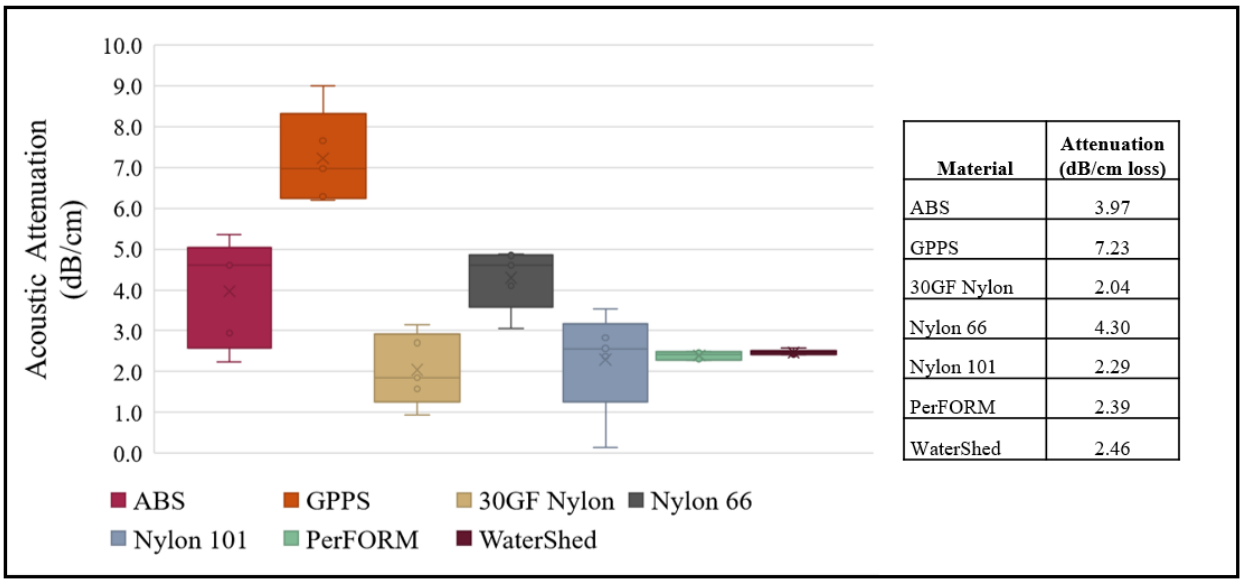

Material	Attenuation (dB/cm loss)
ABS	3.97
GPPS	7.23
30GF Nylon	2.04
Nylon 66	4.30
Nylon 101	2.29
PerFORM	2.39
WaterShed	2.46

Figure 3-13. Attenuation results of various materials determined with 3 MHz transducer element.

To compare our IM process results with industry-produced IM results, we tested ABS (CYCOLAC Resin MG47 – Americas, UL Prospector, Overland Park, KS, USA), GPPS (STYRON 666D, UL Prospector, Overland Park, KS, USA), 30% glass-filled nylon (Durethan BKV130 000000, UL Prospector, Overland Park, KS, USA), and nylon 101 (Zytel 101F NC010, UL Prospector, Overland Park, KS, USA) squares (n=5) injection molded by a commercial IM manufacturer, Total Plastic Solutions (TPS, Lynchburg, VA, USA). The purpose of this was to

eliminate error from our acoustic testing setup and focus on comparing the outputs of a benchtop IMM and industry-standard IMM. The acoustic impedances of the materials injected by TPS were sanded to a flat face and acoustically tested in the same fashion. Instead of 8x25x25 mm^3, the TPS squares were 12.7x76.2x76.2 mm^3 (0.5x3x3 in). A comparison of these samples and our samples is in **Figure 3-14** shows that our IMM produces plastics slightly higher in acoustic impedance than those produced in industry, but the difference is small, <4% for all materials except 30% glass filled nylon which differs by 17%.

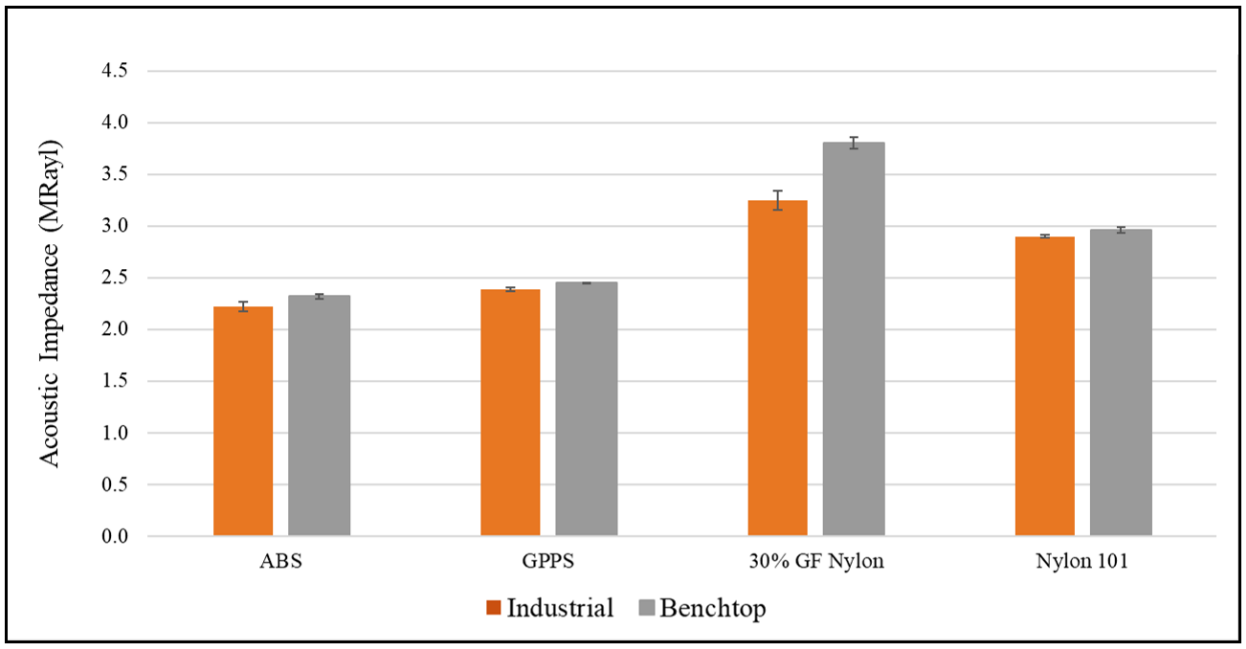

Figure 3-14. Commercially (Total Plastic Solutions, Lynchburg, VA, USA) produced (Industrial) plaque samples acoustic impedances compared to our (Benchtop) material samples for ABS, GPPS, 30% glass-filled nylon, and nylon 101.

3.4 Discussion

IM is a growing manufacturing method for medical devices and pharmaceutical products due to the minimal solubility found in IM as compared to other processes [1], high quality and repeatability of parts, FDA approved materials, and mass manufacturing capabilities in short amounts of time. The goal of this chapter was to investigate injection molding as a feasible

prototyping method for histotripsy transducers and assess injection molded materials' properties for the purpose of transducer element lenses. The materials injection molded and acoustically tested were ABS, GPPS, 30% glass-filled nylon, nylon 6/6, and nylon 101. Although 5 functional samples of each material were formed with our in-house IMM, discovering the inputs for each material required an extensive trial and error process. The APSX-PIM is designed for prototyping and IM feasibility, and while it indeed serves its intended purpose, the exploratory focus can make it difficult to achieve interpretable or consistent results when determining the best inputs for a material. This variability between equivalent runs is not characteristic to IM, and this machine is still being updated and refined by its suppliers as the first of its kind: an at-home benchtop IMM for affordable, simplified IM. Designing a part and mold for IM and discovering the optimized IM inputs can be a steep learning curve, as expected with any unfamiliar equipment. However, with pre-set inputs for each material and a tested mold design, running and monitoring the machine is simple and straightforward. On our IMM, ideal parts can be created with a sufficient number (<3) of runs when these optimized IM inputs are used.

The material shrinkage in our injection molded parts was greater than literature values, but this could be due to the warping occurring at the edges of the part as shown during simulation. Overall, part shrinkage was not observable to the naked eye and did not affect part function. However, for increasingly large components, shrinkage is expected to be observable and the injected material should be considered when generating the mold design. The parts here were easily sanded to account for slight concavity due to the thickness of the samples (8 mm) compared to machine capabilities. This post-processing is anticipated for similarly thick components but is not expected to be the case for element lenses, which are at most 3.1 mm thick through any surface. Component

resolution and consistency for successfully injected components from idealized IM inputs was achieved.

The ideal acoustic impedance for a material for focused ultrasound devices would likely be the geometric mean (*Eq.* 1.3) of the PZT and submerged medium the transducer is used in, degassed water. In this case, with PZTs Pz36 and SM111, the ideal acoustic impedance of a lens would be 4.55 and 7.05 MRayl, respectively. This contributes to why lenses constructed from PerFORM, having an acoustic impedance of 5.12 MRayl, higher than many plastics, is commonly used for prototype histotripsy transducers and especially so with Pz36. While a material with an even higher acoustic impedance would be ideal for best acoustic energy transmission with SM111, utilizing additional matching layers can further enable acoustic wave propagation [13]. For a material's acoustic impedance to be acceptable, the impedance would have to be between the impedance of the submerged medium (water) and PZT. All injection molded materials presented in this chapter have acceptable acoustic impedance values that could likely be used for transducer lenses. However, some materials may be more favorable than others. Based on the acoustic testing results, injection molded 30% glass-filled nylon has the highest acoustic impedance. This indicates that, based on acoustic impedance, 30% glass-filled nylon may be a viable replacement for 3D printed PerFORM and, when paired with Pz36 piezoceramics, may not need a matching layer. When paired with SM111, 30% glass-filled nylon will likely require a matching layer to achieve sufficient peak negative pressures for histotripsy treatment. Nylon 6/6 and nylon 101 are most similar to WaterShed in acoustic impedance indicating that these nylons may be a replacement option for WaterShed. These materials would likely require a matching layer when paired with SM111 to achieve sufficient transducer output. Additionally, nylons are commonly known to be hygroscopic [14], so assessment of water absorption of the injection molded element lenses is

recommended when investigating these materials for histotripsy devices. Although ABS is lower in acoustic impedance than other explored injection molded materials, ABS could be a viable lens housing option when paired with one or multiple matching layers. Idealizing matching layers for optimized acoustic output will require further exploration and testing with element lenses of these materials. When considering acoustic attenuation, 30% glass filled nylon is still a preferred material with an observed low attenuation of -2.04 ± 0.88 dB/cm. This is lower than both PerFORM and WaterShed, indicating that 30% glass-filled nylon may be more suited for transducer lenses than either 3D printed material. According to these results, nylon 101 is the next preferable material with a measured attenuation of 2.29 ± 1.28 dB/cm. GPPS had a surprisingly high observed attenuation, 7.23 ± 1.15 dB/cm. Due to the high variability of molecular weight across polystyrenes, attenuation could decrease in other polystyrene variations. These attenuation results are based only off of 3 MHz data, and additional frequencies should be tested to more extensively characterize attenuation for these injection molded materials.

When compared to literature, the injection molded materials had similar acoustic impedances, different by <18%, indicating that processing minimally affects the material properties related to acoustic impedance and sound speed. This difference was fairly consistent which could indicate a need to refine the testing setup. To assess our impedance results apart from experimental error that could be introduced from the testing setup, we compared our in-house IMM and materials to similar materials injected on an industry-standard machine. Results indicated that the material properties obtained on our benchtop IMM versus an industry-standard machine are different by <4%, with the exception of 30% glass filled nylon which differed by 17%. The difference in these measurements is not considered extreme.

IM offers the exploration of additional materials for transducer housings. Reinforced plastics like the 30% glass-filled nylon presented here, polyether ether ketone (PEEK), polyethylene terephthalate (PET), polyamide-imide (PAI), or other polystyrenes (PS) offer higher flexural modulus values that would likely correlate to higher acoustic impedances. However, additionally investigated plastics and plastic composites must still have processing temperatures and melt flow rates conducive to IM, within the specifications of the utilized IMM.

3.5 Conclusions and Future Work

Based on the investigation presented in this chapter, 30% glass-filled nylon is the most favorable replacement for PerFORM for prototype histotripsy transducers (out of the materials tested in this study) due to its high acoustic impedance, 3.80 ± 0.05 MRayl and low attenuation, -2.04 ± 0.88 dB/cm. Nylon 6/6 and nylon 101 have acoustic impedances similar to WaterShed, 3.05 ± 0.03 and 2.96 ± 0.04 MRayl, respectively, and nylon 101 has a lower attenuation, making it further preferable for a transducer lens. However, further investigation of water solubility is recommended for all plastics and especially nylons. ABS, with exploration into an idealized matching layer, could also be used to create a functioning transducer lens since it has a lower acoustic impedance of 2.32 ± 0.03 MRayl. IM on our in-house table-top IMM, when compared to literature, seems to produce materials with similar acoustic impedances, with an average difference of 0.23 ± 0.22 MRayl between experimental and literature values. Additional testing for delamination after hours of use, ease of resin and backing adherence during construction, and water absorption rate for all potential materials is recommended for future exploration. Materials with high modulus values but sufficiently low processing temperatures and melt flow rates based on IMM specifications could also be investigated for IM transducer applications.

Further refinement of IM inputs for the APSX-PIM is needed in future testing, with suggestions of particular values to refine shown in **Table 3-1**. Although the trial and error process for determining IM inputs can be tedious and designing a proper mold can be a sharp learning curve, once inputs are determined for a material and the mold is tested and installed, operation and production of components is rapid and simple. Initial investment costs for a mold can be high, however, a mold can produce hundreds or thousands of parts without needing to be replaced. Even complicated, highly detailed parts can require little-to-no post processing apart from the removal of gates and runners [2]. Especially when compared to 3D printing which has little to no depreciation in expense per part and long manufacturing times, IM is a promising production method for histotripsy transducers that has been shown to create consistent, detailed components in seconds or minutes out of materials with comparable acoustic properties.

3.6 References

[1] P. H. Kauffer, *Injection molding : process, design, and applications*, New York: Nova Science Publishers, 2011.

[2] I. I. Rubin, *Injection molding : theory and practice / [by] Irvin I. Rubin* (SPE monographs., no. Accessed from https://nla.gov.au/nla.cat-vn1865067). New York: Wiley, 1973.

[3] S. Rangarajan, "Injection Molding Variables," *POPULAR PLASTICS AND PACKAGING,* vol. 55, no. 7, pp. 55-55, 2010.

[4] O. Ogorodnyk and K. Martinsen, "Monitoring and control for thermoplastics injection molding a review," *Procedia Cirp,* vol. 67, pp. 380-385, 2018.

[5] M. P. J. W. Groover and Sons, *Fundamentals of modern manufacturing : materials, processes, and systems*. Hoboken, NJ: John Wiley & Sons (in English), 2010.

[6] *General Design Principles for DuPont Engineering Polymers*. (2000). DuPont Engineering Polymers Design Guide - Module I. DuPont. [Online]. Available: https://www.dupont.com/content/dam/dupont/amer/us/en/mobility-materials/public/documents/en/General%20Design%20Principles%20for%20Engineering%20Polymers.pdf

[7] P. Rossman, J. Zagzebski, C. Mesina, J. Sorenson, and R. Mazess, "Comparison of speed of sound and ultrasound attenuation in the os calcis to bone density of the radius, femur and lumbar spine," *Clinical physics and physiological measurement,* vol. 10, no. 4, p. 353, 1989.

[8] "Plastics Shrinkage Rate & Mold Shrinkage Rate." Intertech Taiwan. https://www.taiwanmoldmaker.com/solution/plastics-shrinkage-rate-mold-shrinkage-rate (accessed March 31, 2022, 2022).

[9] T. Irvine, "Formulas for Calculating the Speed of Sound," *Retrieved,* vol. 6, no. 19, p. 2015, 2000.

[10] "Poisson's Ratio." Engineering Toolbox. https://www.engineeringtoolbox.com/poissons-ratio-d_1224.html (accessed April 4, 2022.

[11] Common Plastic Molding Design Material Specification [Online] Available: https://www.engineersedge.com/plastic/materials_common_plastic.htm

[12] Nylon 6/6 (Polyamide) [Online] Available: https://www.polytechindustrial.com/products/plastic-stock-shapes/nylon-66

[13] V. T. Rathod, "A review of acoustic impedance matching techniques for piezoelectric sensors and transducers," *Sensors,* vol. 20, no. 14, p. 4051, 2020.

[14] V. Miri, O. Persyn, J.-M. Lefebvre, and R. Seguela, "Effect of water absorption on the plastic deformation behavior of nylon 6," *European Polymer Journal,* vol. 45, no. 3, pp. 757-762, 2009.

Chapter 4. Injection Molded Focused Ultrasound Transducer

4.1 Injection Molding Transducers Introduction

Current histotripsy transducers are made using 3D printed methods, SLA and SLS [1-3], but injection molding (IM) could be a promising manufacturing alternative. IM can create detailed, consistent components quickly and affordably. The range of materials offered through IM is also preferable to 3D printing. This chapter investigates and presents, for the first time in literature, prototype focused ultrasound transducers made from injection molded components.

When designing a part for IM, consideration must be made for the materials used and mold design. For example, to maintain part tolerances, the mold must be designed to account for shrinkage of the injected material [4]. The location of the parting line, or where the two mold faces meet, should affect the placement of the part cavity within the mold to avoid undercut features. Undercut features can be injected with the use of split cavity molds or collapsible cores [5], but this increases the expense of the mold and production times for a simplified IMM such as the APSX-PIM. Sufficient draft angles, ejector pins, and the location of those ejector pins are significant considerations when designing an IM mold [4, 5]. Ejector pins lay flush with the part face but are used to eject the part when the component has cooled and the mold has returned to its homed position.

For a transducer lens mold design that can be used on the benchtop APSX-PIM, the design must be adjusted to avoid undercuts, have sufficient internal and external draft angles and ejector pins for part removal, and preservation of the most important feature: the face of the acoustic lens. This chapter will explore these design considerations and outcomes.

4.2 Methods

4.2.1 Injection Molding Design and Inputs

A rectangular transducer lens design with a focal length of 78 mm was modified for IM. The original and modified design is shown in **Figure 4-1**. A previous original design used for 3D printed lenses had slits for excess matching layer used between the PZT and lens to be extruded during construction. These slits caused undercuts in the mold design and were moved to the front face of the lens. The same height tab stops inside the lens face were used in both designs to maintain the matching layer quarter-wavelength thickness. The modified lens has 2.5° draft angles externally and 3° internally. Earlier iterations of the design with preliminary 3D printed mold testing indicated that more extreme draft angles would better ensure part removal.

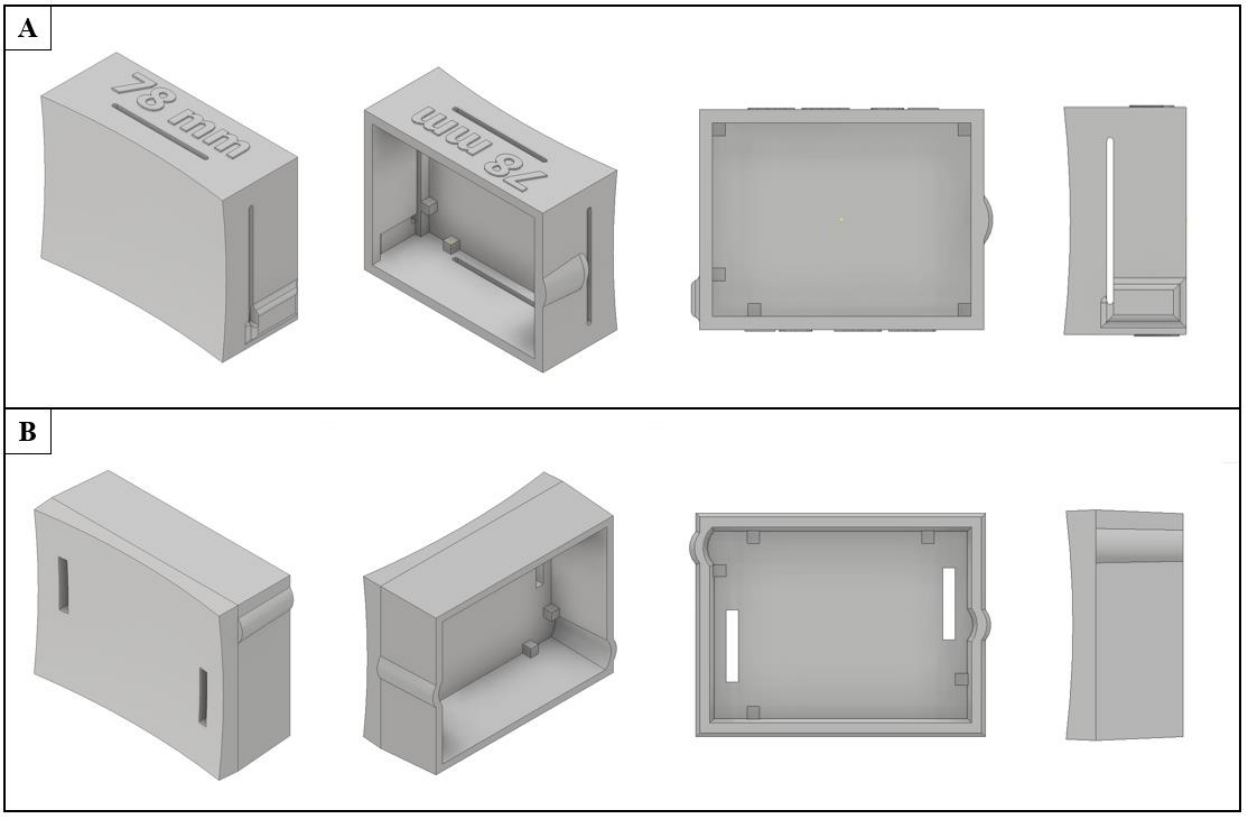

Figure 4-1. CAD renderings of 78 mm focus element lenses, (A) original and (B) redesigned for injection molding. Internally, both have the same height matching layer tab stops. From left to right, isometric front, isometric back, back, and side views.

A mold was designed from the modified lens. The initial and final CAD designs of this mold (SolidWorks 2021, Dassault Systèmes SolidWorks Corporation, Waltham, MA, USA) are shown in **Figure 4-2**. The mold was designed then modified to include ejector pins, an ejector retainer plate with springs, and backer plate. When fully homed, the machine pushes the backer plate to slide the ejector pins forward a maximum of 0.178 in for simple part removal. The blank mold was supplied by APSX, LLC (Blue Ash, OH, USA) and was machined by Total Plastic Solutions (Lynchburg, VA, USA) for ~$1600.

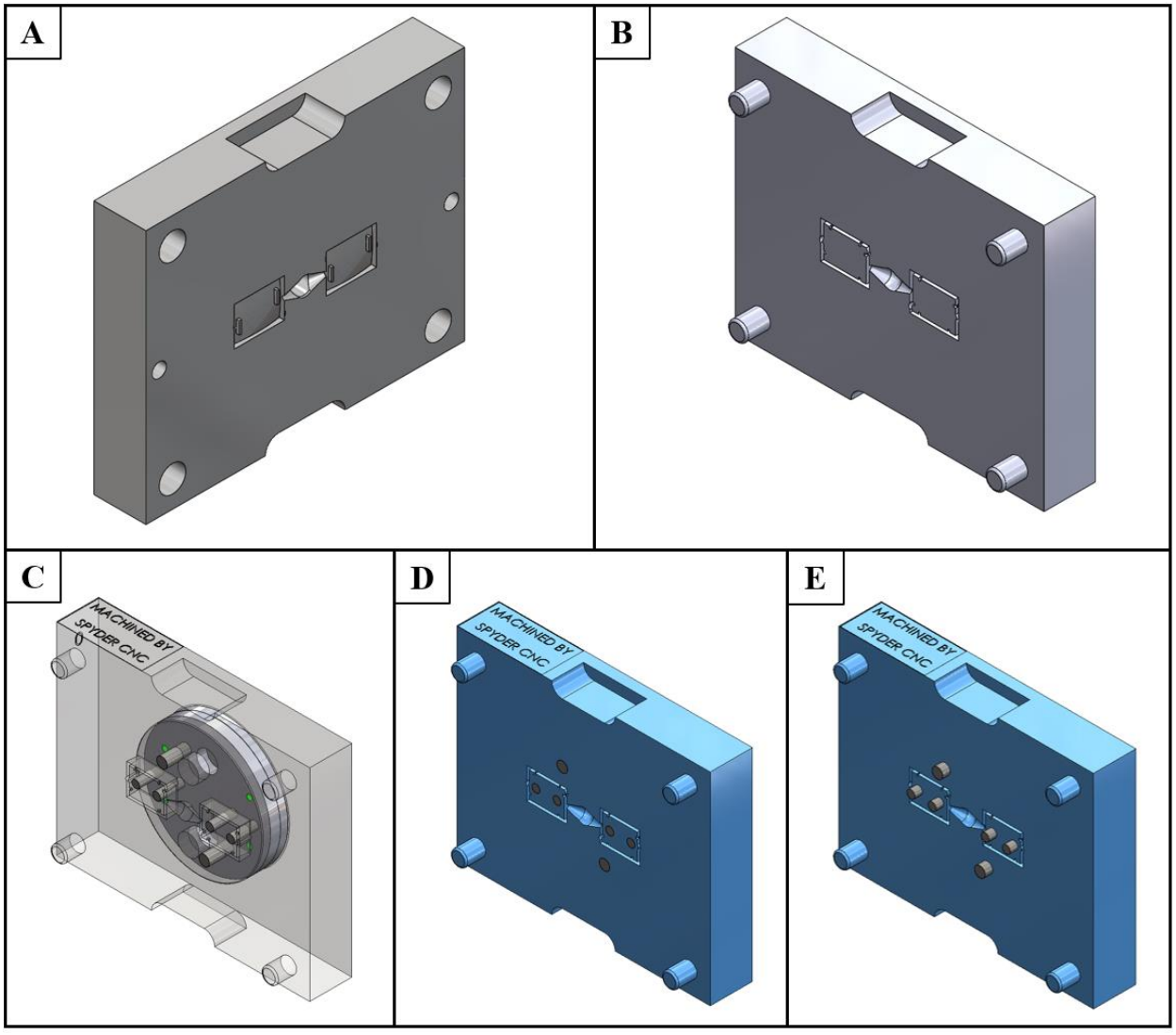

Figure 4-2. Final CAD renderings from a commercial IM manufacturer (TPS, Lynchburg, VA, USA), (SolidWorks 2021, Dassault Systèmes SolidWorks Corporation, Waltham, MA, USA). (A) side A of mold,

(B) side B of mold without ejector pins, (C) rendering where backer plate, ejector pins, and ejector pin retaining plate are visible, (D) ejector pins flush with mold face, (E) ejector pins fully extended 0.178 in.

Similar to Section 3.2.1, simulation of the element lens was run to prepare for injection considerations. Two simulations were run using Fusion 360's Injection Molding simulation tool (Autodesk Fusion 360 2020, San Rafael, CA, USA (Fusion 360). The simulations were run without a sprue and runner system, but the gate was set to the location representative of the mold design. The first simulation was run with generic ABS at an injection temperature of 230°C. The second simulation was run for generic PA6 (nylon 6/6) at an injection temperature of 250°C. These materials were chosen since they are two of the intended materials for element lens injection.

ABS black, 30% glass-filled nylon, nylon 6/6, and nylon 101 were injected on the APSX-PIM with the inputs found in **Table 4-1** to form element lenses. Inputs were determined by trial and error with insight from inputs determined in Chapter 3. For ABS, nylon 6/6, and nylon 101, a PEEK insulator (Mold Insulator (PEEK), Advanced Production Systems LLC., Blue Ash, OH, USA) was placed between side A of the mold and the injection valve to prevent the plastic from prematurely cooling. Stickers were placed on the front face of the molds for venting.

Table 4-1. Element lens injection molding inputs for 4 materials: ABS, 30% glass-filled nylon, nylon 6/6, and nylon 101 on the APSX-PIM.

	ABS Black	**30% glass filled nylon**	**Nylon 6/6**	**Nylon 101**
Dry Time (hr)	2-5	4-6	4-6	5-6
Dry Temp (Celsius)	80-85	80-85	80-85	80-85
Barrel Temp (Celsius)	245	250	265	295
Mold Temp (Celsius)	38	51	51	52
Min Barrel Temp (Celsius)	175	200	200	200
Inj. P (Bar)	120	110	120	100
Hold P (Bar)	10	20	20	5
Clamp Force (Kg)	2000	2000	2000	2000
Holding Time (mSec)	10000	10000	10000	10000
Cooling Time (mSec)	90000	90000	80000	90000
Heater Boost (Sec)	0	0	0	0
Clamp Time (mSec)	14200	14500	14200	14200

Cut Off Amount (cu-cm)	12.0	12.0	12.0	12.0
First Stage (cu-cm)	2.0	3.1	3.1	2.0
Valve Fill Position	180	180	180	180
Hopper Multiplier	50	50	50	40

4.2.2 Single Element Testing

To further investigate IM as a prototyping method for histotripsy transducers, single elements were constructed from the same injection molded ABS, 30% glass-filled nylon, nylon 6/6, and nylon 101 presented in Chapter 3. Five lenses of each material were used to make elements. The lenses were paired with rectangular, 710 kHz SM111 (STEMiNC, Miami, Florida, USA) PZTs. An aluminum oxide (Al_2O_3 White #500 Grit Abrasive CAS# 1344-28-1, AGSCO Corporation, Libertyville, IL, USA) and resin (INF-114-2 Infusion Resin Part A, INF-212-2 Infusion Hardener Part B, Pro-Set, Dallas, TX, USA) combination matching layer (see Section 1.3) was used for each material, put between the PZT and plastic lens. Since this document presents a preliminary analysis, the same matching layer used for WaterShed and SM111, which has an experimentally measured acoustic impedance of 6.82 MRayl, was used for all materials. The elements were backed with epoxy (Marine Epoxy A-side Resin 314, B-side Hardener 143, TAP Plastics, Stockton, CA, USA), and the backing housings were made from WaterShed plastic.

Single elements were tested in degassed water based on the schematic, **Figure 4-3**. The elements were characterized with a rod hydrophone (HNR-0500, Onda Corp., Sunnyvale, CA, USA) giving pressure outputs. Additionally, an impedance analyzer (AIM4300, Array Solutions, Mesquite, TX, USA) was used to complete an electrical impedance test for the elements. The impedance analyzer is connected directly to the element for assessment.

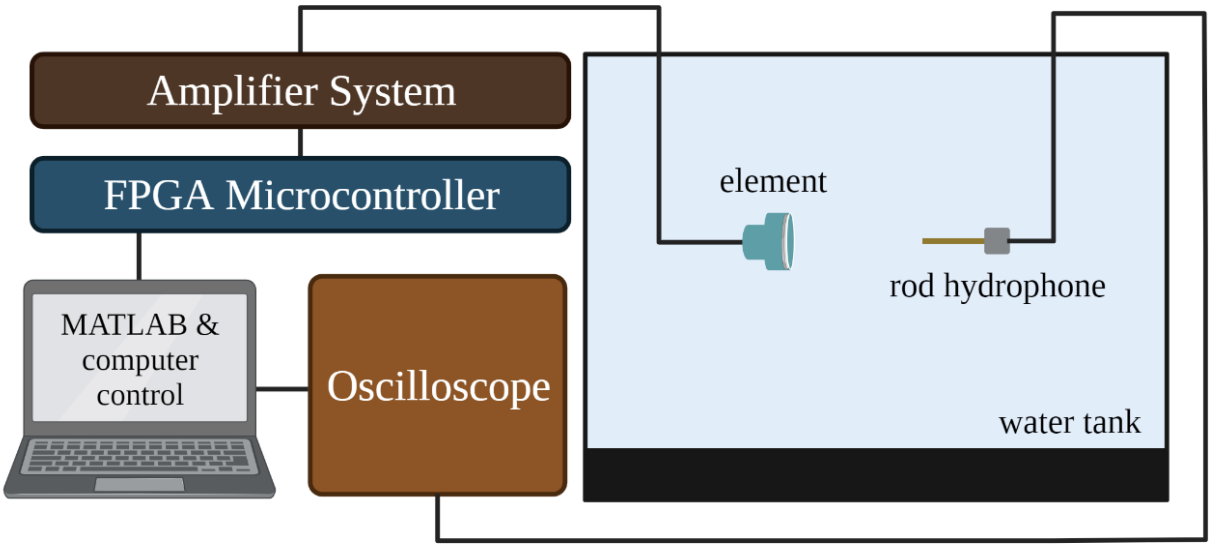

Figure 4-3. Element characterization testing setup schematic with single element and rod hydrophone in water tank with element connected to amplifier and FPGA microcontroller system which is controlled by the computer and MATLAB code. The hydrophone is connected to the oscilloscope which reads the measured waveform and sends data to the computer for analysis.

4.3 Results

4.3.1 Injection Molding Design and Inputs

Simulations of injection molding the lenses with ABS and nylon 6/6 were run and results are presented in **Figure 4-4**. Yellow arrows indicate the injection location of the simulation. These results show that, for both materials, the mold fills easily. No visual defects are expected, but weld lines could be apparent on the back face of the lens. This is especially beneficial to know for the tab stops since the height of these requires good resolution to maintain a desired matching layer thickness. Warpage is more evident in the nylon part (B) as compared to the ABS (A), up to 0.16 mm versus 0.10 mm, respectively. The warpage is expected to occur at the corners of the element face, but this amount of warpage is minimal.

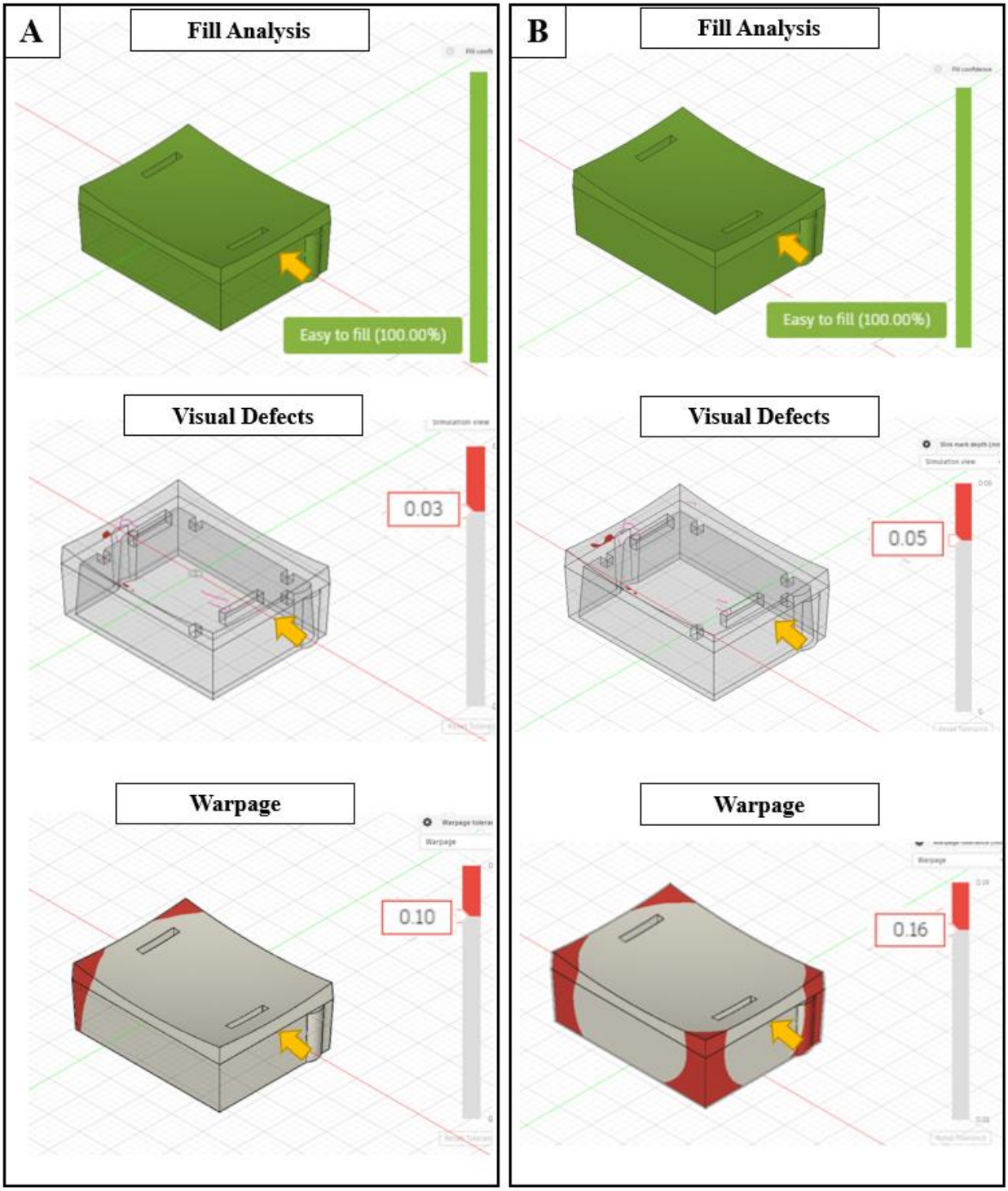

Figure 4-4. Fusion 360 simulation results of mold fill, visual defects, and warpage for a single element lens. (A) ABS results injected at 230°C and (B) PA6 injected at 250°C. The yellow arrow indicates the injection location and pink lines indicate weld lines. Warpage values are in millimeters.

The molds were machined and loaded into the machine successfully. The finished mold is pictured in **Figure 4-5**. The ejector pins were fit with a tight clearance, 0.0007 in so that plastic would not flash into the ejector pin cavities. The ejector pins worked well and removed the part from the mold as long as overpacking is avoided. Overpacking occurs when too much plastic is forced into the mold cavity preventing the part from being removed. To prevent this, the first stage amount (see Section 3.2.1) is slowly increased until the removed part appears fully filled.

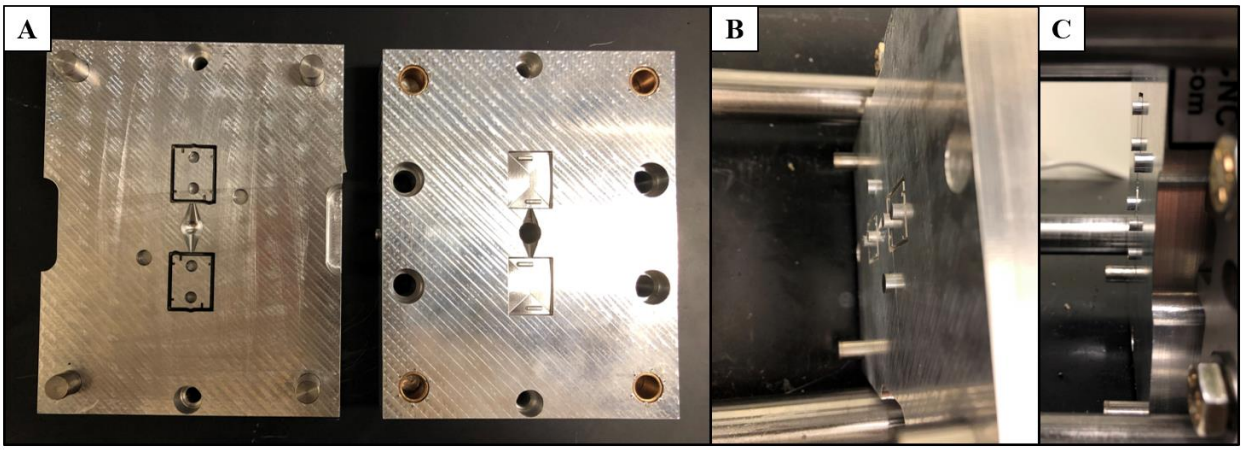

Figure 4-5. Real life machined mold for rectangular element lenses. (A) real life images of sides A (right) and B (left). (B and C) top and side views of ejector pins in machine's homed position. Ejector pins eject 0.178 in.

Rectangular, 78 mm focus lenses were injected from ABS, 30% glass filled nylon, nylon 6/6, and nylon 101. Resultant lenses are pictured in **Figure 4-6**. All lenses were injected with high resolution, with matching layer tab stops and front face slits. Each run took <2 minutes, producing 2 lenses at a time. The front faces of the lenses had a smooth, consistent curvature, and no warpage was apparent. Full part fill was achieved for all material, but the occasional lens injected with 30% glass nylon did not achieve full fill, as pictured in **Figure 4-6** (C). For glass filled nylon, this was not observed in 85% of runs. For nylon 6/6 and nylon 101, flashing was observed, requiring some post-processing to clear matching layer slits. This flashing was more extreme in nylon 101, but was removed easily with tweezers and a small knife.

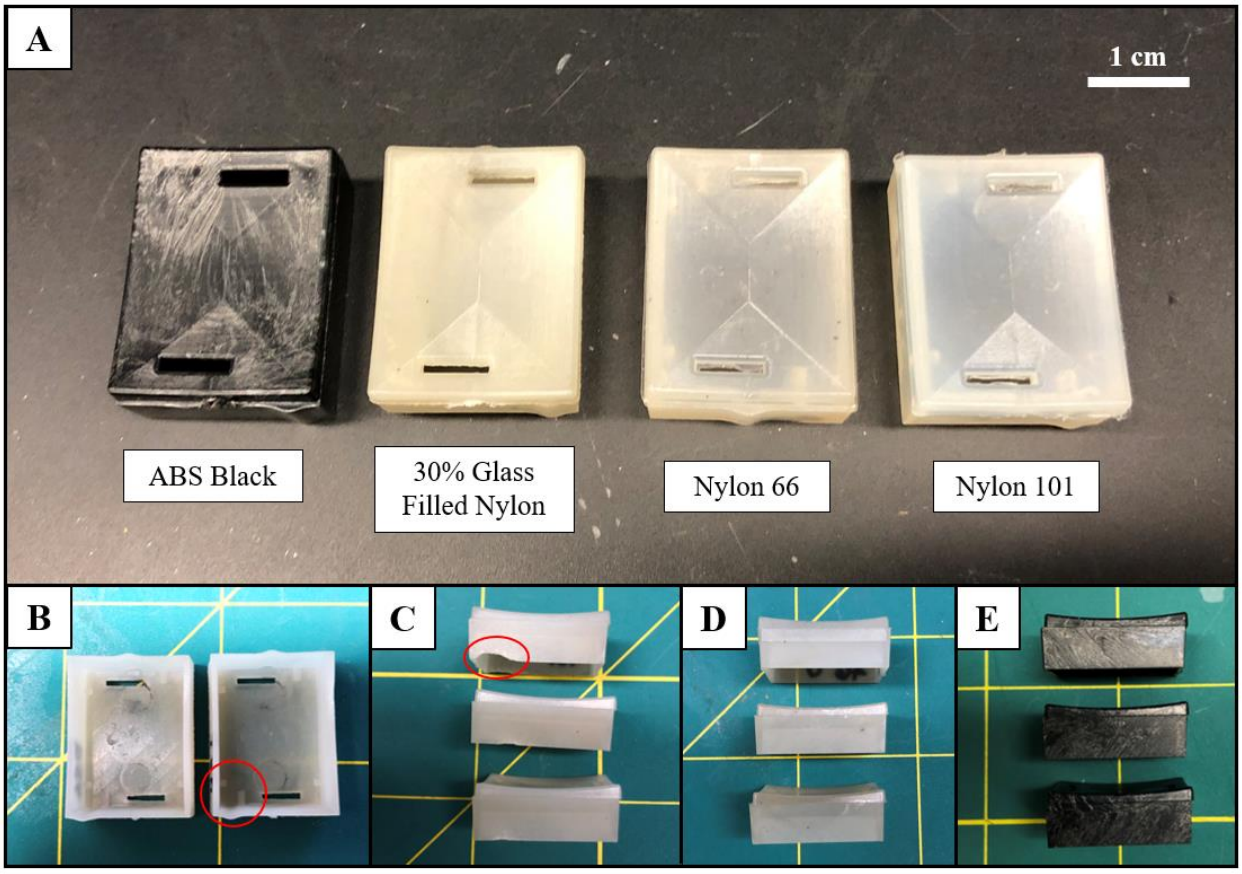

Figure 4-6. Resultant 78 mm focus lenses injected from ABS, 30% glass-filled nylon, nylon 6/6, and nylon 101. (A) front face of elements of injected materials, (B) back of 30% glass-filled lens, circle highlighting good resolution of matching layer tab stops, (C) 30% glass filled nylon side view with partial fill highlighted, (D) side view of nylon 6/6 lenses, and (E) side view of ABS lenses.

4.3.2 Single Element Testing

5 elements of each material lens were constructed. The lenses were made with SM111 710 kHz PZTs and an aluminum oxide matching layer with a compositional acoustic impedance of 6.82 MRayl. Samples of constructed elements are pictured in **Figure 4-7**. These elements were constructed in the same way current WaterShed elements are made, with a two-day manufacturing process that clamps the elements together allowing the epoxy to harden. The various material lenses did not have difficulty adhering to the lens backs or matching layer. After scraping away excess, the matching layer hardened flush with the front face of the element. Additionally, after

handling the element lenses in the construction process, slight peeling was observed on 2/5 of the ABS element lens faces (not pictured).

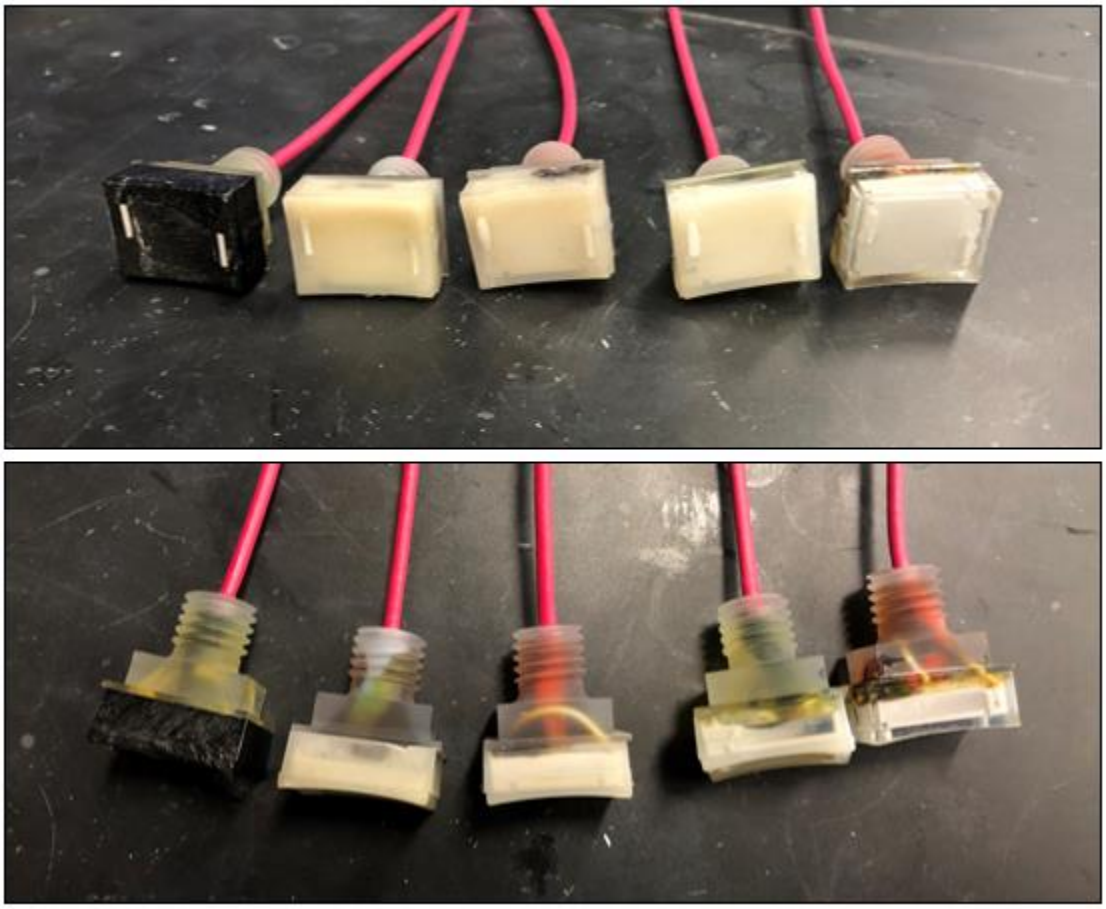

Figure 4-7. Life images of injection molded-lens 710 kHz elements. Top and side views. From left to right, ABS, 30% glass filled nylon, nylon 6/6, and nylon 101.

The elements were characterized individually and electrical impedance data was assessed. On the day of testing, the very first element tested, made from nylon 6/6, stopped producing a waveform when voltage input was increased from 30 to 80V. Even after voltage was decreased from 80 to 50V, the element did not produce a pressure waveform. This element was replaced with a different nylon 6/6 element which produced a waveform at 80V. No issues were observed in any other elements. With the exception of the two nylon 6/6 elements tested, one element of each material was characterized. All element data was collected at a voltage input of 80V, corresponding

to a peak negative pressure of ~1.5 MPa. These results are pictured in **Figure 4-8** and **Figure 4-9**. All waveforms had a shape comparable to the control, 3D printed WaterShed plastic, and, more importantly, in a shape characteristic of a single cycle histotripsy pulse. Peak negative pressures of the injection molded materials were 1.48 ± 0.07 MPa while the peak negative pressure for the 3D printed material, WaterShed, was 1.46 MPa. Peak positive pressures of the injection molded materials were 1.62 ± 0.09 MPa while the peak positive pressure for the 3D printed material was 1.66 MPa. Electrical impedance and phase data show that all injection molded elements have peaks around the 710 kHz range, as desired. More dramatic slopes could possibly be achieved through a more idealized matching layer for each material.

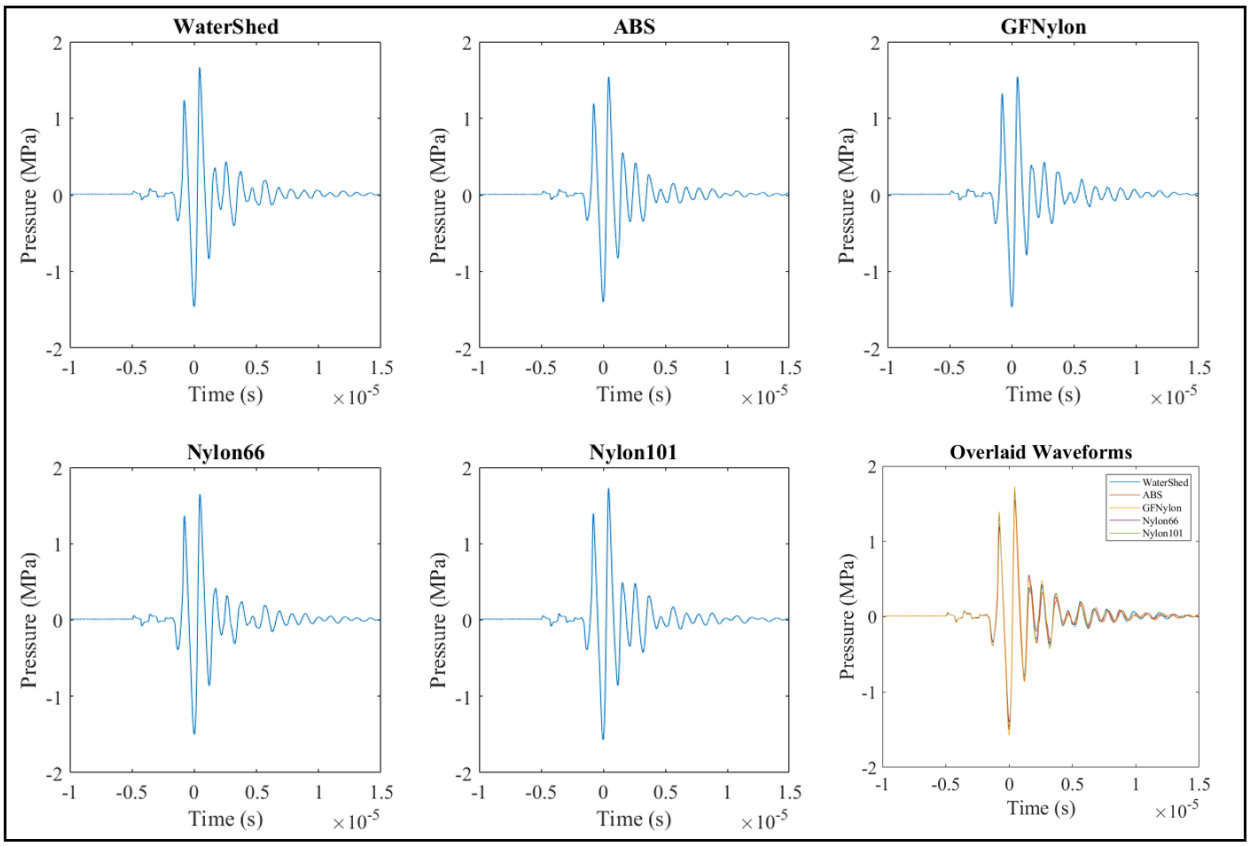

Figure 4-8. Pressure waveforms of injection molded-lens 710 kHz elements tested at 80V input corresponding to peak negative pressures of 1.48 ± 0.07 MPa. Watershed is the 3D printed comparison material while ABS, 30% glass-filled nylon, nylon 6/6, and nylon 101 are injection molded.

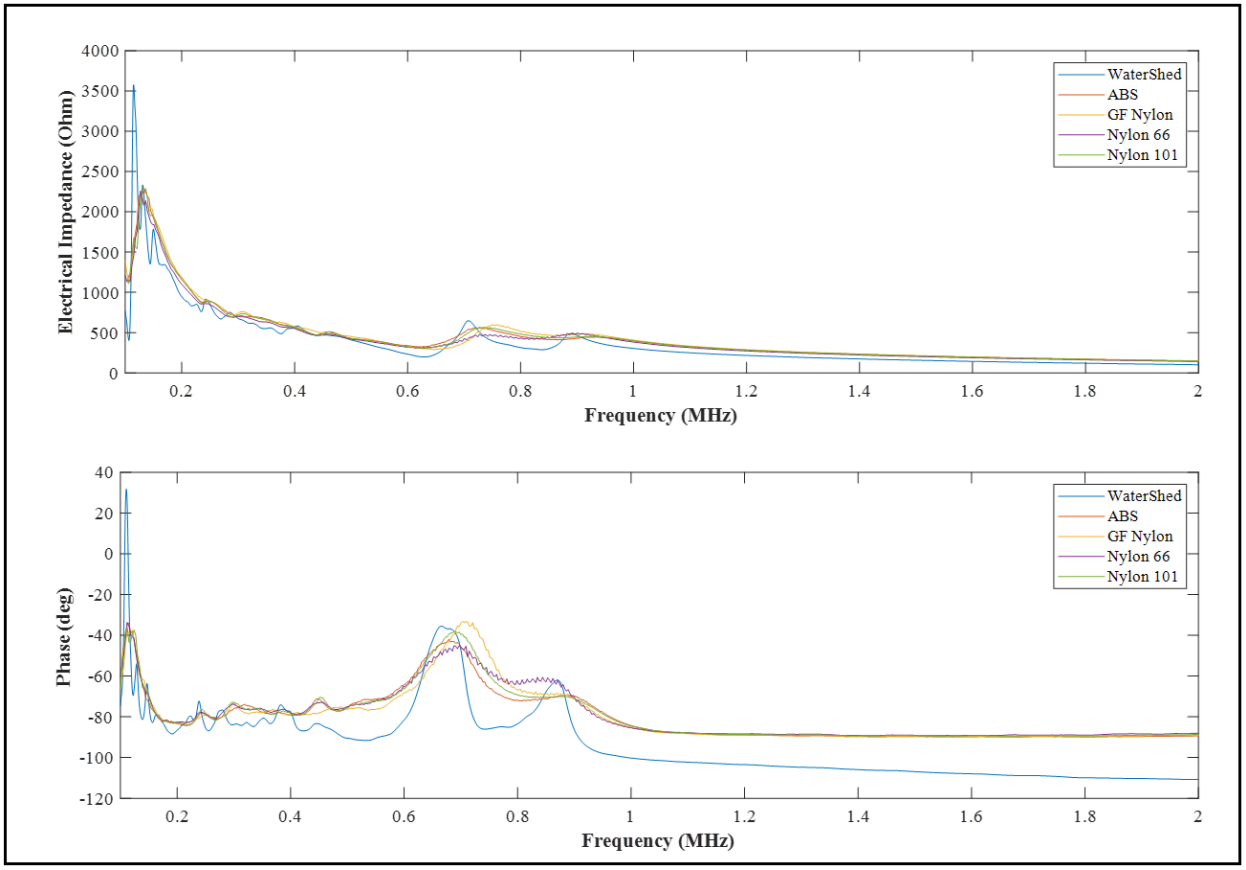

Figure 4-9. Electrical impedance and phase graphs for injection molded-lens 710 kHz elements.

4.4 Discussion

For the first time in literature, IM was used as a rapid prototyping method to construct focused ultrasound transducer elements. ABS, 30% glass filled nylon, nylon 6/6, and nylon 101 were investigated as element housings. Simulations showed substantial part fill but small warpage for the corners of the element face. This warpage is not expected to be significant as long as the front face maintains an appropriate curvature relative to our lens focus for most of the lens face. No warpage was observed in the injected lenses; however, this determination could change for more extreme element curvatures. No substantial shrinkage was observed in the injection molded lenses and all lenses easily housed the PZT and wiring. When investigating IM for larger components such as the transducer scaffold or larger lenses, shrinkage will be a more significant

consideration. Therefore, these larger components will need to be designed with shrinkage in mind, specific to each material [4, 5]. The use of the same mold for a component may not be applicable to materials with more extreme shrinkage properties.

Flashing observed in nylon 6/6 and nylon 101 was minimal, but did require post processing for these lenses. This flashing could likely be minimized or eradicated by increasing clamp force or decreasing injection rate, the latter of which is not a current feature on the APSX-PIM. Each run took less than 2 minutes, producing 2 lenses per run consistently and with preserved detail. All materials produced lenses that could be used to make elements, indicating that from a manufacturing perspective, all materials are promising candidates for further IM investigation for histotripsy. This was further confirmed through acoustic testing. When characterized, the IM elements produced pressures similar to 3D printed elements. This demonstrates feasibility of making focused ultrasound transducers that can be used in histotripsy array transducers as well as a wide range of other focused ultrasound therapies. Additionally, this chapter demonstrates feasibility for single element applications. For example, single element transducers are often used for low intensity focused ultrasound applications such as skull and blood brain barrier transmission for various neuromodulation applications [6-8].

The elements presented in this chapter have a focus of 78 mm. This focus was chosen for best comparison to current elements produced in our lab from 3D printed lenses. A more focused lens would supply greater pressure gain for the purpose of histotripsy applications for shallower targets [9]. Future work is planned to investigate IM of lenses with a range of focal distances for specific clinical applications. Additionally, the same matching layer composition was used for each lens material for simplicity and feasibility testing, but more idealized matching layers are suggested specific to the geometric mean (*Eq.* 1.3) between each material and the selected PZT.

This would also likely increase the acoustic output for injection molded elements and will be explored in future studies.

As mentioned in 3.4, nylon is hygroscopic [10], therefore water absorption rate should be investigated for the presented materials. Delamination within the element of the matching layer, PZT, or lens could occur after a substantial run time and should also be investigated.

4.5 Conclusions and Future Work

IM with our table-top APSX-PIM successfully produced focused transducer lenses from 4 materials: ABS, 30% glass-filled nylon, nylon 6/6, and nylon 101. All lenses were produced accurately, consistently, rapidly, and with retained part features. Acoustic testing showed that elements could successfully generate focal pressures similar to 3D printed transducer elements.

In the future, a mold should be designed for more focused lenses and different transducer geometries in order to more fully characterize the capabilities of IM methods for developing transducers for specific clinical applications. Additionally, improved matching layers should be optimized for each IM material and PZT type in order to optimize the acoustic output obtained from the transducers. It is recommended that a modular transducer with injection molded elements be created and characterized for histotripsy and other applications. To fully produce an injection molded element, mold designs for the element backings should also be explored. Similarly, transducer scaffold designs should be investigated for creating array transducers with IM. Using our benchtop IM system, a transducer could be built with maximum dimensions of ~2x4.5x6 in^3, whereas a larger IMM would be needed to produce transducers larger than this.

Results show the feasibility of using a novel IM process for constructing focused ultrasound transducers, allowing for a wide range of explorable applications for designing and

making prototype histotripsy transducers for histotripsy applications and other focused ultrasound methods.

4.6 References

[1] Y. Kim, A. D. Maxwell, T. L. Hall, Z. Xu, K. Lin, and C. A. Cain, "Rapid prototyping fabrication of focused ultrasound transducers," *IEEE Transactions on Ultrasonics, Ferroelectrics, and Frequency Control*, vol. 61, no. 9, pp. 1559-1574, 2014, doi: 10.1109/TUFFC.2014.3070.

[2] G. E. Stocker, M. Zhang, Z. Xu, and T. L. Hall, "Endocavity Histotripsy for Efficient Tissue Ablation–Transducer Design and Characterization," *IEEE Transactions on Ultrasonics, Ferroelectrics, and Frequency Control*, vol. 68, no. 9, pp. 2896-2905, 2021, doi: 10.1109/TUFFC.2021.3055138.

[3] A. D. Maxwell, K. J. Haworth, C. K. Holland, S. A. Hendley, W. Kreider, and K. B. Bader, "Design and Characterization of an Ultrasound Transducer for Combined Histotripsy-Thrombolytic Therapy," *IEEE Transactions on Ultrasonics, Ferroelectrics, and Frequency Control*, vol. 69, no. 1, pp. 156-165, 2021, doi: 10.1109/TUFFC.2021.3113635.

[4] I. I. Rubin, *Injection molding : theory and practice / [by] Irvin I. Rubin* (SPE monographs., no. Accessed from https://nla.gov.au/nla.cat-vn1865067). New York: Wiley, 1973.

[5] *General Design Principles for DuPont Engineering Polymers*. (2000). DuPont Engineering Polymers Design Guide - Module I. DuPont. [Online]. Available: https://www.dupont.com/content/dam/dupont/amer/us/en/mobility-materials/public/documents/en/General%20Design%20Principles%20for%20Engineering%20Polymers.pdf

[6] A. Bystritsky *et al.*, "A review of low-intensity focused ultrasound pulsation," *Brain stimulation,* vol. 4, no. 3, pp. 125-136, 2011.

[7] H. Baek, K. J. Pahk, and H. Kim, "A review of low-intensity focused ultrasound for neuromodulation," *Biomedical Engineering Letters,* vol. 7, no. 2, pp. 135-142, 2017.

[8] A. Fomenko, C. Neudorfer, R. F. Dallapiazza, S. K. Kalia, and A. M. Lozano, "Low-intensity ultrasound neuromodulation: An overview of mechanisms and emerging human applications," *Brain stimulation,* vol. 11, no. 6, pp. 1209-1217, 2018.

[9] M. G. Mallay, J. K. Woodacre, T. G. Landry, N. A. Campbell, and J. A. Brown, "A Dual-Frequency Lens-Focused Endoscopic Histotripsy Transducer," *IEEE Transactions on Ultrasonics, Ferroelectrics, and Frequency Control,* vol. 68, no. 9, pp. 2906-2916, 2021.

[10] V. Miri, O. Persyn, J.-M. Lefebvre, and R. Seguela, "Effect of water absorption on the plastic deformation behavior of nylon 6," *European Polymer Journal,* vol. 45, no. 3, pp. 757-762, 2009.

Chapter 5. Conclusion

5.1 Conclusions

Results presented in this thesis demonstrate that injection molding is a novel, viable method for manufacturing prototype histotripsy transducers and focused ultrasound transducers for other applications. 3D printed prototype histotripsy transducers were presented in Chapter 2 with *in vivo* studies for comparative analysis for alternative prototyping methods. These studies showed effective histotripsy treatment with 3D printed prototype transducers. Injection molding with a benchtop plastic-injection molding machine, the APSX-PIM, and quantification of injection molded material acoustic properties was presented in Chapter 3. ABS, GPPS, 30% glass filled nylon, nylon 6/6, and nylon 101 were injection molded into ~8 mm thick test squares. This investigation revealed that 30% glass filled nylon is the most similar in acoustic impedance to PerFORM, a currently used 3D printed material for transducer lenses, and nylons 6/6 and 101 are most similar to WaterShed, another 3D printed transducer material. ABS appears to be viable material option as well with appropriate acoustic matching layers. Based on experimental sound speed, acoustic impedance, and attenuation results, 4 injection molded materials, ABS, 30% glass filled nylon, nylon 6/6, and nylon 101, are viable options for acoustic lenses with preference for 30% glass filled nylon. These injection molded plastics should be further tested for water absorption and delamination. In Chapter 4, these 4 materials were used to inject element housings on our benchtop injection molding machine. A mold was designed for a rectangular lens with a focus of 78 mm and ¼ wavelength height tab stops for a 710 kHz PZT. The resulting lenses of each material were used to create single elements which were acoustically tested. The injection molded elements produce waveforms and pressures comparable to 3D printed elements. The

results of this chapter showed that injection molding is a feasible manufacturing method for detailed, consistent, mass production of transducer element lenses. Injection molding is a preferable method to 3D printing for histotripsy transducer applications due to the more affordable production cost, consistent component detail and resolution, fast production time, range of possible plastic materials, and because of the ability to produce the components in-house on our benchtop machine.

5.2 Future Directions

The feasibility of injection molded transducer elements lays a foundation for multiple future investigations. First, the matching layer should be idealized for the most promising housing material and PZT combination. For example, an idealizing matching layer composition for 30% glass-filled nylon and Pz36 or SM111 PZT would have an acoustic impedance of 11.3 or 7.3 MRayl, respectively. This would further enable acoustic transmission of the element. Alternative lens focus designs should be considered for better energy propagation as well. Following this, it is recommended that a modular transducer similar to the style presented in the *in vivo* studies in Chapter 2 be constructed to create a histotripsy transducer capable of cavitation bubble clouds. This transducer could be characterized and used for *ex vivo* and *in vivo* studies. Addition transducer components can be redesigned and a mold created for injection molding. The element backing should be redesigned to avoid undercuts and overhangs, possibly replacing the screw threads of the current design. A small transducer scaffold can be created in the benchtop injection molding machine if the scaffold is less than ~2x4.5x6 in^3. The plastic used for this should be strong or possibly fiber-reinforced so that the scaffold maintains its shape over time. These injection molded prototype transducers can be used for histotripsy or can be applied to other focused ultrasound

applications such as low intensity focused ultrasound for blood brain barrier disruption and neuromodulation [1-3].

In parallel, alternative materials for injection molding, as suggested in Section 3.4, can be investigated with acoustic properties quantified. These materials should have high a flexural modulus, likely correlating to a higher acoustic impedance, and have melt flow rates and processing temperatures within the specifications of injection molding processes. Overall, here injection molding has been shown for the first time in literature to be a feasible process for creating focused ultrasound transducers which could be used for histotripsy or other focused ultrasound applications.

5.3 References

[1] H. Baek, K. J. Pahk, and H. Kim, "A review of low-intensity focused ultrasound for neuromodulation," *Biomedical Engineering Letters*, vol. 7, no. 2, pp. 135-142, 2017.

[2] A. Bystritsky *et al.*, "A review of low-intensity focused ultrasound pulsation," *Brain stimulation*, vol. 4, no. 3, pp. 125-136, 2011.

[3] A. Fomenko, C. Neudorfer, R. F. Dallapiazza, S. K. Kalia, and A. M. Lozano, "Low-intensity ultrasound neuromodulation: An overview of mechanisms and emerging human applications," *Brain stimulation*, vol. 11, no. 6, pp. 1209-1217, 2018.

Appendix A. APSX-PIM Specifications

	SAE	Metric
Piston Dia [in / cm]	1	2.54
Injection Volume [cu-in / cu-cm]	1.83	30
Injection Pressure [PSI / BAR]	5000	345
Clamping Force [lbs / tons]	11023	5
Opening Stroke w/ & w/o Ejector Plate [in / cm]	5.5-7.0	13.97-17.78
Max Processing temp [F / C]	600	315
Weight [lbs / kgs]	250	113
Standard Mold Size [in / cm]	4.8" (W) X 6.0" (H)	12.19cm (W) X 15.24cm (H)
Machine Dimensions [in / cm]	43" (L) X 10" (W) X 15" (H)	109cm (L) X 25.4cm (W) X 38cm (H)
Shipping Crate Dimensions [in / cm]	48" (L) X 16" (W) X 19" (H)	.22cm (L) X 40.6cm (W) X 48.3cm (H
Steel Bar Frame Diameter [in / cm]	1	2.54
Tie Bar Top Clearance [in / cm]	5	12.7
Min Power Supply [V]	115	
Heating Power [W]	1250	
Plastic Materials for Injection	Polycarbonate (PC), Acetal (Delrin), ABS, PC/ABS, Nylon (PA6), Polypropylene (PP), Polystyrene (PS), Polyethylene (PE), Thermoplastic Polyolefin (TPO)	
Warranty	1 year	

Appendix B. 3D Printed Injection Molds

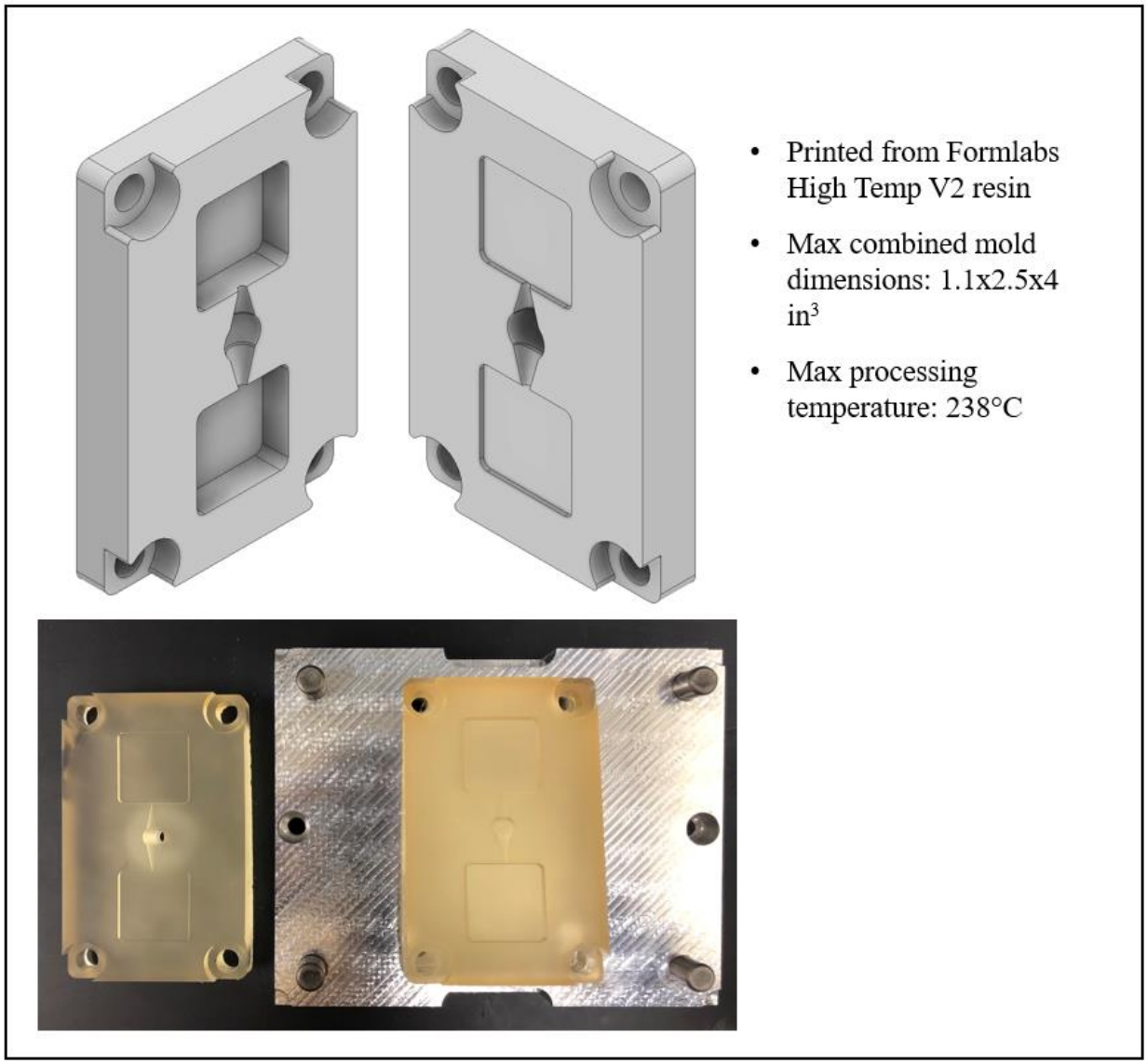

Figure B-01. 3D printed mold inserts for 8x25x25 mm^3 squares.

Appendix C. MATLAB Function for Material Acoustic Impedance Calculation

Below is the MATLAB function used to calculate sound speed and acoustic impedance. The function shown here is specific to ABS and values for names, thickness, and density were adjusted for each material.

```
function material_vals_ABS_mod

names = ['1','2','3','4','5'];
thickness = [12.71,12.54,12.56,12.6,12.74]./10^3; %mm converted
to m, measured with calipers
density = 1040; %kg/m
timeDif = zeros(1,length(names));
waterSpeed = 1484; %m/s distilled water

%control
avgControl = 2.1601e-06; %seconds

%load files of interest
for i =1:length(names)
    file_name = strcat('ABS_', names(i),
'_3MHz_20.0V_HS_20220407.mat');
    load(file_name, 'focusWave', 'timeValues');

    [~, ind_i] = min(focusWave); %tilda means it won't save the
value, we only need the index
    timeDif(i) = timeValues(ind_i); %not a time difference yet,
just time value, s

end

timeDif = abs(timeDif - avgControl);
velocity = transpose((-
waterSpeed.*thickness)./(waterSpeed.*timeDif-thickness)); %m/s
materialImp = velocity.*density./1e6; %MRayls, (Rayl = kg/m2/s)

save ABS_values_mod velocity materialImp

end
```